2014

Catalytic Activity of Heteropoly Tungstophosphoric Acid supported on Partially Reduced Graphene Oxide Prepared by Laser and Microwave Irradiation

Mark Paul Jimena Dailo

CATALYTIC ACTIVITY OF HETEROPOLY TUNGSTOPHOSPHORIC ACID SUPPORTED ON PARTIALLY REDUCED GRAPHENE OXIDE PREPARED BY LASER AND MICROWAVE IRRADIATION

A thesis submitted in partial fulfillment of the requirements for the degree of Master of Science at Virginia Commonwealth University

By

MARK PAUL J DAILO

B.S., Chemistry, University of California Irvine, Irvine, California 2007

Director: M. SAMY EL-SHALL

Professor, Department of Chemistry

Virginia Commonwealth University

Richmond, Virginia

Fall 2014

Acknowledgments

I have many people that I want to acknowledge that have supported, guided, and directed me in carrying out my thesis.

I want to thank my family: my mother, Marlita Jimena, my late father, Crispin Dailo, and my brother, Melvin Dailo. Thank you for your love, support, and everything. I am grateful to be part of the God loving and educated family. All this hard work is the fruit of how you have raised me. You are truly a pattern of hard work, patience, and endurance.

I want to thank my dear and lovely wife, Hongwei Dailo for loving me, understanding, and supporting me. I do not know how I can finish my thesis without you. Thank you for all your motivation and encouragement day in and day out. Also, thank you for taking care of our baby girl, Naomi Grace during my preparation.

I want to thank my research advisor, Dr. M. Samy El-Shall for the opportunity to work in the lab. It was a privilege to work with you and thank you for your advice, support and guidance throughout my thesis. Thank you for your dedication to this field and all your encouragement for the growth and advancement of this research.

I want to thank Assistant Professor, Dr. Sherif Moussa, for his help while he was a post-doctorate associate in the lab and his support and advice. Thank you for leading me to the right direction in the project, for troubleshooting the laser and other essential equipment in the lab, and

for your patience. Thank you for the advice and feedbacks in all the part of this thesis. It is truly a privilege to work with you.

I want to thank Dr. Joseph Turner for all his help and assistance in troubleshooting and setting up of the instruments in the instrumental lab. I appreciate the time and effort you spent in making sure the instruments are working properly.

I want to thank my committee members. Dr. Frank Gupton, Dr. James Terner, and Dr. Hani El-Kaderi. Thank you for investing your time to guide, support, and direct me in carrying out this thesis.

I want to thank all my fellow lab members: Natalie Herring, Abdallah Zedan, Khaled Abouzeid, Sean Platt, Vitaly Kisurin, Ahmed Said, Amr Mohammed, Hany El-Azab, Julian Bobb, and Parichehr Afshani. Thank you for all your encouragement and help.

Finally, thank you VCU Chemistry Department for a privilege to be part of a great community in pursuit of success. Thank you for providing all the necessary help and advice throughout my duration here. Thank you for all the faculty and staff who endeavor to provide the best help for students in their success.

Table of Contents

List of Figures

List of Tables

Abstract

CATALYTIC ACTIVITY OF HETEROPOLY TUNGSTOPHOSPHORIC ACID SUPPORTED ON PARTIALLY REDUCED GRAPHENE OXIDE PREPARED BY LASER AND MICROWAVE IRRADIATION

By Mark Paul J Dailo, M.S

A thesis submitted in partial fulfillment of the requirements for the degree of Master of Science Chemistry at Virginia Commonwealth University.

Virginia Commonwealth University, 2014

Director: M. Samy El-Shall, Professor, VCU Department of Chemistry

The solid acid catalyst of the Keggin-type 12-tungstophosphoric acid ($H_3PW_{12}O_{40}$, HPW) is supported on graphene oxide (GO) and partially reduced graphene oxide (PRGO) nanosheets for acid-catalyzed reactions. HPW is a new class of catalyst with a good thermal stability and high Bronsted acidity in order to replace common mineral acids. However, it has low specific surface area. Therefore, we investigate the possibility of GO and PRGO as a catalytic support for HPW. The synthesis of HPW supported on GO and PRGO is prepared using microwave and laser irradiation without using any chemical reducing agents. The HPW/GO catalysts are characterized by Ultraviolet-visible spectroscopy (UV-Vis), Fourier Transform Infrared Spectroscopy (FT-IR), Raman Spectroscopy, X-ray Photoelectron Spectroscopy (XPS), X-ray Diffraction (XRD) techniques, and Transmission Electron Microscopy (TEM). Also, the surface acidity is measured by a non-aqueous titration of n-butyl amine. Furthermore, the application for catalysts is tested by three acid-catalyzed reactions: Esterification, Friedel-Crafts acylation, and

Pechmann condensation. The greatest acidity for the microwave irradiation method is the loading of 85 wt% HPW and 60 wt% HPW for laser irradiation. The results observed provide an excellent opportunity for GO and PRGO as a catalytic support for HPW for acid-catalyzed reactions.

CHAPTER 1

1. Introduction

1.1 Motivation

The heteropoly solid acids such as 12-tungstophosphoric acid ($H_3PW_{12}O_{40}$, HPW) have been utilized as a Bronsted acid and redox catalysts because they possess unique properties. These properties include strong acidity, high oxidation potential, and redox characteristics [1-11]. These properties make HPW a great homogeneous catalyst to replace common mineral acid catalysts. However, HPW has low surface area (1-5 m^2g^{-1}), low thermal stability, and low porosity [1-3, 5, 7]. Also, HPW forms carbonaceous deposit (coke) on its surface. As a result, HPW catalytic activity decreases over different cycles over time[12]. Therefore, the synthesis and design of heterogeneous catalyst is needed to mitigate the problems of an unsupported HPW catalyst. Catalytic supports, which possess large surface area and good thermal stability, are favorable. Several publications have been reported in the literature exploring support for HPW including carbon nanotubes, silica, mesoporous matrices (MCM-41 and SBA-15), metal oxides (TiO_2, ZrO_2, Al_2O_3, Nb_2O_5)[6, 13-23], metal organic framework (MIL-101)[22]. However, there

are few reported so far about the loadings of HPW on either graphene oxide or partially reduced graphene oxide support which can serve as large surface area for HPW[24-28].

The advances of using reduced graphene oxide as a catalytic support for catalysis have drawn considerable attention. Geim and his coworkers reported the first mechanical exfoliation of graphene from graphite using Scotch tape method in 2004. Eventually, they received the Nobel Prize in Physics in 2010 for their discovery of a new and exciting material. Graphene is an exciting material since it possesses several properties that are used in different applications. Such properties include high intrinsic mobility (200 000 $cm^2v^{-1}s^{-1}$)[29], thermal conductivity (~5000 $Wm^{-1}K^{-1}$)[30], high Young's modulus (~1.0 TPa)[31], large surface area (~2630 m^2/g) [29, 32], good electrical conductivity and optical transmittance (~97.7%)[33, 34]. Its high intrinsic property allows the exploration of new composite materials for supercapacitors, batteries, nanoelectronics, etc. [35, 36]. However, the property which makes graphene viable as a catalyst support is its large surface area and its high thermal stability. A number of publications have been reported related to the loadings of metal including bi-metallic, metal oxides supported on reduced graphene oxide [37-44] and metal free including functionalized graphene with either nitrogen or sulfuric groups [45-47].

1.2 Objective Statement

The objective of this research is to examine graphite oxide and partially reduced graphene oxide as a catalytic support for HPW catalyst in acid-catalyzed organic reactions such as Esterification, Friedel-Crafts acylation (FCA), and Pechmann Condensation. Also, it is necessary to use various characterization techniques for the confirmation of proper loadings to the support and study the catalytic activity which includes conversion, selectivity, yield, and

recyclability. This study will determine the development and future of HPW-GO as a heterogeneous catalyst.

1.3 Approach

The synthesis and design of the HPW-GO catalyst requires the preparation of GO by the oxidation of graphite. HPW is incorporated into the surface of GO by a simple impregnation method. The HPW and GO mixture undergoes laser irradiation method with laser wavelength of 355 nm or 532 nm for the partial reduction of GO. The microwave irradiation was used to load HPW to GO.

The HPW-GO catalysts were characterized by potentiometric titration, UV-Vis, FT-IR, Raman, XPS, XRD, and TEM. The potentiometric titration allows the determination of the surface acidity of the catalysts. This enables the calculation of the number of acidic sites available for catalysis. A greater number of acidic sites show a high catalytic activity. However, not until a significant test for acid-catalyzed organic reactions is developed can the catalytic activity be truly known. The other techniques mentioned above provide the evidence of a successful loading of HPW on the surface of GO and partially reduced GO.

A bulk HPW was used for many different acid-catalyzed organic reactions. Many researchers have tested a supported HPW in acid-catalyzed organic reactions. In this study HPW-GO catalysts were tested in three reactions which include Esterification, Friedel-Crafts acylation, and Pechmann condensation. The products were characterized by GC-MS for the three reactions. Since the product for Pechmann condensation were solid crystals, FT-IR and melting point were used for further characterization. The catalytic activity which includes the conversion and

selectivity of products were calculated for Esterification and Friedel-Crafts acylation. The amount of products for Pechmann condensation was used to calculate its yield. Finally, a possible heterogeneous catalyst not only should have good conversion and high selectivity, it must also have a good recyclability. The recyclability was tested using the best HPW-GO catalysts for each reaction.

1.4 Organization of Chapters

This thesis will be divided into six chapters to provide readers some understanding of the problems with an unsupported HPW, the possibility of graphene in catalysis, and the thorough presentation of the work. Chapter 2 presents a literature review of the HPW's role in homogeneous and heterogeneous catalysis, several examples of materials used for catalytic support for HPW, and the background of graphene in catalysis.

Chapter 3 shows the experimental section which includes the synthesis of GO and the loadings of HPW into the graphene sheets. The catalytic activity of such catalyst was examined using the three acid-catalyzed reactions.

Chapter 4 demonstrates the results and discussion of the characterization techniques for the HPW-GO catalysts such as XRD, XPS, UV-Vis, FTIR, Raman, TEM, and Potentiometric titration.

Chapter 5 indicates the results and discussion of the application of HPW-GO catalyst for Esterification, Friedel-Crafts acylation, and Pechmann Condensation. GC-MS was used to investigate the catalytic activity such as the conversion, selectivity, conversion, and recyclability.

Chapter 6 presents the conclusion of the work.

CHAPTER 2

2. Literature Review and Background

2.1 Homogeneous vs. Heterogeneous Catalysis

According to the International Union of Pure and Applied Chemistry (IUPAC), a catalyst can be defined as a substance in which an increase of the rate of reaction is observed. Furthermore, the standard overall Gibbs energy change is unmodified in the reaction. Also, the catalyst should be present in the reactant and the products of the reaction. It is either used or consumed in the reaction [48]. Also, with a catalyst there is less expenditure of free energy in order to reach the transition state of the reaction. **Figure 1** shows a simple energy diagram. It shows both the catalyzed and uncatalyzed reaction. Also, it shows that the activation energy (E_a) of the catalyzed reaction is lower than the uncatalyzed reaction. In other words the overall speed of the reaction increases. There are two types of catalyst that can be part of the reaction. It can either be a homogeneous or a heterogeneous catalyst. A homogeneous catalyst includes only one phase, while heterogeneous happens at either at the reaction site or near the interface in between phases [48, 49]. The heterogeneous catalyst is advantageous since it is more stable and it degrades slower than a homogenous catalyst. As a result, many scientists have been interested in investigating and improving the field of heterogeneous catalysis.

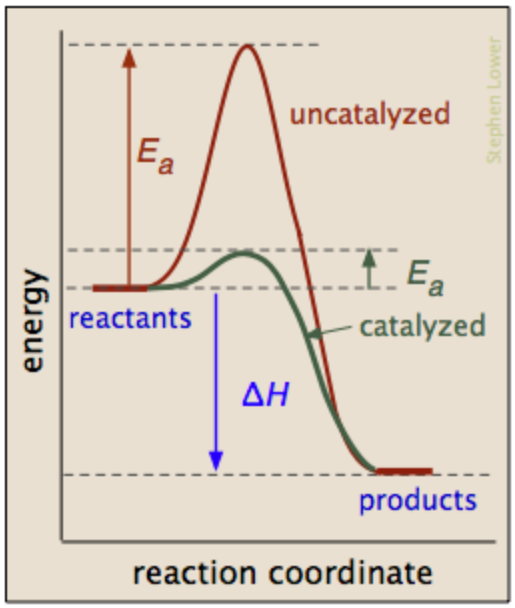

Figure 1. The Energy Diagram [50]

Although homogenous catalysis has been the catalytic route for different acid-catalyzed organic reactions in industry, there is extensive research to replace this type of catalyst with solid heterogeneous catalysts. Homogeneous catalysis has been utilized because of the accessibility of all catalytic sites in the reaction [51]. In other words, each acid site is available for the reaction which makes a reasonable catalyst. Some of the common homogeneous catalysts included the use of mineral acids such as H_2SO_4, HF, HCl, H_3PO_4, etc. [52, 53]. However, the disadvantage of using such a catalyst is that it gives rise to environmental and hazardous effects. This is unwanted in most applications. Moreover, another disadvantage is the difficultly to separate the catalyst from the products. As a result, it is irrecoverable and unrecyclable for the following reaction[54]. The synthesis and design of heterogeneous catalyst helps in producing environmentally friendly and recyclable catalysts. Specific examples will be given in section 2.4, where various literature references on heterogeneous catalyst are discussed.

2.2 Heteropoly Acid

2.3.1 Overview and Structure

Heteropolyacids (HPAs) are very appealing in the field of catalysis as a substitute for the common mineral acids (sulfuric acid, phosphoric acid, etc.) for homogeneous and heterogeneous catalysis. Its first discovery was dated in 1826 by Berzelius and coworkers. The structure and the correct formula were unknown until further studies of Keggin in 1934 emerged[55].

The formula for the α-isomer heteropoly anion is $[XM_{12}O_{40}]^{n-}$. The central atom, X, which includes P^{5+}, Si^{4+}, etc. The metal atom, M, includes W^{6+}, Mo^{6+},V^{5+},etc. **Figure 2**a shows the general structure of Keggin heteropoly anion where XO_4 tetrahedron is in the center and its surroundings include 12 corner- and edge-sharing metal oxygen octahedral MO_6[56]. In this project $PW_{12}O_{40}^{3-}$ was chosen as shown in **Figure 2**b due to its greater acidic property compared to other types of heteropoly acids.

(a) (b)

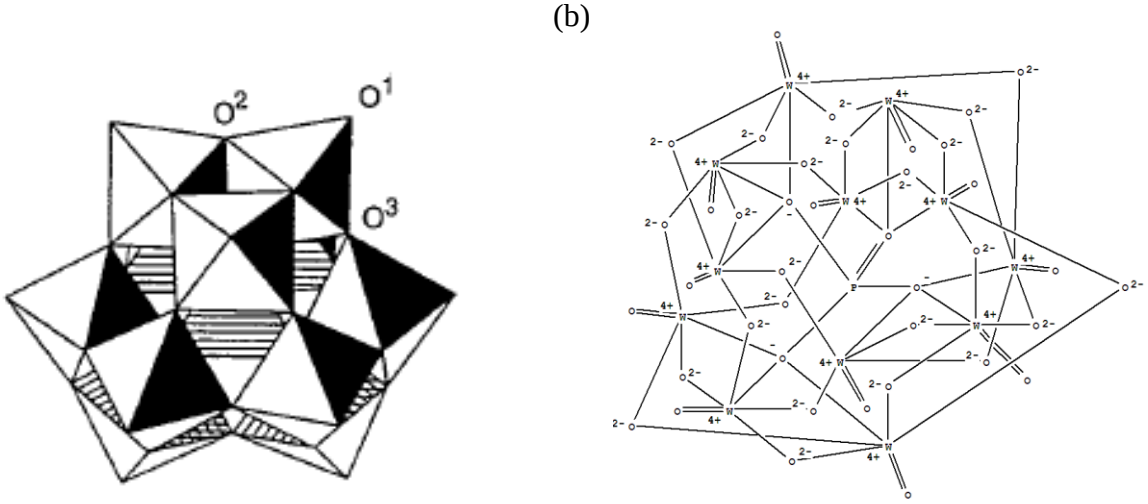

Figure 2.(a) Keggin heteropoly anion $(\alpha XM_{12}O_{40})^{n-}$ The oxygen atoms: terminal (O^1), edge-bridge (O^2), and corner-bridge (O^3)[5, 55, 57]. (b) $PW_{12}O_{40}^{3-}$

2.3.2 Advantages

There are several advantages for HPAs that have drawn interest among researchers that involve not only environmental and economic uses but also its strong Bronsted acidity that has reached the superacid region [5]. A superacid by definition is a medium where the proton's chemical potential is greater as compared to pure sulfuric acid [58]. Moreover, the strength of an acid is determined by how much it dissociates in a solution. In other words, a great acid catalyst is determined by its dissociation constant. This is quantified by an acid dissociation constant (K_a) which is given in **Equation 1.**

A general equilibrium acid dissociation, where HA is an acid, A^- is a conjugate base, and H^+ is the proton: $HA \leftrightarrow A^- + H^+$

$$K_a = \frac{[A^-][H^+]}{[HA]} \qquad \textbf{Equation 1}$$

As a result, the acid dissociation constant is larger which gives a smaller pK_a value. Table 1 reports the pKa of HPAs compared to common acids. Also, the crystalline HPAs acid strength decreases according to a similar trend in table 1, PW>SiW≥PMo>SiMo. The $H_3PW_{12}O_{40}$ has the greatest pK_1 value which corresponds to a strong acid. The acid strength of HPW makes it a good candidate for a heterogeneous catalyst. This explains the choice of catalyst for this work.

Table 1. Dissociations constants of HPAs in Acetone at 25ºC[59].

Acid	pK_1	pK_2	pK_3
$H_3PW_{12}O_{40}$	1.6	3.0	4.0
$H_4PW_{11}VO_{40}$	1.8	3.2	4.4
$H_4SiW_{12}O_{40}$	2.0	3.6	5.3
$H_3PMo_{12}O_{40}$	2.0	3.6	5.3
$H_3SiMo_{12}O_{40}$	2.1	3.9	5.9
H_2SO_4	6.6	-	-
HCl	4.3	-	-
HNO_3	9.4	-	-

Moreover, another advantage of HPAs is their relative high thermal stability. The PW decomposes at 465ºC, SiW (445ºC), PMo(375ºC), SiMo (350ºC)[60]. As HPAs decompose, they lose it acidity strength. Thus, a thermally stable acid has a beneficial in recyclability of catalysts. Finally, HPAs are very soluble in polar solvents: lower alcohols, water, esters, ethers, water, etc. However, they are insoluble to non-polar solvents mainly hydrocarbons.

2.3.3 Problems with Bulk HPAs

Although unsupported HPAs can be an effective and efficient catalyst, they still pose several problems. Therefore, development of a different support for HPAs is valuable as it will discuss in detail in section 2.5. The activity of the catalyst depends on how many acidic sites are available for a reaction. One main problem of bulk HPAs is their low specific surface area (1-5 m^2g^{-1})[1], which can become a limitation to maximizing its catalytic activity in various reactions. However, it has been reported that it has greater catalytic activity since the reaction occurs on bulk HPAs as well as its surface when the polar character is found in the reactants [61]. On the other hand, the utilization of solid supports is recommended the activity is increased for non-polar reactants by increasing the acidic sites.

Another problem with bulk HPA catalysts is the formation of carbonaceous deposit known as coke on the catalyst surface [5]. It occurs in organic reactions which deactivates the catalysts. As a result, it is difficult to regenerate HPAs for subsequent reactions [12]. The coke remains on the surface of the catalyst because of the strong adsorption and low solubility in liquid phase and low volatility in gas phase. In acid catalysis, the coke is produced from the transformation of reactive compounds such as oxygenated compounds, alkenes, alklypolyaromatics, etc. [62]. In some cases, burning these deposits on the surface happens between 500-550ºC for the case of zeolites. However, it cannot be applied for bulk HPAs because of their low thermal stability, which is below this temperature range. The supporting of HPAs with supports can inhibit the formation of coke[63]. In other words, the support acts as a barrier in order to prevent the formation of coke. With all the known disadvantages of unsupported HPAs, the design and development of solid support is a requirement for future applications involving this type of reaction.

2.3 Different Supports for HPAs in Acid-Catalyzed Organic Reactions

2.4.1 Overview

The development of solid supports is an integral part in increasing the acidic sites that are available in catalysis for a specific reaction. A large surface area for the support is considerably advantageous for this type of application in order to increase the available acid sites for the reaction. Different scientists have reported the surface area of various supports that have been used for HPAs which includes MCM-41 (~1000m^2/g)[5], MCM-48 (755 m^2/g) [64],Y-type zeolite/silica (620 m^2/g), SiO_2 (306 m^2/g) [1], active charcoal (450m^2/g) [13], Nb_2O_5 (50m^2/g) [65], SnO_2 (62.3 m^2/g)[4], and Modified Clay AT-Mont(390 m^2/g)[66]. These solid supports for

HPAs are useful in various acid-catalyzed reactions and it will be discussed in more detail in the next sections.

There are different types of interaction between the HPAs and the different catalytic support. The OH groups and the protons surrounding the HPAs have interaction within the support. This interaction enhances the catalytic site[67]. Also, HPAs Bronsted acid site protons are transported to the catalytic support basic OH group. Furthermore, the strong binding of the HPAs and the support is the result of strong adsorption via electron transfer biding and electrostatic binding[25]. These interactions for the support help stabilize the catalyst on the surface or pores of the support.

2.4.2 Esterification Reaction

Esterification reaction is an essential and key organic reaction for producing esters between carboxylic acids and alcohols. Esters are used in different applications from manufacturing perfumes, plastics, flavoring extract, glass, pharmaceutical, etc. [68]. The common routes for catalyzing this reaction is using hydrochloric acids and toxic chemicals such as methyl iodide or dimethyl sulfate [69]. This research will also provide another route for increasing the catalytic activity of a given reaction. Therefore, the ultimate replacement of such toxic and hazardous chemicals in this reaction with a cost-effective and reliable catalyst will be beneficial to the environment.

For example, Khder and et. al [20] presented a work on the Esterification of n-octanol with acetic acid using MCM-41 as a catalytic support for HPW. The reaction uses 0.05 g of the catalyst and the mixture of the reactants using 2 mmol of acetic acid and 2 mmol n-octanol at 80^{o}C for 1 hour. The results show how the 60 wt% of the catalyst gives an almost 100% yield

and has a selectivity of about 99 % to mainly octyl acetate. However, the loadings above 60 wt% showed a decrease in catalytic activity. The catalyst can be recycled twice resulting in a yield of 98.7% on the second run and 97.1% on the final run.

Another work presented by Singh and et. al. shows the use of 12-Tungstophosporic acid (TPA) supported on Mobile Composition Matter (MCM-48) for biodiesel production [64]. They synthesized the TPA/MCM-48 using an incipient impregnation method. The MCM-48 was supported with various loadings of TPA. The Esterification reaction occurred with reactants oleic acid and methanol. The percent conversion is related to the increase in the percent loadings. This can be attributed to the total acidity of the catalysts. The best conversion of their catalyst is 96% from 40% loadings. However, since the loadings of 30 and 40% do not have much difference, 30wt% was used with 95% conversion in their study. They have studied the effect of mass of catalyst used in the reaction, and the mole-ratio of the reaction. They observed that the conversion increases with the percent conversion. Therefore, the optimum condition for the reaction time is 8 hours. The catalysts prepared have a recyclability of four times which shows a very promising support for biodiesel production because of high catalytic activity at lower loadings.

Furthermore, Bhorodwaj and et. al developed a catalyst using dodecatungstophosphoric acid, HPW (DTP) supported on an acid modified Montmorillonite clay (AT-Mont) and tested it for Esterification of acetic acid with n-butanol [66]. In this study, the Montmorillonite clay contains silica, iron oxide, as impurities. The clay was purified using a sedimentation method. The DTP was loaded on the support using the incipient wetness impregnation method. The Esterification reaction was performed by mixing n-butanol with acetic acid. They studied the best amount of loadings to yield the best conversion and they found that to be 20% loadings.

Also, different reaction times were studied and found that increasing the reaction to 12 hours gave the best conversion. Then the reaction temperature that gave the best yield is at 150^0C. All these conditions were applied to obtain the best conversion. The best conversion of their catalyst is 88.0% with loadings of 20% DTP/AT-Mont with a reaction time of 12 hours. AT-Mont can be considered a very stable support for the DTP based on the results and its recyclability. AT-Mont is a promising support due to low cost, environmental compatibility and operational simplicity.

Moreover, the mechanism of the esterification reaction of alcohols with acetic acid using zeolites is displayed in **Figure 3** as proposed by Kirumakki and et. al [70].The general mechanism involves the use of Bronsted acid sites while others mentioned the use of Lewis acid sites by low coordination metal ions [71, 72]. Since alkenes are formed as side products, we can deduce that the mechanism goes via a protonated alcohol intermediate which is displayed in this mechanism below [73]. In this reaction the acetic acid is adsorbed on the catalytic surface where it forms a protonated acetic acid as an intermediate. The electrons in the oxygen of the alcohols are nucleophiles to attack the electron deficient carbocation. Resulting from this is a bond between oxygen and carbon. Finally, a series of electron rearrangement and dehydration occurs for the formation of the ester product. The results found by Kirumakki and et.al showed that there is a competition of adsorption in the acid sites of the catalyst resulting in the reduction of catalytic efficiency.

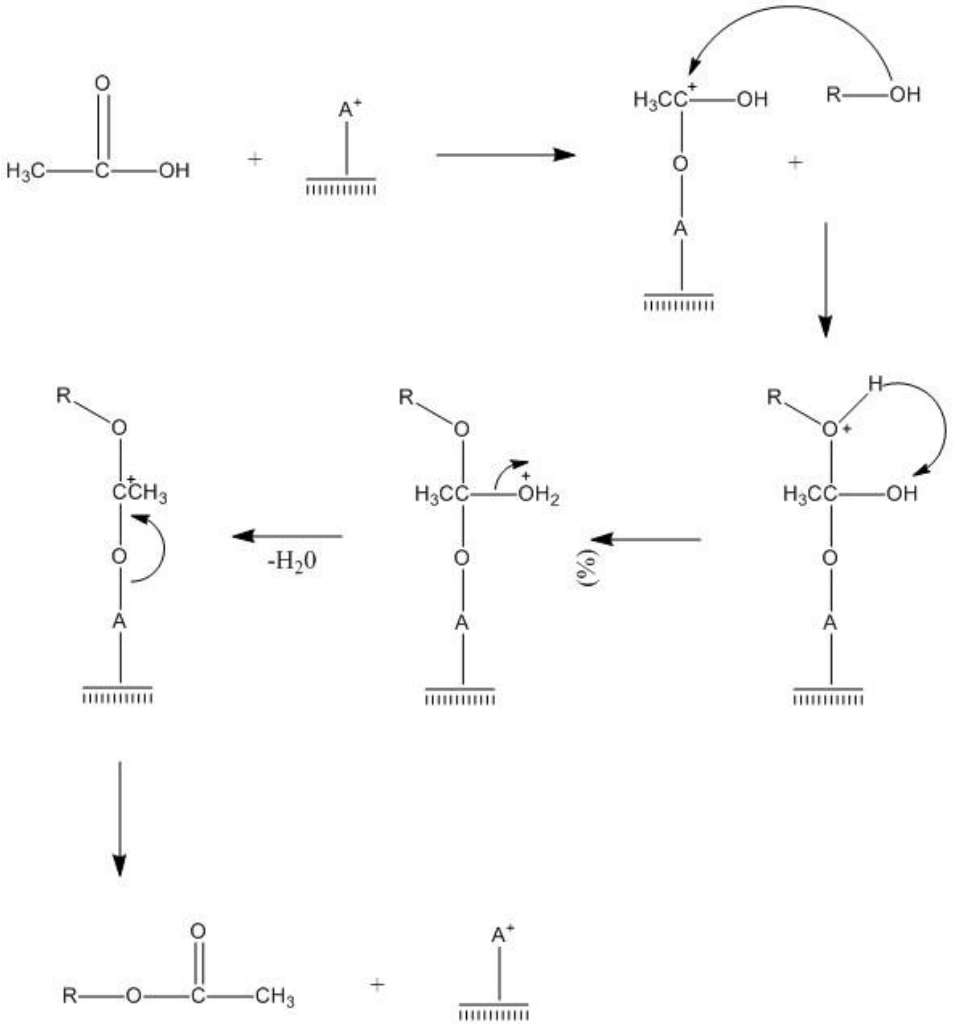

Figure 3. Proposed Mechanism for Esterification

2.4.3 Friedel-Crafts Acylation

Friedel-Crafts Acylation is used in synthesizing substituted aromatic ketones. This reaction is a crucial step in making intermediates for various processes in pharmaceuticals, and cosmetics[74]. The reaction happens through the combination of an aromatic compound and a carboxylic acid derivative such as acid chloride, acid anhydride, etc. with an acid catalyst. The mechanism involves the acylating agent interaction with the acid catalyst and produces acyllium ion intermediates [75].

Kozhevnikov and et. al [12] obtained a very high activity of acylation of anisole with acetic anhydride using SiO_2 support. The PW/SiO_2 was synthesized via the impregnation of HPA into the Aerosil 300 silica and it was stirred for about 6 hours at room temperature. The reaction was carried by mixing the reactants in a condenser with the PW/SiO2 catalysts without any solvent for 2 hours. They obtained 98% para-methoxyacetophenone (p-MOAP), and 2.1% ortho-methoxyacetophenone (o-MOAP) using the catalyst 40% PW/SiO_2. It is attributed that the decrease of catalytic activity is from the dehydration of water in the catalyst surface since it decreases the number of acidic sites. Moreover, strong acidic sites are able to deactivate coke faster. Furthermore, the catalysts were reusable with some gradual decline of catalytic activity. The first run of 40% PW/SiO_2 obtained 98.0 % p-MOAP yield while the second run gave 82%. The results show an improvement in the yield compared to the common mineral acids; therefore, PW/SiO2 is very promising catalyst for heterogeneous catalysis.

Another research using MCM-41 as a support for HPW was studied by Khder and et. al [20]. The synthesis of the HPW/MCM-41 was achieved through the impregnation method for 4

hours. The catalyst was dried and calcined in a furnace at 350^0C for 4 hours. 60% HPW/MCM-41 provided the greatest conversion of acetic anhydride at 99.2% with 99.5% yield for para-methoxyacetophenone (p-MAP) having 0.5% yield for ortho-methoxyacetophenone(o-MAP). The recyclability was obtained from using the 40wt% HPW/MCM-41 showing no significant loss of activity. They were able to recycle the catalyst for about 5 times. There results showed a great advance in HPW support.

In addition to the results of the yield of supports for HPW, we want to know what happens to the reactants as they interact with the catalyst. Khder and et. al [20] proposed a mechanism in **Figure 4** for the acylation of anisole and acetic anhydride being an electrophilic substitution reaction. The Bronsted acid sites of this reaction generate an acylium ion ($R\text{-}CO^+$) from actyling agent. The strength and number of Bronsted acid sites determines the catalytic activity of the reaction. Therefore, an increase in acidic sties means an increase in the yield of the catalyst. In the mechanism the reaction between the acetic anhydride and a Bronsted acid site generates the adsorption of acylium ion on the active site [76, 77]. The final products are obtained by the reaction of anisole with the adsorbed acylium ion. However p-MAP is more selective than the o-MAP products. Steric hindrance can make p-MAP more favored than o-MAP. Moreover, the Bronsted acid sites generate the acylium ion while the Lewis acid site tends toward the p-MAP. The ortho site is more electron deficient due to the strength of the Lewis acid site, which in turn prohibits the attack of the acylium ion to the para position. As a result, the p-MAP has higher selectivity than o-MAP.

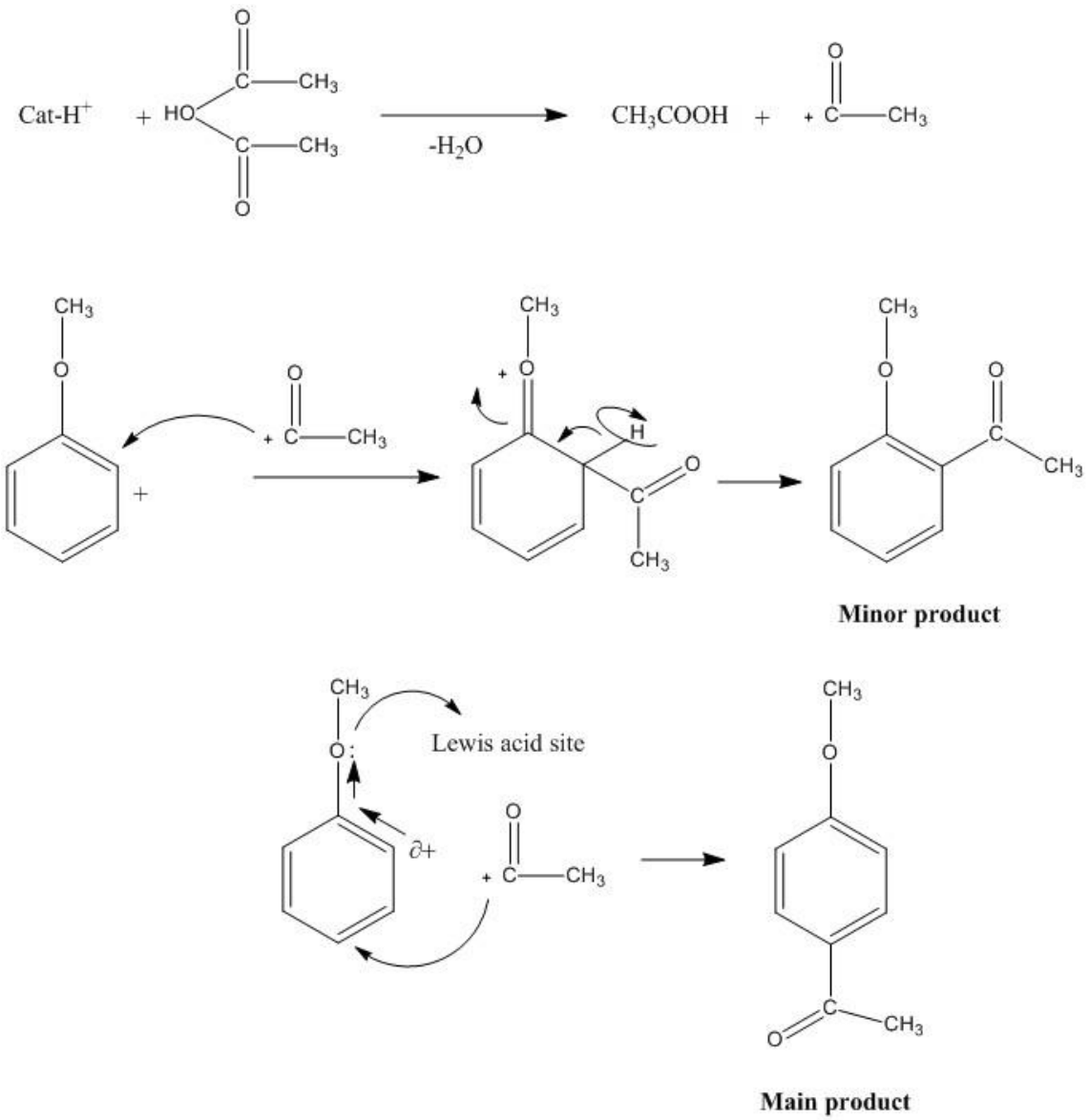

Figure 4. Proposed mechanism of Friedel Crafts Acylation

2.4.4 Pechmann Reaction

Pechmann reaction is an important reaction in organic synthesis to produce substituted coumarins in food industry, cosmetic, and optical brightening agents [78]. Different synthetic routes for coumarins includes Perkin, flash vacuum pyrolysis, Knoevenagel and Reformatsky reactions, Wittig reaction, and Pechmann condensation [79]. The most common route is using Pechmann condensation because it involves using phenol and β-keto ester as the reactants and it gives great yield of coumarins having substitutions in the benzene ring or pyrone or both [80]. Currently the development of a heterogeneous catalyst is being investigated by researchers especially using HPW supported on some types of material to provide a great yield of coumarins.

Khder et.al obtained a great yield for 7-hydroxy-4-methyl coumarin using 60% HPW supported on MCM-41. The reaction was reached by combining 10 mmol of resorcinol and 20 mmol of ethyl acetoacetate with 0.1 g HPW/MCM-41 catalyst at 120^{o}C for 1 hour. Then it was stirred in 10 ml ethanol after the completion of reaction. Ethanol was evaporated as the product is being recrystallized. The maximum catalytic activity is related to the acidity of the surface. They measured that the 60wt% have higher surface acidy compared to the other loadings of HPW [20]. Also, they claimed that using this catalyst showed a higher catalytic activity in a smaller amount of catalyst, lower temperature, and shorter reaction time.

Ghodke et.al reported using zirconia(IV) as a support for phosphotungstate (12-TPA/ZrO_2) using it as a catalyst for Pechmann condensation [80]. The synthesis of ZrPW was obtained using the sol-gel method to get a high ion exchange capacity and protonating ability. The Pechmann condensation reaction was completed by mixing 15mmol methyl acetoacetate (MA) and 10 mmol resorcinol (R) and stirred with the 0.20 g catalyst for 8 hours at 130^{o}C in oil-

bath and microwave irradiation (250W) at 130^{o}C for 30 min. In both cases, the final product became solid after cooling. The result of their catalytic activity using conventional heating is that yield is dependent on the reaction time and the best yield is 8 hours. Also, the catalytic yield increases when more catalyst is added in the reaction because the number of active sites increases also in the catalyst. The conventional heating gave the best yield at 58.12% while the microwave gave 61.82%. Although it is promising to use zirconia as a support, its yield doesn't exceed the yields of other types of support.

Also, a possible mechanism is presented by Ghodke et. al for the Pechmann condensation reaction as shown in **Figure 5**[80]. It shows that this process goes through transesterification which is continued by intramolecular hydroalkylation and dehydration reactions [80]. Furthermore, other researchers such as Sudha and et. al described the carbonyl group on ethyl acetoacetate involves the chemisorption on the Bronsted acids sites of the catalyst and the nucleophilic attack of resorcinol in order to form the 7-hydroxy-4-methyl coumarin[81]. Therefore, it is significant to design catalysts having more acidic sites in order to enhance their catalytic activity.

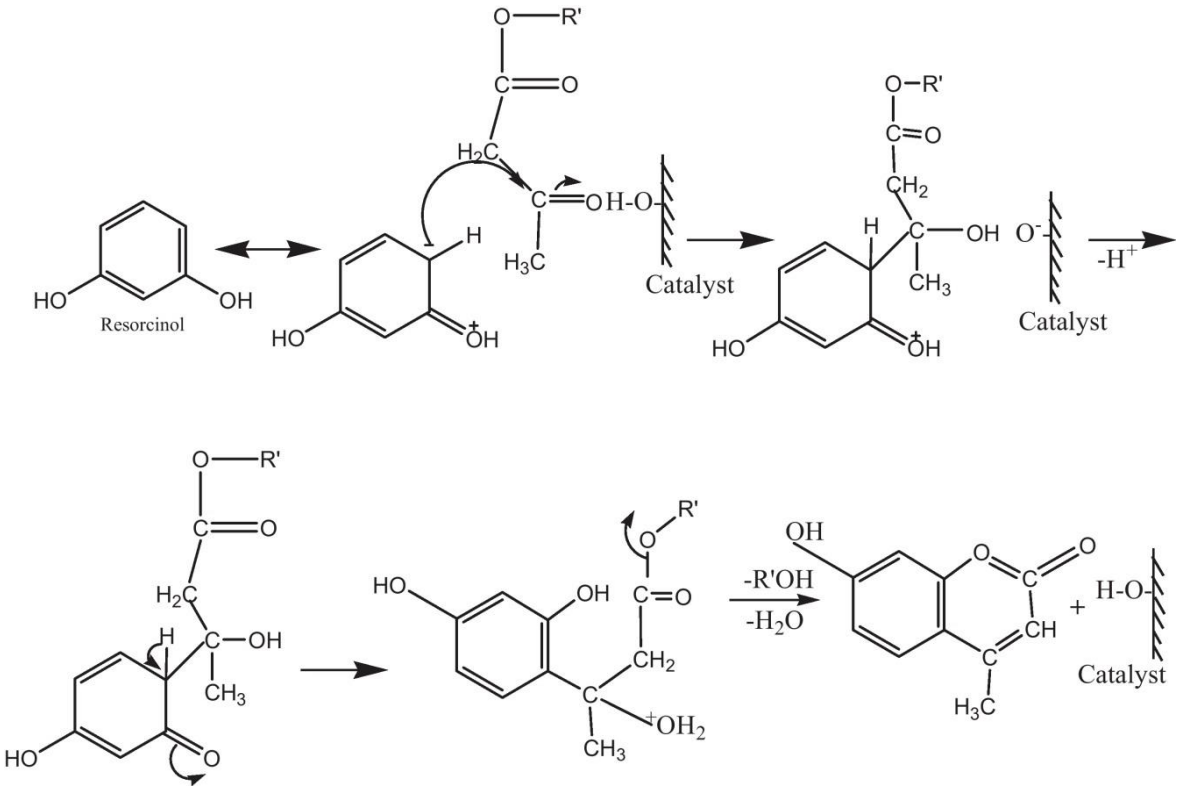

Figure 5. Possible mechanism for Pechmann Condensation

2.4 Graphene

2.2.1 Overview

The first successful extraction of graphene sheets was reported by Geim and Novoselov in 2004. They showed the mechanical exfoliation or repeated peeling of bulk graphite yields to the one-atom thick, sp^2 hybridized planar graphene sheet. Then, it was transferred into the silicon dioxide in a silicon wafer [82]. The Nobel Prize in Physics recognized the two for their "groundbreaking experiments regarding the two-dimensional graphene"[83]. Since then, scientists have been studying the different properties of graphene in various applications. Furthermore, mechanical exfoliation is a simple method for producing one-atomic thick graphene sheets. However, it is not feasible to produce graphene in a larger scale. Therefore, it is necessary to use another synthetic route for large production, which will be discussed later.

The growth of graphene is emerging quickly as a future carbon-based catalyst. Graphene is considered a building block for all other dimensions of carbons. **Figure 6** shows that graphene can be bound into 0D buckyballs, rolled into 1D nanotubes, and piled up to 3D graphite[36]. Multi-walled and single-walled nanotubes have been studied comprehensively for catalysis, energy and electronic device, drug delivery, and polymer fillers [84]. However, due to the discovery of graphene, scientists have been exploring its valuable applications. The advantages of using carbon based nanomaterials are its electrochemical and mechanical stability, high surface area, and high degree of functionalization [45]. Moreover, graphene is being investigated for different applications such as energy storage and devices, catalysis, sensors, conductive films,

polymer nanocomposites, etc. [85]. Therefore, more study is being conducted with graphene in this field of science.

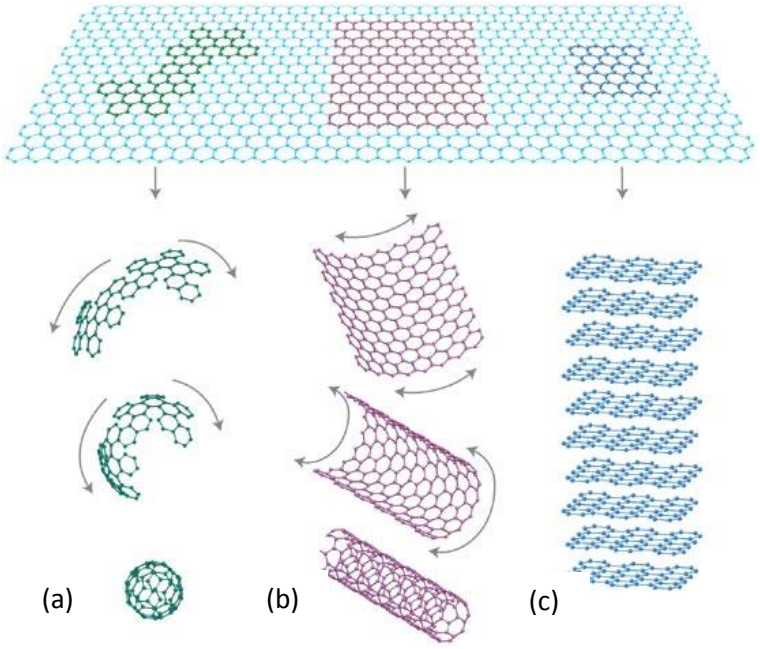

Figure 6. Graphene as a 2D building material for (a) buckyballs (0D) (b) nanotubes (1D) (c) graphite (3D) [36]

2.2.2 Synthetic Routes

There are various routes of synthesis of graphene and they can be categorized into two major classes (a) top-down (b) bottom-up approach. The top-down approach is where graphene is obtained by beginning with macroscopic structures and going into smaller ones. On the other hand, bottom-up begins with atomic scale and building up to reach the desired size. Some examples of top-down approach include pulsed laser deposition, scotch tape stripping, ion

sputtering, and ball milling. Bottom-up approach includes chemical vapor deposition(CVD), pyrolysis, and ion implantation [44, 86].

An alternate synthetic route for mechanical exfoliation in producing graphene sheets from graphite is the usage of chemical methods. The disturbance of the π- π interaction between the sheets is obtained using solvents and then individual sheets are stabilized separately [87]. However, the most prevailing synthetic route for preparing graphene is using GO. This is an example of a top-down approach. This route has been developed by Hummer's and Offeman [88], Staudenmaier [89], and Brodie[90]. GO is produced by the oxidation of graphite using strong oxidation acids. The use of GO as a precursor for producing graphene has several key features. It is hydrophilic; therefore, it can form stable aqueous colloids. Then it can develop into macroscopic structure using different solution processes. Furthermore, graphite as a raw material is very inexpensive using chemical methods with [91].

The Hummer's and Offeman method used in this project is an example of top-down approach where graphene layers were synthesized from bulk graphite. Among the other synthetic routes, this is commonly used because graphite oxide can be made in a larger scale compared to others. Graphene can be obtained from graphite oxide through chemical reduction using reducing agents (i.e. hydrazine, $NaBH_4$, $LiAlH_4$, etc.) [37, 92, 93] via microwave-assisted synthesis, laser-assisted synthesis [39, 94, 95], and thermal exfoliation[96]. This method was used because of it is economical, great yield of product, and reproducible.

El-Shall discusses two methods of synthesis for heterogeneous catalysis on supporting metal nanoparticles on graphene. These methods are mainly laser and microwave synthesis[95].The microwave heating method is advantageous over other methods of heating

because of uniform and rapid heating of the reaction mixture[37, 93, 97]. The rapid heating is due to the solvent and dielectric of reactants. This results in the increase in the internal temperature in the reactants and GO. The hydrazine hydrate has been employed as a reducing agent for GO. Using this method enables better control of the reduction of GO. It is fulfilled by varying either the microwave heating time or power. As a result, reduction of GO is due to the fast deoxygenation and formation of C-C and C=C bonds[93]. Furthermore, laser irradiation in solution has been utilized to facilitate the reduction of GO[39]. The advantage of this method is the elimination of chemical reducing agent. Also, GO in water solution creates a favorable environment for laser irradiation. The time required for the deoxygenation of GO varies from few to several minutes depending on the wavelength of laser either 355nm or 532nm and the concentration of GO in solution. The reduction of graphene is visible by color changes in solution. The change of color of GO from light brown to black suggests deoxygenation. However, when the solution turns to colorless, it indicates that the solution bleached out. The formation of CO_2 gas, water vapor and graphitic powder results in the GO being decomposed[98]. These two methods provides opportunities for concurrent reduction of GO and formation of metal nanoparticles supported on the defect sites obtained in reduced GO. These methods create many opportunities for synthesis of graphene in various different applications.

The other reduction method for GO is thermal annealing [96, 99, 100]. Acik and et. al studied the role of oxygen upon thermal reduction of GO[99]. They have tested the effects of oxygen at annealing temperatures between 60-850ºC using 10^{-4} to 10^{-5} Torr. The exfoliation of graphene sheets occurs by heating GO at high temperatures. The high temperature produces enough pressure to isolate the single layer graphene [101]. It is shown that increasing the annealing time increases the reduction of oxygen which is present in GO. The annealing process

causes a structural damage that happens to the GO due to the release carbon dioxide[102]. Also, there is a loss of mass to the GO by 30% during the process of exfoliation. This gives rise to the topological defects and vacancies found in reduced graphene oxide sheet[103]. The thermal reduction method is very useful in the reduction process of GO to reduce graphene oxide sheets.

2.2.3 Graphene in Catalysis

Graphene is being investigated extensively especially in the field of catalysis. It has attractive properties including large surface area, promising electronic, mechanical, and thermal features which allows it to be used as a substrate for inorganic nanoparticles to generate a highly dispersed composites [43]. There are two types of catalysts that are utilized by graphene which encompasses metal based or metal free graphene. The metals are usually loaded to graphene and use it as a support for catalysis. The metal free graphene is used a catalyst alone or it can be functionalized. Metals[42, 104], metal oxides[39, 94, 105], biomaterial[106-108], small organic compound[109, 110], polymer[111, 112], metal organic frameworks[113, 114], and other carbon materials (i.e. fullerenes or nanotubes)[115-118] are some examples of materials that can be incorporated into graphene.

Scientists are interested in catalysis as one of the applications in graphene research. Metal supported on graphene nanocomposites is one of the topics that have been addressed by researchers. Metals including Pt, Pd, bimetallic, and metal oxides have been published in the literature. Moussa and et. al. have developed a laser reduction method for Pt, Pd, CoO and Pc-CoO nanoparticle catalysts for carbon monoxide oxidation [39]. This method presented the deposition of the different loadings of the nanoparticles on the surface of the reduced graphene oxide sheets. The catalytic activity of Pd and CoO was found to have increased a considerable

amount compared to the unsupported Pd and CoO. They reported that formation of certain alloy nanoparticles favored the oxidation of CO to CO_2. This study provides evidence that graphene can be used as a support in catalysis. Also, using a support for catalysis increases the results of the reaction.

Furthermore, Seger and et.al investigated the use of graphene as a support for Pt nanoparticles for electrocatalyst in fuel cells [104]. The borohydride reduction of H_2PtCl_6 in suspended GO was used for the deposition of Pt nanoparticles onto graphene sheets. There were three methods they used in order to prepare GO-Pt electrodes. The best method was found to be the deposition of GO-Pt with tetrahydrofuran solution in a carbon Toray paper. It has been observed that the Toray provided a better stability for the GO-Pt film. This setup was used as the electrocatalyst for the anode of the fuel cell, while Pt in carbon black was used as the cathode. The supported in comparison with the unsupported was tested for the Galvanostatic fuel cell. A similar result was found on the open-circuit voltage; however, the voltage varied as the current was obtained from the cell. The maximum power for a supported Pt is 161 mW/cm^2 while the unsupported is 96 mW/cm^2. Although the deposition of Pt-GO composited into the electrodes was quite complex, this result provides a window for more exploration of graphene sheets used as support for electrocatalyst in fuel cells.

Another important application for using graphene as a support for catalysis is the catalytic production of liquid hydrocarbons from synthesis of gas. Moussa et. al developed iron-based nanoparticles supported on graphene for Fischer-Tropsh synthesis[41]. The goal of this work is to design a catalyst that enhances the selectivity for long-chain hydrocarbons and low methane production. They have synthesized Fe-K and Fe-Mn nanoparticles via impregnation method and microwave irradiation with further reduction using thermal furnace. The results

indicated that these catalysts showed a great selectivity and activity for C_8 and greater hydrocarbons. The Fe-K supported on graphene was compared to support using carbon nanotubes and found that one using graphene had the probability for forming carbon dioxide and methane gas. The catalytic activity presented here might be due to the uniform dispersion of the iron nanoparticles over the support and the defect sites on the graphene sheet to help hold the nanoparticles. However, more work is required to understand the interaction of the nanoparticles with the defect sites in the graphene sheets.

In addition to metal supported on graphene sheets for electrocatalyst in fuel cells, metal oxides are supported on graphene for photocatalysis applications. Xu et. al investigated the photocatalytic activity of ZnO/graphene composite [105]. Designing an environmental heterogeneous photocatalyst provides a way to convert photon energy to chemical energy [119]. The method they used for making the composites requires the coating of ZnO into GO. The chemical reduction using hydrazine was utilized to convert GO to graphene. The photocatalytic activity was investigated using the degradation of methyl blue under UV light. ZnO/graphene reaction rate constant increased almost five times when compared to pure ZnO. The sample that gave the best photocatalytic activity is 2.0 wt% graphene. A further increase in the loadings of graphene resulted in a decrease of catalytic activity due to increase absorbance and scattering of photons in the photosystem. This work shows how using graphene as a support increases catalytic activity.

Also, gold nanoparticles and graphene hybrids are used as a catalyst for Suzuki reaction. Li and et.al successfully modified graphene with gold nanoparticles[120]. The synthetic route involves the reduction of chlorauric acid in sodium dodecyl sulfate. This was used as both a surfactant and reducing agent. The Au-graphene hybrids were found to be stable in suspension

with water for months. This was tested for the Suzuki reaction of iodobenzene and phenylboronic acid. This reaction facilitates the formation of C-C bond of biaryls. The results show that the conversion of 8wt% Au-graphene is 76.5% and selectivity of 85.8%. The gold size for this is about 2-3nm. Also, 21wt% Au-graphene shows 59.8% conversion having 11.2% selectivity. The gold size for this is approximately 7.5nm. The smaller size of gold attributes to more catalytic sites available for catalysis. Therefore, control of the size is very crucial in the catalytic activity.

Although there is much more research on metal based graphene, the work on metal free graphene is a good possibility for other types of applications in catalysis. Zhang et. al explored the synthesis of amino-functionalized graphene for oxidation reduction reaction(ORR) for fuel cells[46]. The way to functionalized graphene with a nitrogen containing group is by using a one-pot solvothermal method using GO and ammonia. **Figure 7** shows where the nitrogen can be doped into the graphene structure. The three locations where nitrogen functionalization occurs is either pyridinic, graphitic, and pyrollic. The pyridinic nitrogen is at the edge of the graphene plane, graphitic nitrogen replaces the carbon in the graphene structure, and pyrrolic nitrogen is in between two carbon atoms[121]. Each type of nitrogen in the graphene structure contributes to the different aspects of the ORR catalysis. The total amount of nitrogen in their work is 10.6% (atom%). The amino and graphitic types are responsible for the electron transfer number and potential. Furthermore, the graphitic and pyrrolic is used in increasing the current density in ORR.

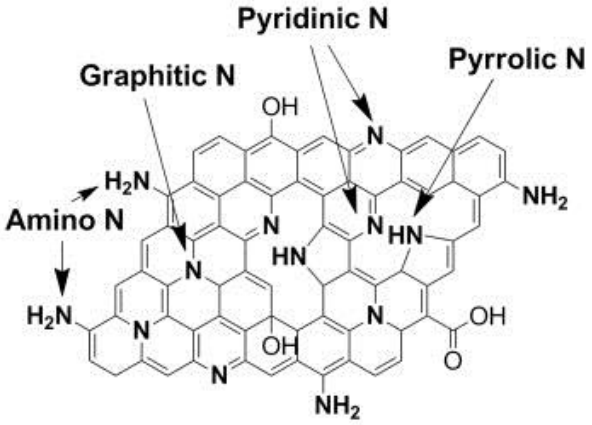

Figure 7. The various nitrogen atoms doped in the graphene structure such as graphitic, pyridinic, pyrollic, and amino groups[46].

Moreover, another application for metal free graphene catalysis is the sulfonation of graphene. A work done by Ji and et.al demonstrates its application as a solid catalyst[47]. This is used in acid catalyzed reaction for the hydrolysis of ethyl acetate.

Figure 8 shows the sulfonation of graphene. The synthesis involves using sulfonic aryl radicals and anchoring it to the surface of the reduced graphene. They also noted that most solid catalysts are unstable in water because of water poisoning acid sites. However, the sulfonated graphene has desirable stability in water. This is shown in the results of hydrolysis rates and repeatability. There result shows that this solid catalyst can has a hydrolysis rate of an average 64.0% and using it for five reactions. This catalyst activity was compared to the Nafion NR50 and it surpasses its hydrolysis rate. The high catalytic activity is due to its high acid exchange capacity and it has a number of active sites available for catalysis.

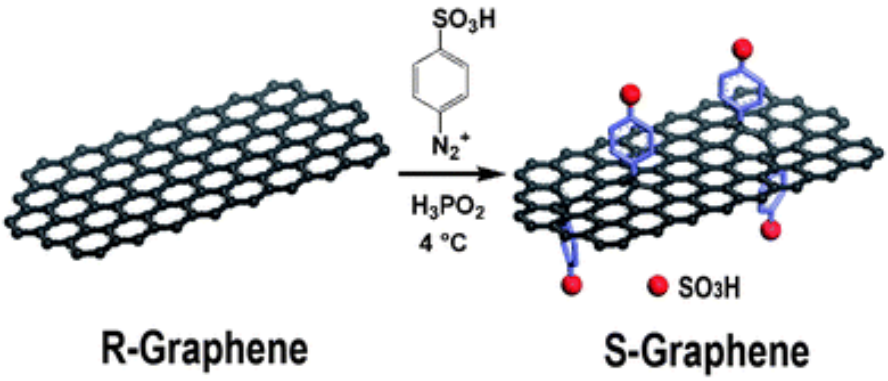

Figure 8. Sulfonation of Graphene[47]

CHAPTER 3

3. Experimental

3.1 Overview

The primary preparation of the HPW-GO catalyst is the synthesis of GO followed by the loading of HPW into GO. Then the catalyst undergoes laser or microwave irradiation. Several characterization techniques such as XRD, XPS, UV-Vis, FTIR, Raman, TEM, and potentiometric titration are utilized to check the successful loadings of HPW on the GO and partially reduced GO. Then, the application for acid catalyzed reactions was tested for three acid-catalyzed reactions: Esterification, Friedel Crafts acylation, and Pechmann Condensation. GC-MS was utilized to check the selectivity, conversion, and recyclability of the catalysts. **Figure 9** shows an overview of the entire project.

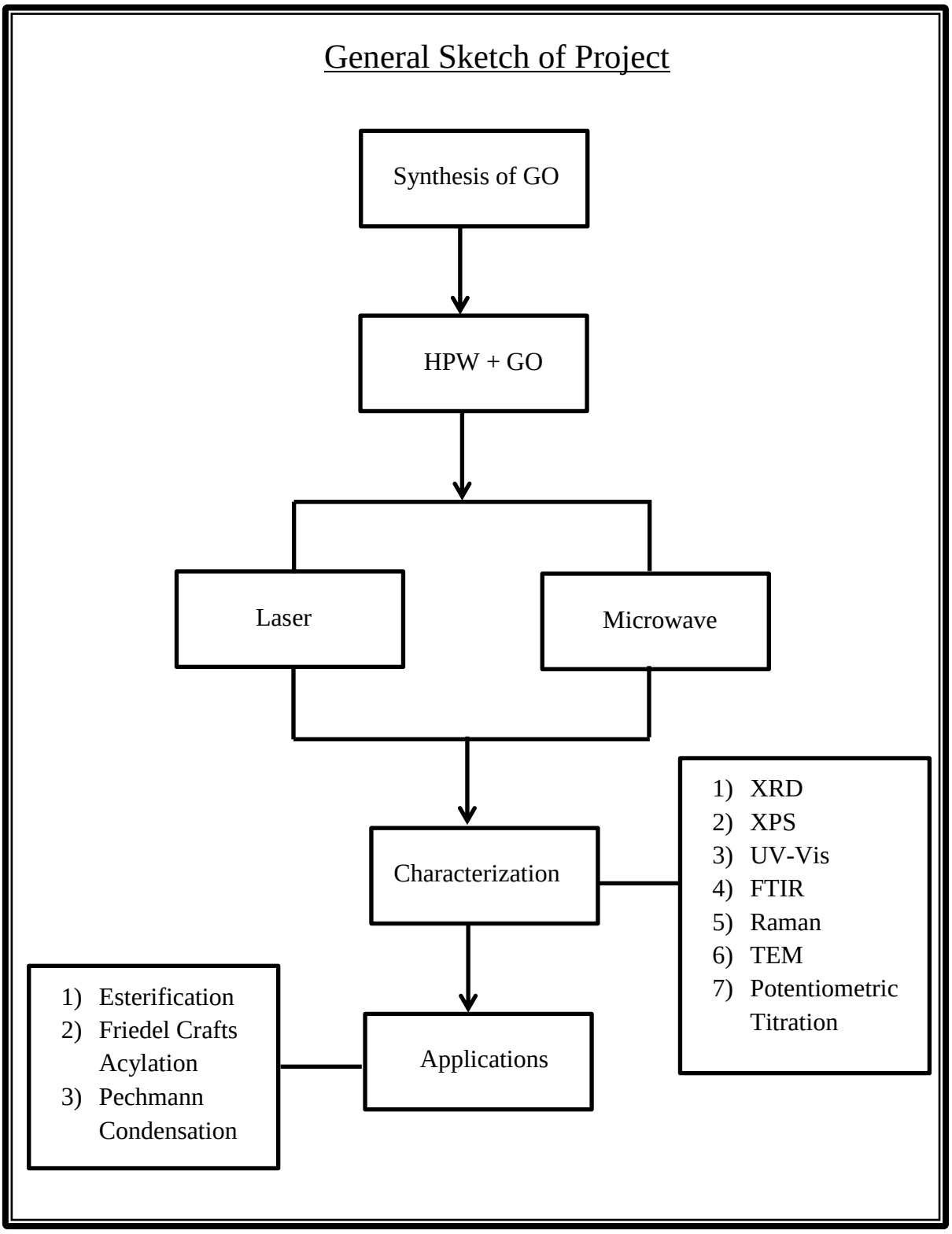

Figure 9. A General Sketch of the Project

3.2 Materials

3.2.1 Graphite Oxide Preparation

The graphite powder was purchased from Alfa Aesar (www.alfa.com, stock # 14734, Ward Hill, MA) having 200 mesh and 99.9999% (metal basis) purity. Sulfuric acid was purchased from Fischer Scientific (www.fishersci.com, Pittsburg, PA). The Sodium Nitrate was purchased from Sigma Aldrich (www.sigmaaldrich.com, product #S5506, St. Louis, MO). The potassium permanganate was purchased from J.T Baker (www.avantormaterials.com, product #3227-01, Center Valley, PA). The hydrogen peroxide was purchased from VWR (www.us.vwr.com, catalog #AAAL14000-AP, Philadelphia, PA).

3.2.2 Heteropoly Tungstophosphoric Acid

The phosphotungstic acid hydrate shown in **Figure 10** was purchased from Sigma-Aldrich (www.sigmaaldrich.com, product # P4006, St. Louis, MO). It has a molecular weight of 2880.5 g/mol measured by anhydrous basis.

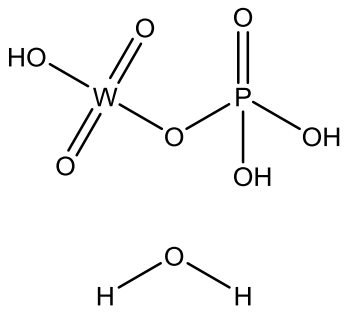

Figure 10. Phosphotungstic acid hydrate

3.2.3 Esterification

The acetic acid was purchased from Mallinckrodt Baker (www.mbigloballabcatalog.com, product #9515, St. Louis, MO). The 1-octanol was purchased from Sigma-Aldrich (www.sigmaaldrich.com, product # 95446, St. Louis, MO).

3.2.4 Friedel-Crafts Acylation

The anisole was purchased from Acros Organics (www.acros.com, CAS #100-66-3, Morris Plains, NJ). The acetic anhydride was purchased from Sigma Aldrich (www.sigmaaldrich.com, product # 320102, St. Louis, MO).

3.2.5 Pechmann Condensation

The resorcinol was purchased from Sigma Aldrich (www.sigmaaldrich.com, product # 398047, St. Louis, MO). The ethyl acetoacetate was purchased from Sigma Aldrich Aldrich (www.sigmaaldrich.com, product # 00410, St. Louis, MO).

3.3 Preparation of Graphite Oxide

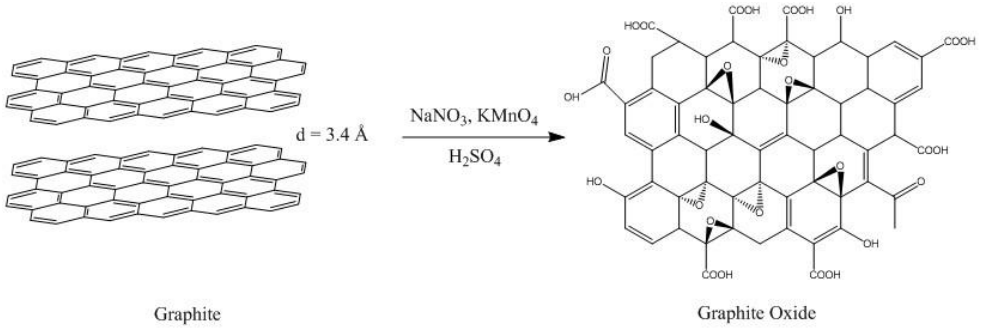

Figure 11. The Synthesis of Graphite to Graphite Oxide

The Hummer and Offeman method was used to synthesized GO from graphite powder [88]. The H_2SO_4 was cooled in an ice bath until it reached 0ºC. A 2.5 g $NaNO_3$ was grinded and mixed into the solution for 15 minutes. Then, 4.5 g of graphite powder was added to the mixture and it was stirred for 20 minutes. It followed the careful addition of the 15.0 g $KMnO_4$ crystals and stirred for 15 minutes. Then, the solution was heated for 3 hours at 35ºC. 230.0 mL deionized water was added into the mixture and stirred for 20 minutes. Then, 700.0 mL deionized water at 80ºC was added. After 20 minutes 20.0 mL of 10 wt% H_2O_2 was added into the mixture. Finally, the yellowish brown cake was washed, filtered and dried overnight at 60ºC **Figure 12** shows the synthesized GO.

Figure 12. Graphite Oxide

3.4 Preparation of HPW-GO Catalysts

3.4.1 Laser Synthesis

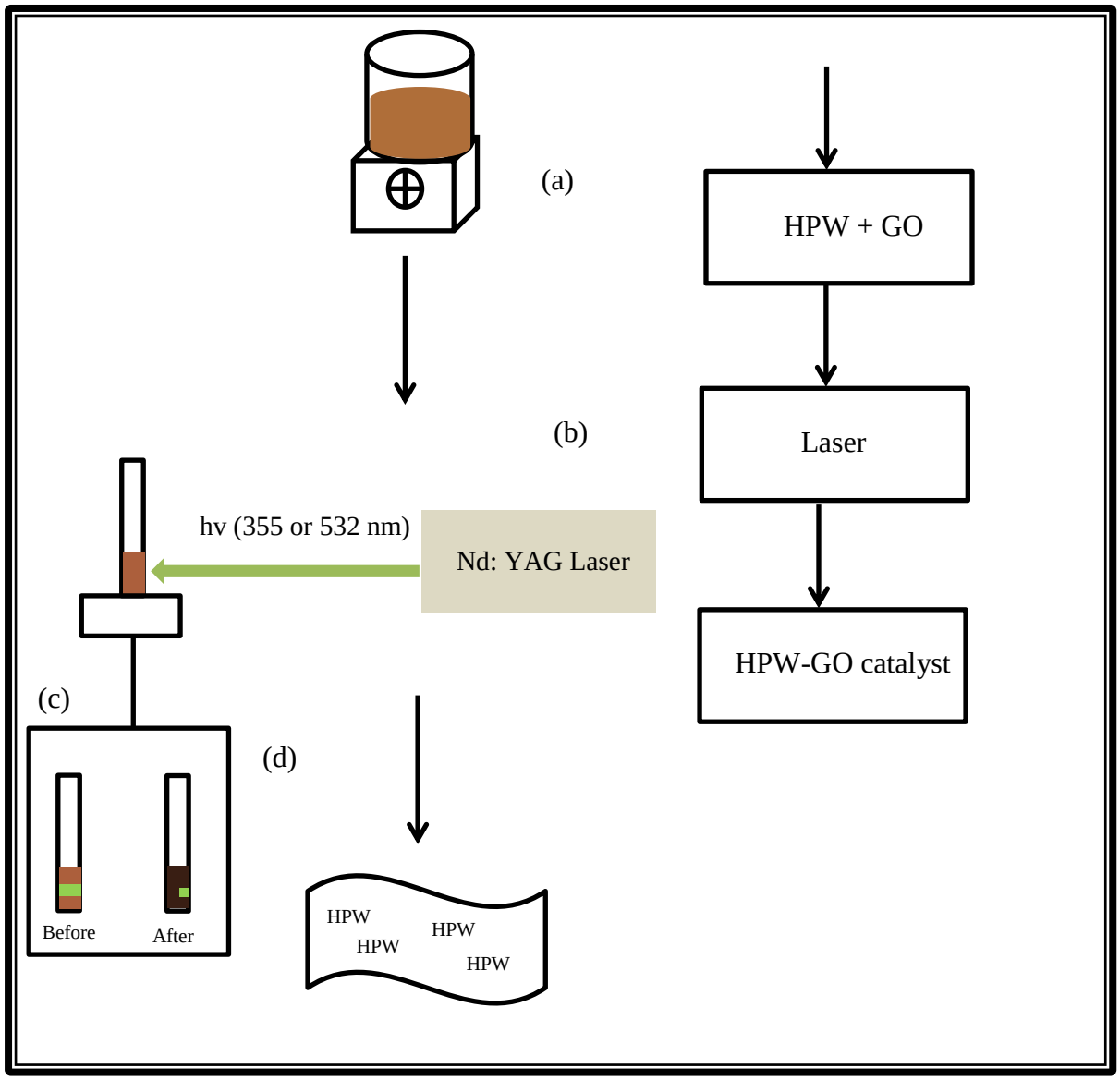

Figure 13. Laser Irradiation Diagram. (a) impregnation of HPW into GO (b) Laser setup (c) before laser irradiation of HPW-GO catalyst in Nd: YAG laser (d) after the laser irradiation.

A 50.0 mg GO was mixed with 100.0 mL deionized water and the solution were sonicated for 1 hour. Different loadings (wt%) of HPW were stirred in the GO solution for 1 hour (**Figure 13**a). The amount of HPW added was calculated based on **Equation 2**. Then 5.0 mL HPW-GO solution were irradiated by a pulsed Nd:YAG laser (unfocused, 2^{nd} harmonic: λ = 532 nm , 7.0W, hv= 2.32eV, or 3^{rd} harmonic: λ = 355nm, 4.0W, hv = 3.49eV, pulse width τ = 7ns, repetition rate = 30Hz, Spectra Physics LAB-170-30) in a test tube while stirring. The HPW-GO solution shows a dark brown color before laser irradiation and the laser beam deflected by the solution (**Figure 13**c). Then gradually as the time increases, the solution turned into black and the laser beam was absorbed by the solution (**Figure 13**c). The irradiation time for 532 nm is 4 minutes while 355 nm is 9 minutes. The irradiation time was determined based on the darkest color of the solution. In other words, laser irradiation was stopped once the desired color was reached. Otherwise, the solution gradually turns into colorless and the GO bleaches out or is destroyed. Also, the laser irradiation setup is shown in **Figure 13c**. Finally, the solution was dried overnight at 60^{o}C.

$$\text{HPW(wt\%)} = \frac{\text{Amount of HPW(g)}}{\text{Amount of GO (g)+Amount of HPW(g)}} x100 \qquad \textbf{Equation 2}$$

3.4.2 Microwave Synthesis

Varying amounts of GO depending on the HPW added was mixed with 150.0 mL deionized water and the solution were sonicated for 1 hour or until GO is fully dispersed. 0.5 g of HPW was stirred in the different loadings of GO solution for 1 hour. Then the HPW-GO solution was irradiated in a conventional microwave (Avanti Model #MO7191TW, 700W) shown in **Figure 14**. The reaction time is 90 seconds and it is stopped every 30 seconds to prevent spilling inside the microwave. The initial color before microwaving is brown, and once the reaction finishes the color turned to almost black. Then the solution is dried overnight at 60ºC. After drying, the sample is calcinated at 350ºC.

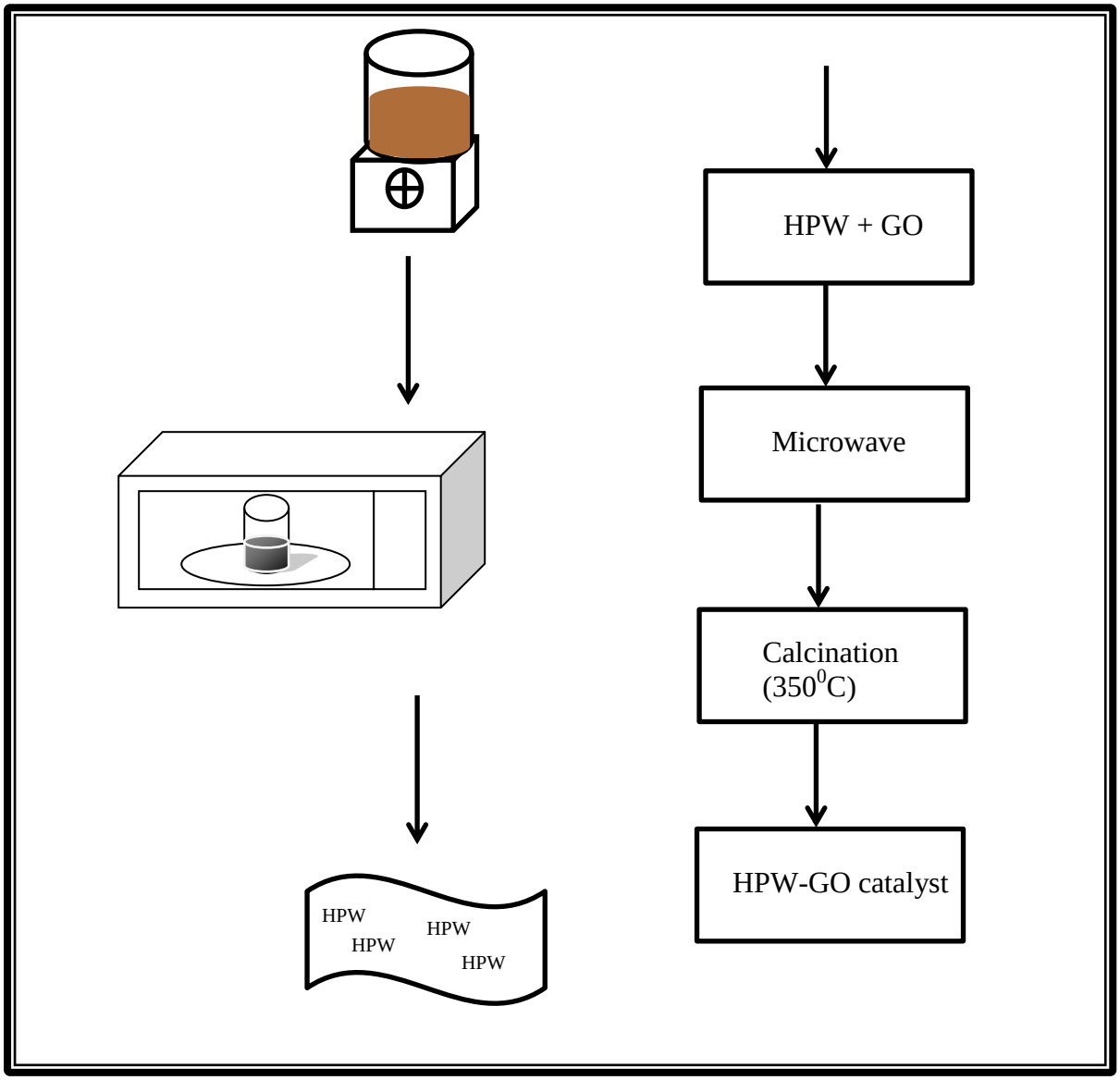

Figure 14. Microwave Irradiation Setup

3.5 Characterization

The UV-Vis spectra were measured using HP Agilent 8453 with single beam diode array. The catalysts were diluted and sonicated in deionized water for the measurement of UV-Vis. The

FTIR spectra were measured with Nicolet-Nexus 670 FTIR with 4 cm^{-1} resolution and 32 scans. The catalysts were mixed with potassium bromide and made into a pellet for FTIR. The Raman spectra were measured by a Thermo Scientific DXR Smart Raman Spectrometer with an excitation wavelength of 532nm. The sample was focused on the laser with a power of 10mW. The samples were placed directly on the Raman. The XRD patterns were measured using an X'Pert Philips Materials Diffractometer with Cu $K_{\alpha 1}$ radiation. The XPS analysis was conducted using Thermo Fischer Scientific ESCALAB 250 with monochromatic Al KR. The TEM was measured using Jeol JEM-1230 TEM equipped with Gatan Ultrascan 4000SP 4K x 4K CCD Camera. The TEM was prepared by one drop of dispersed catalyst in ethanol in the grid. The acidity of the solid samples was investigated using potentiometric titration [122, 123]. 0.05 g of the catalyst was suspended in acetonitrile, and stirred for 3 h. Then it was titrated using 0.05 N n-butylamine in acetonitrile at 0.05 ml/min. The Orion 420 digital A model was used to obtain the electrode potential.

3.6 Catalytic Activity

3.6.1 Esterification Reaction

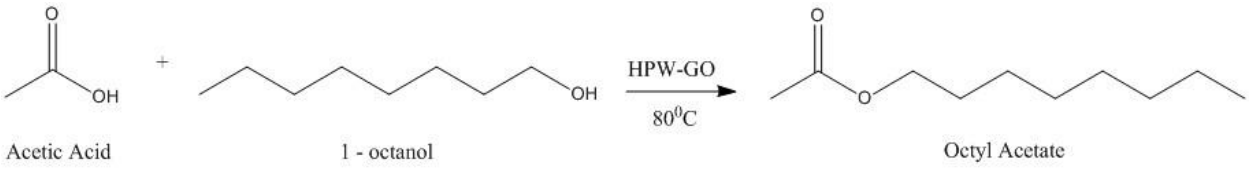

Figure 15. The Esterification Reaction. Acetic Acid and 1-octanol catalyzed by HPW-GO yields to Octyl Acetate.

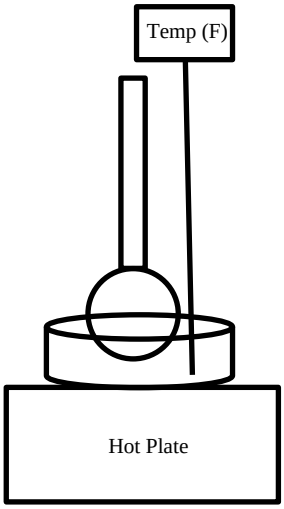

Figure 16. The condensation reaction setup for the acid-catalyzed reactions

Figure 15 shows the chemical reaction for the Esterification reaction using the HPW-GO catalyst. **Figure 16** displays the condensation reaction setup. 0.04 g of the HPW-GO catalyst was added into 10 mmol of acetic acid and 10 mmol of 1-octanol. The solutions were continuously stirred in a round bottom flask at 80ºC under a reflux condenser in an oil bath for 1 h. The product of the reaction were filtered and analyzed by GC-MS (HP G100C Series II) with an Electron Impact Desorption ion source for laser synthesis and GC-MS (Varian Cp-3800 GC coupled with Varian Quadrupole MS) for microwave synthesis. The catalytic activity were calculated using **Equation 3** and **Equation 4**.

$$Conversion(\%) = \frac{(peak\ area\ of\ unreacted\ 1{-}octanol){-}(peak\ area\ of\ reacted\ 1{-}octanol)}{peak\ area\ of\ unreacted\ 1{-}octanol}\ x\ 100$$

Equation 3

$$Selectivity\ (\%) = \frac{peak\ area\ of\ octylacetate}{peak\ area\ of\ octylacetate{+}other\ products}\ x\ 100$$

Equation 4

3.6.2 Friedel-Crafts Acylation

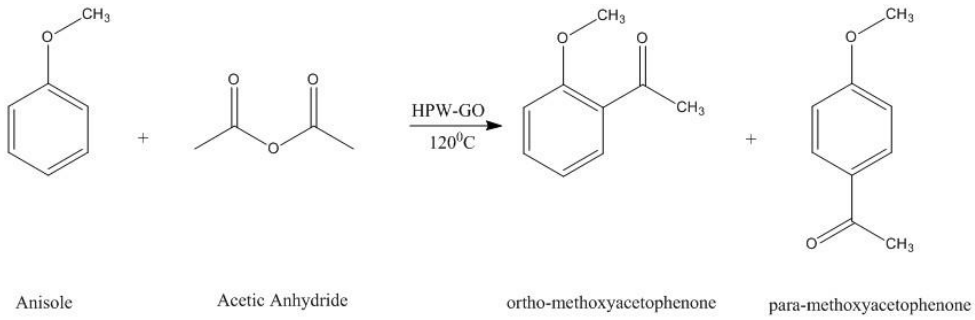

Figure 17. The Friedel-Crafts Acylation Reaction. Anisole and Acetic Anhydride yields to ortho-methoxyacetophenone and para-methoxyacetophenone.

The Friedel-Crafts acylation reaction is shown in **Figure 17**. A 0.02 g HPW-GO catalyst was added into 4.0 mmol of anisole and 1.0 mmol of acetic anhydride. The solutions were stirred in a round bottom flask at 120ºC under a reflux condenser in an oil bath for 2 hours. The product of the reaction were filtered and analyzed by GC-MS (HP G100C Series II) with an Electron Impact Desorption ion source for laser synthesis and GC-MS (Varian Cp-3800 GC coupled with Varian Quadrupole MS) for microwave synthesis. The catalytic activity were calculated using **Equation 5** and **Equation 6**.

$$Conversion\ (\%) = \frac{peak\ area\ of\ unreacted\ AA - peak\ area\ of\ reacted\ AA}{peak\ area\ of\ unreacted\ AA}\ x\ 100 \qquad \textbf{Equation 5}$$

$$Selectivity\ (\%) = \frac{peak\ area\ of\ o-and\ p-MAP}{(peak\ area\ of\ o-MAP)+(peak\ area\ of\ p-MAP)}\ x\ 100 \qquad \textbf{Equation 6}$$

3.6.3 Pechmann Reaction

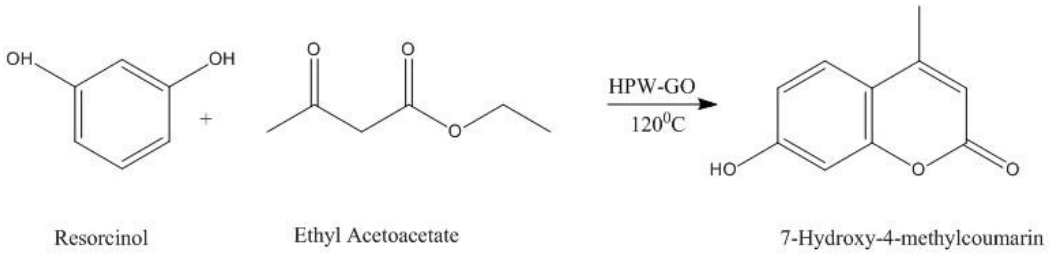

Figure 18. The Pechmann Reaction. Resorcinol and Ethyl Acetoacetate catalyzed by HPW-GO yields to 7-Hydroxy-4-methylcoumarin

Figure 18 shows the Pechmann reaction using the HPW-GO catalyst. 0.02 g catalyst was used in 2.0 mmol resorcinol and 4.0 mmol of ethyl acetoacetate. The solutions were stirred in a round bottom flask at 120ºC under a reflux condenser in an oil bath for 2h. The product sample was analyzed by GC-MS (HP G100C Series II) with an Electron Impact Desorption ion source for laser synthesis and GC-MS (Varian Cp-3800 GC coupled with Varian Quadrupole MS) for microwave synthesis, FTIR, and the melting point. The percent yield was calculated using **Equation 7**. The melting point was measured using the Sigma Aldrich MEL-TEMP capillary melting point apparatus.

$$Yield\ (\%) = \frac{Obtained\ weight\ of\ the\ product}{Theoretical\ Yield\ of\ the\ product}\ x\ 100 \qquad \textbf{Equation 7}$$

CHAPTER 4

4. Characterization of HPW-GO catalysts

This chapter provides the results and discussion of the characterization techniques used for the HPW-GO catalysts that were prepared by both laser and microwave irradiation methods. The characterization of the HPW-GO catalyst was an important aspect of this project to provide evidence of successful loadings of HPW onto the surface of partially reduced GO for the laser method and GO for the microwave method. Here we discuss several characterization techniques since it is insufficient to cover one or two techniques in order to provide evidence for the HPW-GO catalyst. The various techniques that were investigated in this project include XRD (4.1), XPS (4.2), UV-Vis (4.3), FTIR (4.4), Raman (4.5), TEM (4.6), and Potentiometric Titration (4.7). Each technique was used to determine the characteristic feature of GO, HPW, and HPW-GO catalyst as prepared by the two synthesis approach.

4.1 XRD

XRD is an analytical technique that is used for determining specific information about the unit cell dimensions. Also, it is used for the identification of phases in crystalline material. The inner shell electrons of the target material are ejected to produce specific X-ray spectra [124]. **Figure 19**A shows the XRD spectra of GO, HPW, HPW-GO after laser irradiation at 532nm and 355nm. The GO characteristic diffraction peak is observed at $2\theta = 10.9^{o}$. The d-spacing for GO is 8.14Å which is higher compared to the d-spacing of bulk graphite at 3.34Å.

This is the result when the hydroxyl and epoxy groups are inserted in the lateral and terminal sides of the sheets due to the oxidation of graphite [8, 11, 18]. The characteristic peak of HPW is observed at the following 2θ= 9.4º, 11.1º, 18.6 º, 21.4º, 23.9º, and 26.1º. This corresponds to the HPW characteristic peaks reported by Soled et.al [125]. There is an observation of a change from yellow golden color of HPW and GO solution before laser irradiation. Also, the solution turned black after laser irradiation. This is due to the characteristic peak of GO at 2θ = 10.9º disappearance in both the 60wt% HPW-GO catalyst, which suggests the partial reduction of GO and sp^2 carbon sites being restored. In **Figure 19**B, the comparison of GO with Laser Converted Graphene (LCG) is shown. This also shows the disappearance of the characteristic peak of GO at 2θ = 10.9º. This coincides with the results we obtained for the HPW-GO catalysts in **Figure 19**A. Moreover, the two characteristic peaks in the case of 60wt% HPW-GO 532nm occurs at 2θ = 21º and 27.5º. The smaller intensity of both peaks suggests the adsorption of HPW onto the surface as the other peaks for HPW are not present. In addition, the characteristic peaks for HPW-GO 355 nm are more intense compared to the HPW-GO 532 nm. Also, an additional peak is observed at 60wt% HPW-GO 355nm at 2θ = 6º. This might be from HPW peaks at 2θ= 9.4º that shifted to a lower 2θ value. The XRD peaks suggest that there is a good dispersion of HPW adsorbed into the surface of the PRGO. Furthermore, it was observed that there is a slight increase in intensity at HPW-GO irradiated at 355nm which indicates a poor dispersion or agglomeration of the HPW crystals compared to the HPW-GO irradiated at 532nm [20]. Also, HPW is amorphous based on the XRD peaks.

Figure 19C shows the XRD spectra of GO, HPW, HPW-GO after microwave irradiation method. As mentioned previously for laser irradiation method, it was also observed that the characteristics peaks for HPW and GO in the microwave irradiated HPW-GO catalyst. The

major difference with this catalyst as prepared is the presence of the characteristic peak of GO at $2\theta = 10.9^{o}$. This is observed in all the loadings of HPW in GO. However, the characteristic peak of GO is present in all the loadings of the catalysts. This suggests that there is no reduction of GO during microwaving. Also, the HPW is polycrystalline based on the XRD peaks. It was observed that the best loading occurred in 85wt% HPW, while the loadings thereafter decreased gradually. This is the result of the agglomeration of HPW on the surface of GO.

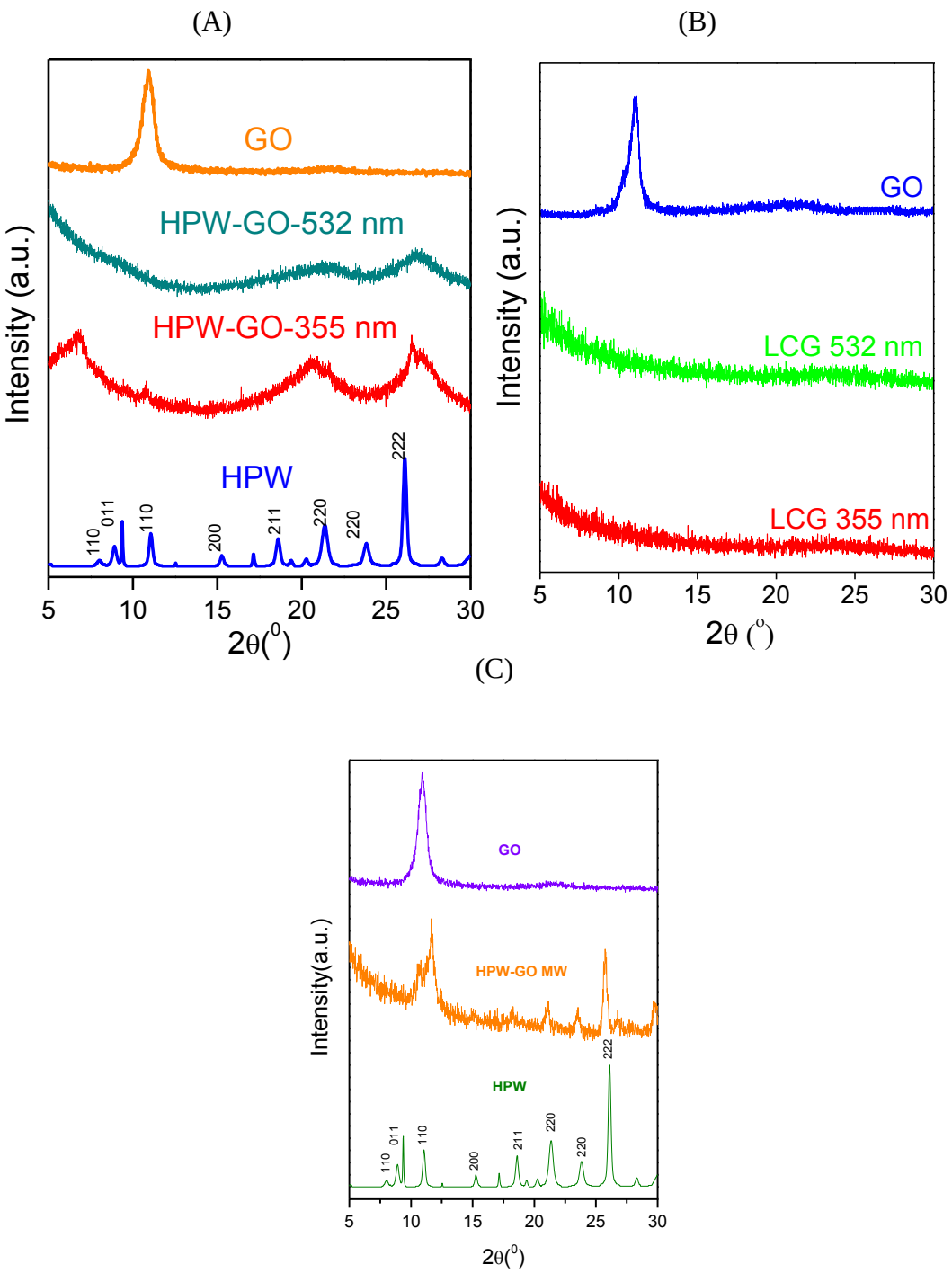

Figure 19. (A) XRD-patterns of GO as compared to of HPW-GO catalysts prepared by 355nm and 532nm irradiation by laser (B) XRD-patterns of GO as compared to partially reduced GO without HPW. (C) XRD-patterns of GO as compared to of HPW-GO catalysts prepared by microwave irradiation.

4.2 XPS

XPS is a common surface analysis technique due to its simple functionalities and data interpretation. It provides analysis on elemental composition by measuring the photoelectron energy that is emitted from the surface of the material[126]. This technique gives us information on the partially reduced GO and the HPW. **Figure 20**a shows the carbon 1s spectra of GO and compares it with the spectra of HPW-GO at 532 and 355nm. The oxygen containing groups shown in the GO spectrum are between 285.5 and 289eV. Also, it shows that the sp^2 bonded carbon C=C is at 284.5eV. The binding energies 285.6, 286.7, 287.7, and 289eV correspond to the carbon 1s of the C-OH, C-O, C=O, HO-C=O groups [39, 97, 98, 127]. The C-O and C=O intensity for HPW-GO decrease compared to GO due to the laser irradiation, which eliminates the oxygen group from the carbon partially. In other words, the moderate peak intensity shows that GO was partially reduced. **Figure 20**b presents the C1s spectra of GO in comparison to the Laser Converted Graphene (LCG). The increase of the sp^2 bonded carbon C=C at 284.5eV means decrease or the disappearance of the oxygen containing groups at 287.7eV. Furthermore, **Figure 20**c demonstrates the Tungsten 4f region of HPW-GO catalysts. The spin-orbit doublet $4f_{7/2}$ and $4f_{5/2}$ is located at 35.8 and 38.0eV [128] for both of the catalysts. **Figure 20**d presents the Phosphorus 2p region at 133 eV for both catalysts is unchanged. This reveals that the oxidation state of phosphorus is constant [129].The XPS results provide evidence the nature of GO after laser irradiation and the loading of HPW on the surface of PRGO.

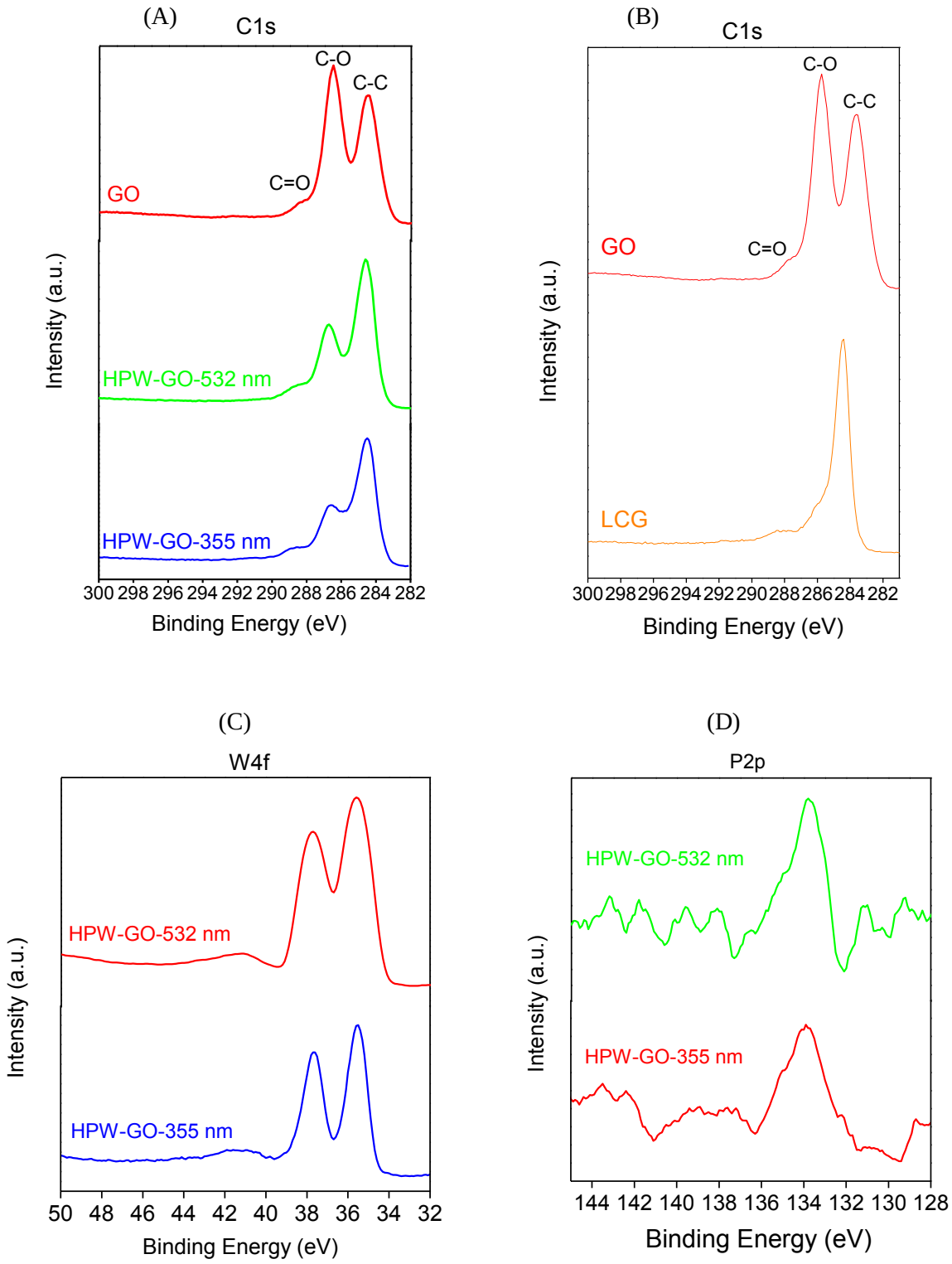

Figure 20. XPS of (a) C1s binding energies of GO compared to the HPW-GO catalysts as prepared by laser irradiation method. (b) C1s binding energies of GO compared to LCG (c) W4f (d) P2p of HPW-GO catalysts as prepared by laser irradiation method.

4.3 UV-Vis

UV-Vis spectroscopy provides the absorption of molecules by either UV or visible radiation at corresponding wavelength. Such absorption relates to the excitation of the outer electrons of the molecules. **Figure 21**A shows the absorption spectra of GO in comparison to LCG at 532nm and 355nm . The UV-Vis spectrum of GO shows two bands: 231 nm and 305 nm. The 231 nm band corresponds to the electronic transition $\pi \rightarrow \pi^*$. Moreover, the shoulder peak at 305 nm relates to $n \rightarrow \pi^*$ transition of C=O bonds [130]. Also, the peak at 305nm disappears after the laser irradiation and the peak at 231nm red shifts to about 270nm. **Figure 21**B demonstrates the spectra of GO in comparison to the HPW-GO catalysts. The characteristic band for HPW can be seen at 265 nm which is attributed to the charge transfer band of $[PW_{12}O_{40}]^{3-}$ heteropolyanion[131]. However, the characteristic band observed is at 269 nm, which is slightly higher that might be due to the HPW crystals used. The HPW-GO catalyst shows a characteristic band at 265 nm for 532 nm and 267 nm for 355 nm. Furthermore, the GO shoulder peak is no longer present. A red shift occurred for the 231nm peak of GO around 270nm after laser irradiation because the electronic conjugation restored in graphene as reported by Abdelsayed and et. al [98]. However, the red shift of 231nm peak of GO and the presence of the charge transfer band occurs at the same wavelength. Therefore, it can be predicted that the only peak that was observed for both the HPW-GO catalysts corresponds to accumulation of both peaks. Furthermore, **Figure 21**C shows the spectra for GO compared to all the loadings of HPW-GO catalysts as prepared by microwave irradiation. The characteristic band for HPW was observed at 269nm. This result is similar to the results for laser irradiation. The HPW-GO catalysts at different loadings of HPW show characteristic bands between 265-269 nm.

(A)

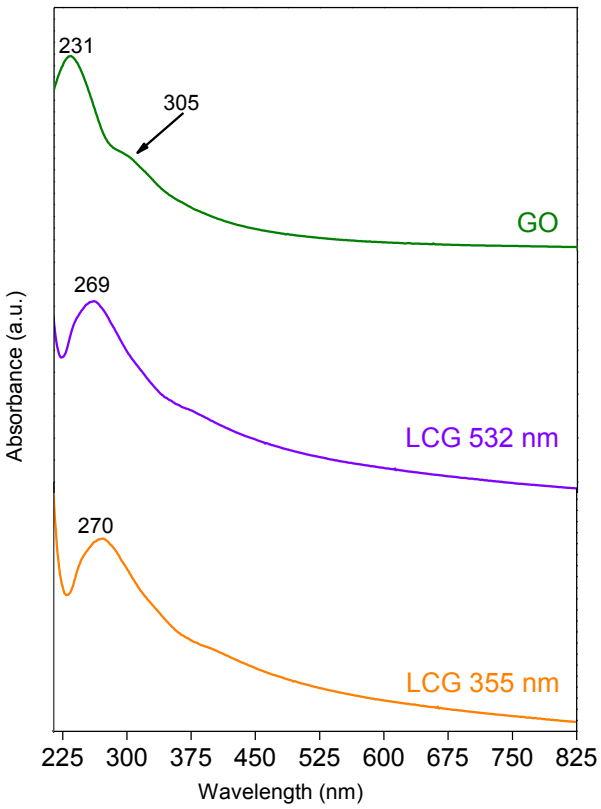

(B)

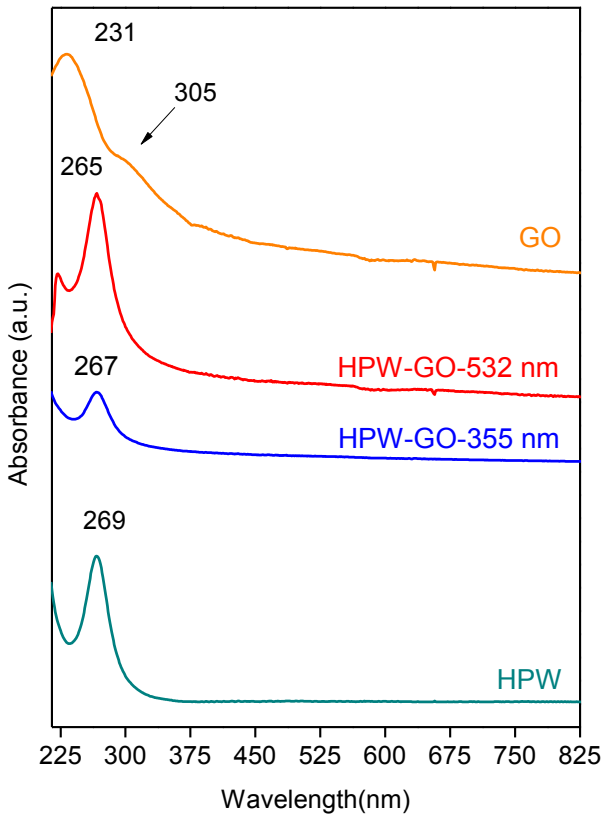

(C)

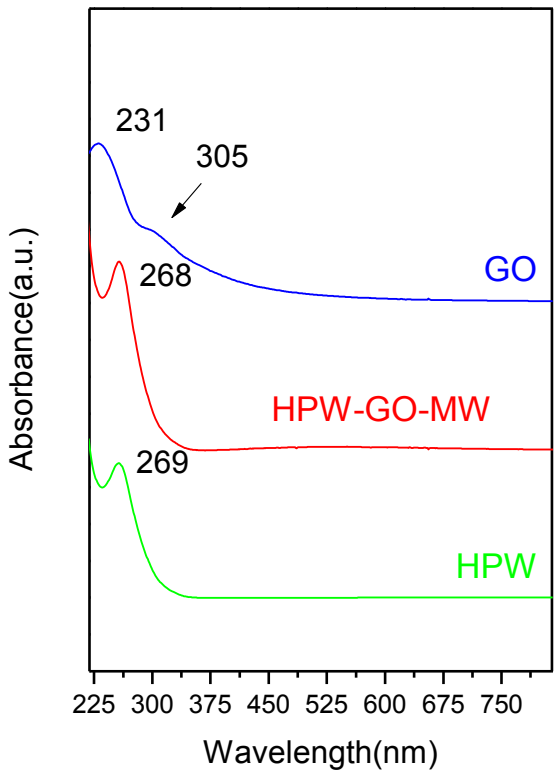

Figure 21. UV-Vis of (A) GO in comparison to the LCG at 355nm and 532nm. (B) GO in comparison to the HPW-GO catalysts as prepared by laser irradiation (C) GO in comparison to the HPW-GO catalysts as prepared by microwave irradiation.

4.4 FTIR

FTIR is used to determine the functional groups expected for HPW-GO catalysts. It utilizes infrared light correlation with specific characteristic absorption of the molecules. The absorption of light by molecules at specific wavelengths results in a change in its dipole moment[132]. Therefore, it produces a vibrational spectrum for functional groups within the molecule that has dipoles. The FTIR spectra of the HPW-GO catalyst in comparison to GO and bulk HPW are shown in **Figure 22** for both preparation methods. **Figure 22**A gives the comparison of GO and LCG. It is observed that the increase in intensity of sp^2 bonded carbon C=C bonds and the decrease of the carboxylic peak C=O. **Figure 22**B shows the spectral data of GO in comparison to bulk HPW and the HPW-GO catalyst as prepared by laser irradiation. FTIR provides with the validation of the presence of the Keggin anion on the surface of the PRGO and its structural integrity at the molecular level. The $PW_{12}O_{40}^{3-}$Keggin anion has a full tetrahedral symmetry where the tungsten atoms are connected by oxygen atoms and phosphorus in its center [133, 134]. The fingerprint region in the IR spectra occurs between 1100 and 500 cm^{-1} and corresponds to the various bands of the bulk HPW. The characteristic bands for HPW are 1081, 982, 889, 797, and 595 cm^{-1}. These bands represent the stretching vibrations of P-O_a, W=O_t, W-O_c-W, W-O_e-W and the bending vibration of P-O [20]. The subscripts a, c, e, and t represents the specific positions: internal, corner, edge-shared, and terminal [19]. The specific positions are labeled in the figure. Furthermore, the peak at 1610 cm^{-1} corresponds to the OH group on the Keggin structure. The characteristic band for GO occurs at 1740 cm^{-1} which is the C=O stretching vibrations for the COOH groups. There is a deformation on the group O-H at 1350-1390 cm^{-1}. Also, the epoxide groups at around 1230 cm^{-1} and the C-O stretching vibrations

occurs at 1060-1100cm^{-1}[135, 136].On the other hand, the characteristic band for PRGO transpires at 1680 cm^{-1}, which represents the aromatic C=C bond [94]. As shown in the figure, the aromatic C=C peak intensity increases in comparison with the C=O peak. Also, HPW-GO catalysts show the presence of HPW on its surface. **Figure 22**C shows the spectra of GO in comparison to HPW-GO catalysts as prepared by microwave irradiation. Furthermore, the characteristic bands for HPW are present in the fingerprint region of the spectra for HPW-GO catalysts. The characteristic bands of the HPW at lower loadings have lower intensity compared to the higher loadings. In other words, the intensity of HPW characteristic bands indicates the amount of dispersion on the surface.

(A)

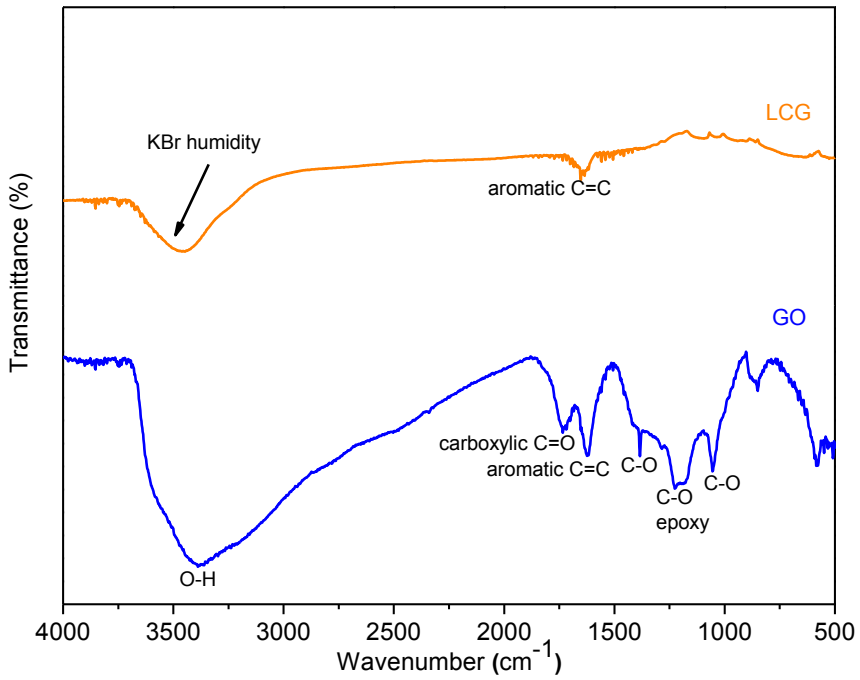

(B)

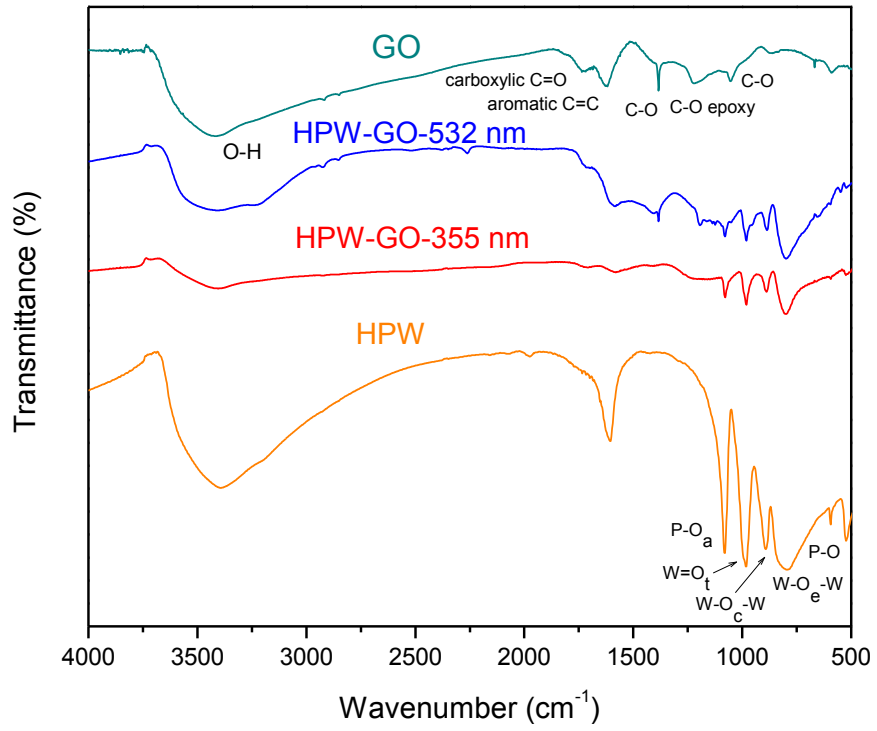

(C)

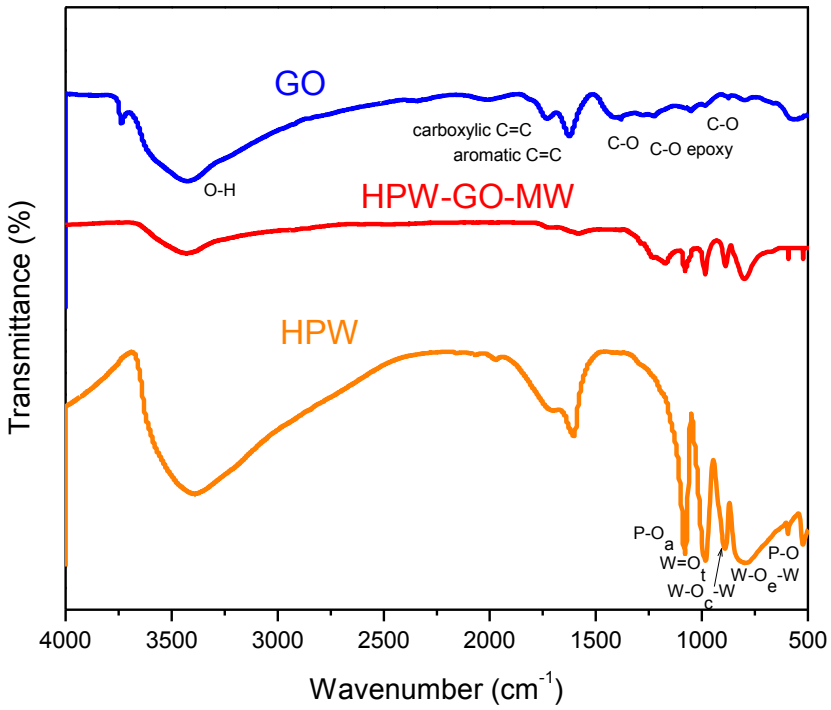

Figure 22. FTIR Spectra of (A) GO in comparison to LCG. (B) HPW-GO catalysts as compared to GO and bulk HPW as prepared by laser irradiation (C) HPW-GO catalysts in comparison to GO and bulk HPW as prepared by microwave irradiation.

4.5 Raman

Raman Spectroscopy is an analytical technique to determine the electronic and structural properties of graphene such as doping levels, defect density, and disorder in its structure[137, 138]. There are three main characteristic peaks that can be seen in graphene which are D,G, and

2D bands. The D band is considered the defect or disorder band. Graphene has some atomic defects in each layer, and stacking defects between two layers[139]. In other words, this peak determines the defects in a material. This disorder induced band occurs at ~1350 cm^{-1}. Also, the G band is the principal mode in graphene. This band is associated with the longitudinal phonon mode which is around 1580 cm^{-1}. This band constitutes the planar configuration of the sp^2 carbon structure which makes it graphene[140]. The G band is due to the emission that occurs at zone-center optical phonons. Also, the other band is a 2D band and is sometimes referred to as the G' band when we refer to the carbon nanotubes. This band is considered the overtone mode and occurs at ~2700 cm^{-1}. Also, the 2D band helps in measuring the layer thickness of the material such as single free layer or bilayer or few layers [137, 138]. **Figure 23**A shows the Raman spectra of HPW-GO-532nm in comparison to GO and bulk HPW. The G band for GO occurs at 1597 cm^{-1}, D band of 1354 cm^{-1}. This corresponds to the peaks reported in the literature[93, 98]. The bulk HPW show bands at 1009, 992, 925 cm^{-1}. These bands correspond to the assymetric and symmetric stretching modes of W=O, which is the terminal oxygen[141]. These characteristic bands for HPW catalyst occur at 1003, 985, 901 cm^{-1}, which is blue-shifted which means that incorporation of HPW to the GO is stable. Furthermore, this result corresponds to what is reported in the literature [64, 142, 143]. The characteristic bands for the HPW-GO catalyst are the G band at 1604 cm^{-1} and D band at 1355 cm^{-1}. The calculation of the intensity ratio of D/G is a indicator of the defect or disorder in a sample[139]. The D/G intensity ratio of GO is 0.97, while the ratio of the HPW-GO catalyst 0.88. This is slightly lower than the ratio of GO. The ratio approaches zero for highly ordered pyrolytic graphite[144]. This results shows a weak disorder induced D-band after laser irradiation of the catalysts. Also, it shows that there is some reduction of the GO because of the decrease of the D/G band ratio. **Figure 23**B

shows the spectra of GO in comparison to HPW-GO catalyst as prepared by microwave irradiation. The D/G intensity ratio of GO is 0.97, while the ratio of the HPW-GO catalyst 0.82. This is slightly lower than the ratio of GO. The ratio approaches zero for highly ordered pyrolytic graphite[144]. This results demonstrates a weak disorder induced D-band after laser irradiation of the catalysts. Both synthesis methods show the characeristic peak of HPW.

(A)

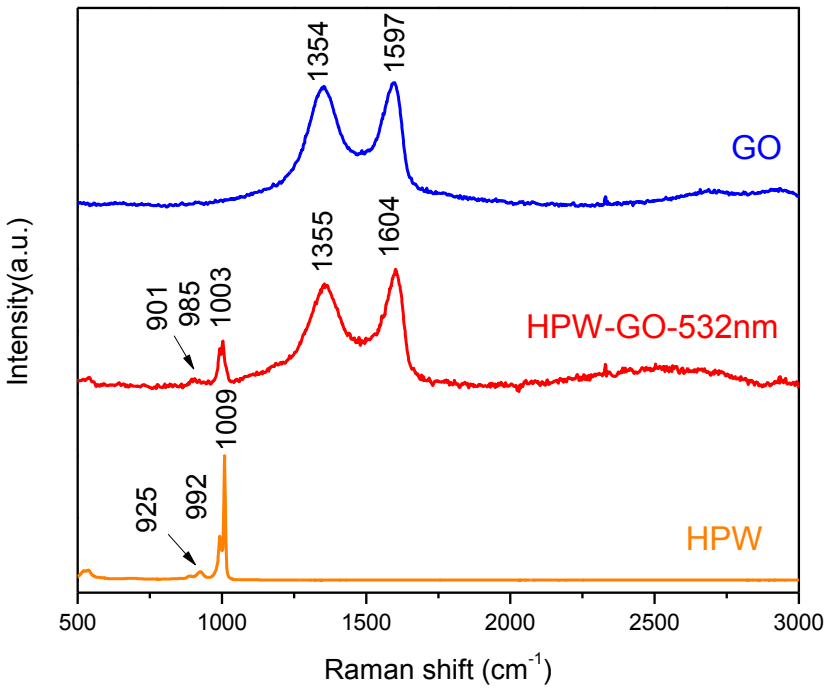

(B)

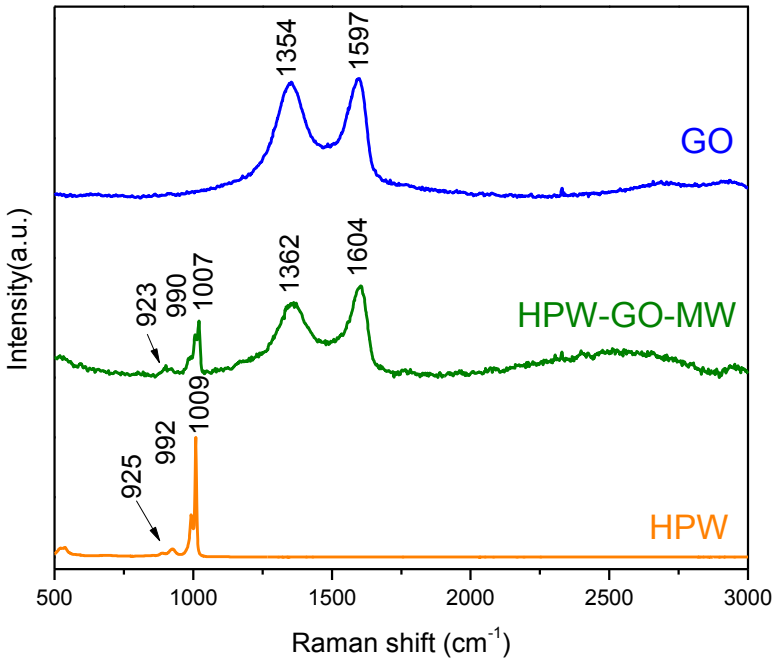

Figure 23. Raman Spectra (A) GO in comparison to HPW-GO catalysts as prepared by laser irradiation (B) GO in comparison to HPW-GO catalyst as prepared by microwave irradiation.

4.6 TEM

TEM is a microscopy technique where electrons beams are emitted through a small scale sample. Then the samples are magnified and an image is captured by a camera. **Figure 24** shows TEM images of Go with different magnifications when compared to HPW-GO 60wt%. The image for GO in **Figure 24**a provides multi-layer in the morphology while **Figure 24**b shows greater magnification of the multi-layer graphene oxide sheets stacked together. The oxidation from graphite to GO affords a way for the extraction of single layer graphene sheets through different reduction techniques. The laser irradiation provides a way for the reduction to happen in the HPW-GO catalyst. **Figure 24**c shows that the surface of the PRGO is loaded with HPW catalyst. This is attributed to the black spheres, which are well-dispersed in the PRGO. **Figure 24**d gives an approximate size of the HPW which is around 10-15nm in diameter. **Figure 24**e provides some creases in the morphology of HPW-GO catalyst while **Figure 24**f shows greater magnification of the multi-layer graphene oxide sheets stacked together. The oxidation from graphite to GO affords a way for the extraction of single layer graphene sheets synthesis. The surface of GO with many vertical creases might be due to the microwave irradiation of GO. Also, it was observed some HPW crystals loaded with the black spheres. This shows a good dispersion of HPW on both surfaces.

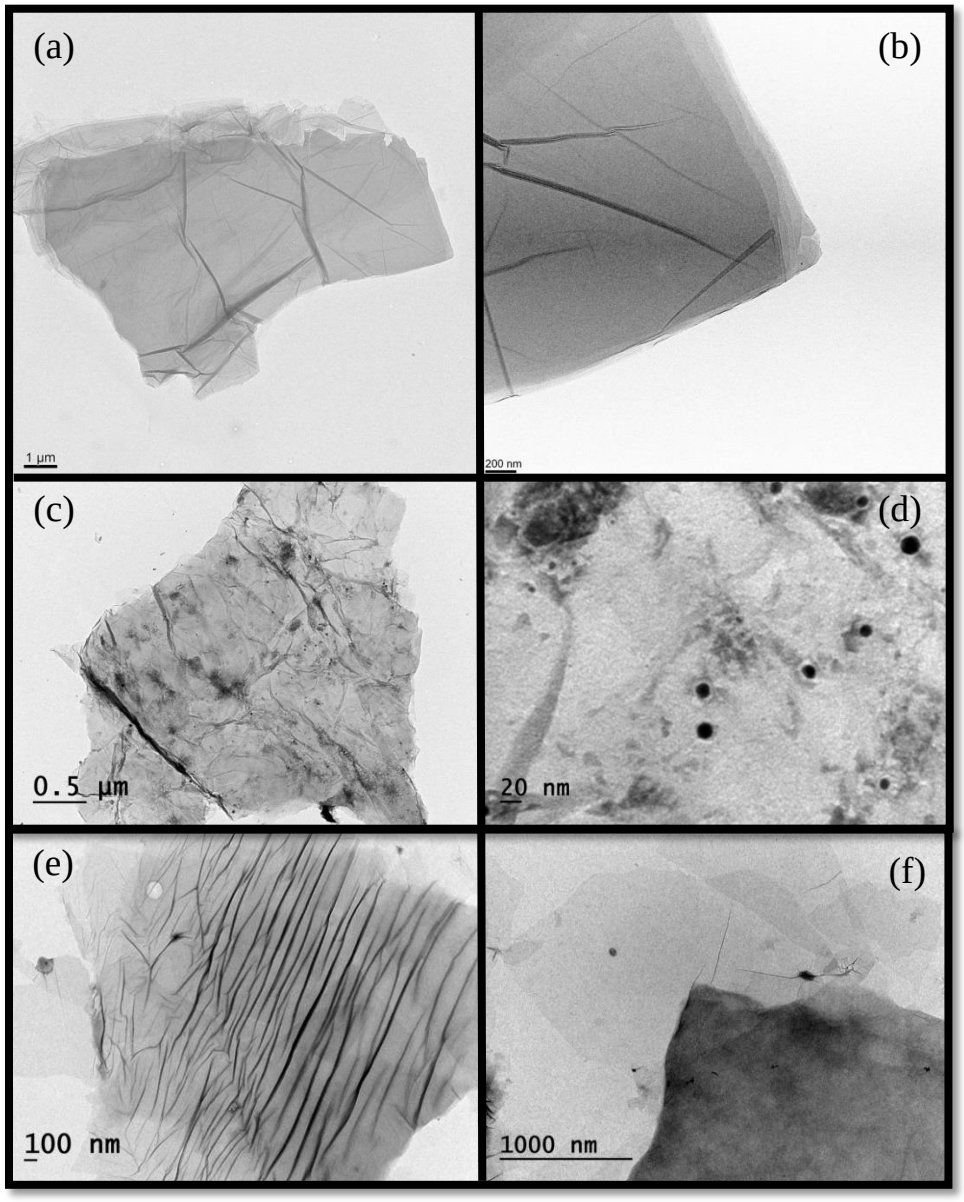

Figure 24. TEM images of (A) GO (a,b) as compared to HPW-GO 60wt% (c,d) as prepared by laser irradiation and (e,f) HPW-GO 85wt% as prepared by microwave irradiation.

4.7 Potentiometric Titration

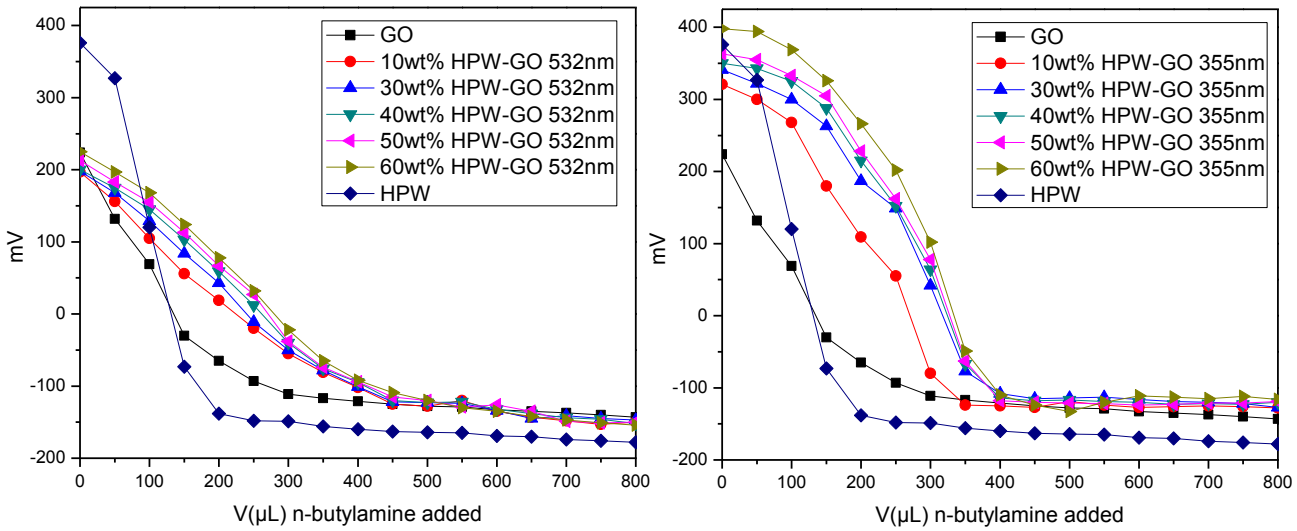

Figure 25. Potentiometric-titration curve as-synthesized (a) 60 %-HPW-GO 532nm and (b) 355 nm compared to both HPW and GO.

Potentiometric titration is used in characterizing the acid strength of the HPW supported on PRGO. The amount of titrant, butylamine, added is measured as a function of millivolts. This method allows to determine the number of acidic sites and their acid strength[145]. The maximum acid strength corresponds to the electrode potential while the total number of acid sites corresponds to the value of mequiv/g solid when the plateau is reached. The following scale has been established to correlate the acidic strength with electrode potential: E>100mV(very strong acid sites), 0<E<100mV(strong sites), -100<E<0mV(weak sites), E<-100mV(very weak acid sites) [69].

Figure 25 shows the titration curves of the HPW-GO catalysts. The different catalysts exhibit electrode potentials between 225-398mV as presented in **Table 2** and **Table 3**, which means that HPW-GO catalysts have very strong acid sites compared to GO and bulk HPW. The basal plane of GO contains some acidic sites that is shown by the results [146]. The number of acidic sites can be calculated using **Equation 3**. A significant increase in the number of acidic sites was observed on the supported HPW which are 2.75 mequiv/g for HPW-GO 532 nm and 3.00 mequiv/g for HPW 355 nm. The acidic sites increases when HPW is well-dispersed at the surface of GO. The increase in acidity is very essential in increasing the yield and conversion of acid-catalyzed organic reactions.

Table 2. The acidic properties of HPW-GO-532nm catalysts

Catalyst	E (mV)	No. of acidic sites (mequiv/g)
GO	224	1.50
10 wt% HPW-GO-532 nm	197	1.25
30 wt% HPW-GO-532 nm	198	1.50
40 wt% HPW-GO-532 nm	200	2.00
50 wt% HPW-GO-532 nm	213	2.25
60 wt% HPW-GO-532 nm	225	2.75
HPW	376	0.20

Table 3. The acidic properties of HPW-GO-355nm catalysts

Catalyst	E (mV)	No. of acidic sites (mequiv/g)
GO	224	1.50
10 wt% HPW-GO-355nm	321	1.65
30 wt% HPW-GO-355 nm	341	1.85
40 wt% HPW-GO-355 nm	350	2.10
50 wt% HPW-GO-355 nm	363	2.40
60 wt% HPW-GO-355 nm	398	3.00
HPW	376	0.20

$$Number\ of\ Acidic\ sites\ \left(\frac{mequiv}{g}\right) = \frac{Normality\ of\ titrant\ (N) x\ Volume\ titrated\ (mL)}{Weight\ of\ catalyst\ (g)} \qquad \textbf{Equation 8}$$

where N = equiv/L

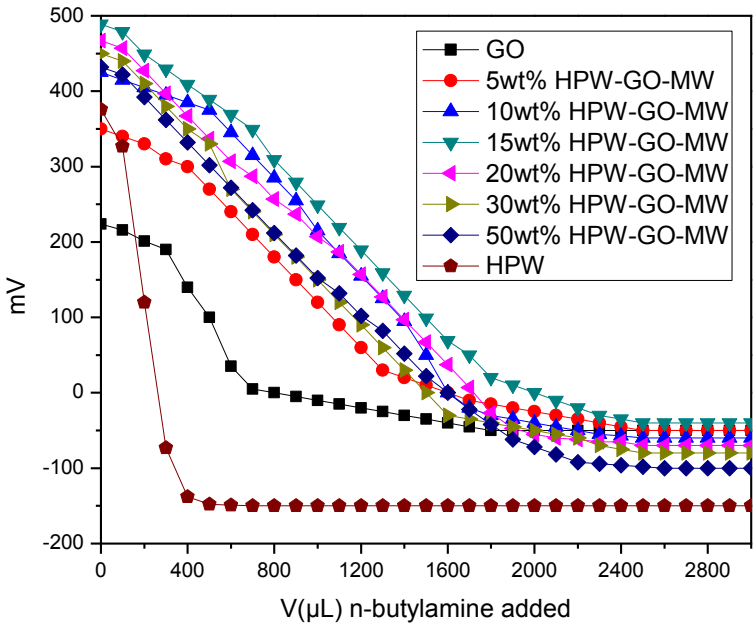

Figure 26.Potentiometric-titration curve different loadings of HPW on GO compared to both HPW and GO prepared by microwave irradiation.

The potentiometric titration curves of the HPW-GO catalysts for the microwave irradiation method are shown in **Figure 26**. The different catalysts exhibit electrode potentials between 224-480 mV as presented in **Table 4**, which means that HPW-GO catalysts have very strong acid sites compared to GO and bulk HPW. The basal plane of GO contains some acidic sites that is shown by the results [146]. However, a significant increase in the number of acidic sites was observed on the supported HPW which is observed to be 10.70mequiv/g for 85wt% HPW. The acidic sites increase when HPW is well-dispersed at the surface of GO. There is a correlation between the loadings of HPW to the number of acidic sites. It was observed that when the loadings reaches 85wt% HPW, the acidic site increases. However, loadings greater than 85wt% gradually decreased in the acidic sites which might be due to the agglomeration of

the HPW on the surface of GO. Furthermore, it is necessary to increase the yield and conversion of acid-catalyzed organic reaction by increasing the acid sites of the catalyst.

Table 4.The acidic properties of HPW-GO-MW catalysts

Catalyst	E (mV)	No. of acidic sites (mequiv/g)
GO	224	1.50
50 wt% HPW-GO-MW	445	8.25
70 wt% HPW-GO-MW	450	9.00
80 wt% HPW-GO-MW	455	10.50
85 wt% HPW-GO-MW	480	10.70
90 wt% HPW-GO-MW	450	9.00
95 wt% HPW-GO-MW	320	7.50
HPW	376	0.20

CHAPTER 5

5. Applications

This chapter presents the application that was used to test the HPW-GO catalysts that were synthesized using laser and microwave irradiation. The application was investigated involves three acid-catalyzed reactions such as Esterification (5.1), Friedel Crafts-Acylation (5.2), and Pechmann Condensation (5.3). The percent conversion, yield, selectivity, and recyclability were obtained from the calculation of the results of GC-MS. The catalytic activity of each reaction is presented for both synthesis methods. Furthermore, comparisons of the results from different catalytic supports for HPW are presented in section 5.4.

5.1 Esterification Reaction

The conversion, selectivity, and yield of the products after each acid-catalyzed reaction were analyzed by GC-MS. The esterification reaction involves the reaction of acetic acid and 1-octanol to yield octyl-acetate. **Figure 27** shows a peak for anisole because it was used as an internal standard. The internal standard is not part of the reaction which should be constant in all samples. It is a useful tool since organics are volatile. Furthermore, it is used for calibration using the peak area of the product as it is compared to the reactant. The acetic acid is the limiting reagent in the reaction; therefore, it is completely consumed. The esterification reaction

terminates once the acetic acid is consumed. The amount of 1-octanol in excess is utilized for the calculation of the percent conversion.

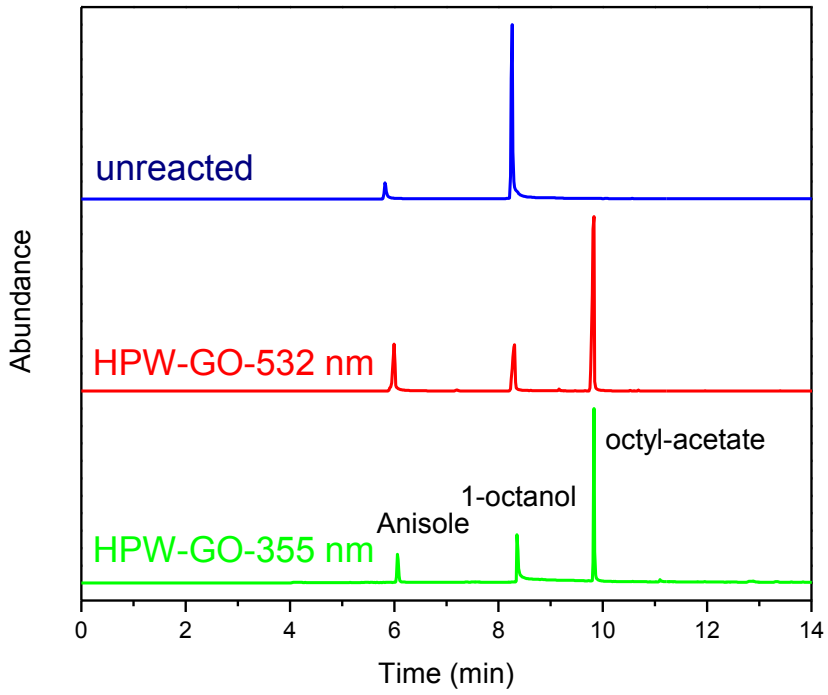

Figure 27. GC-MS of Esterification Reaction for HPW-GO 60 wt% using 355 nm and 532 nm laser irradiation as compared to the unreacted material.

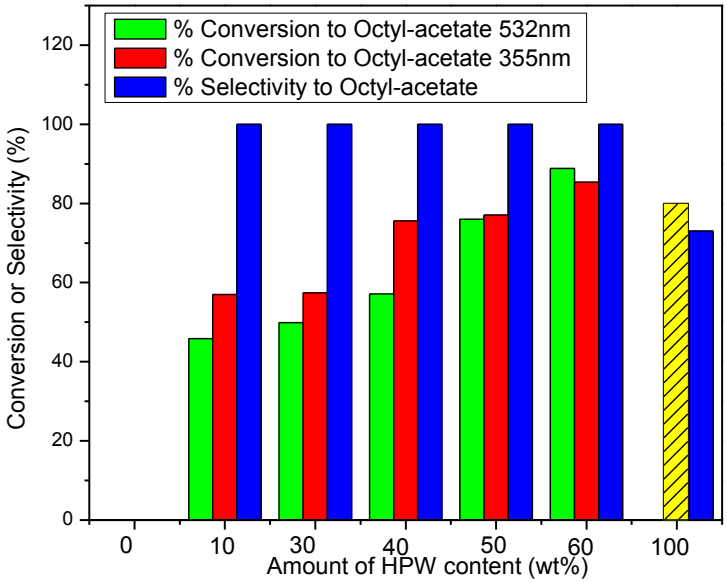

Figure 28. Percent Conversion and selectivity to octyl-acetate of HPW-GO catalysts prepared by laser irradiation.

Table 5. Percent Conversion and selectivity to octyl-acetate of HPW-GO catalysts prepared by laser irradiation.

Catalyst	% Conversion to Octyl-acetate 532nm	% Conversion to Octyl-acetate 355nm	% Selectivity to Octyl-acetate
10 wt% HPW-GO	45.8	56.9	100.0
30 wt% HPW-GO	49.9	57.4	100.0
40 wt% HPW-GO	57.2	75.6	100.0
50 wt% HPW-GO	75.8	77.1	100.0
60 wt% HPW-GO	88.9	85.4	100.0
HPW	79.5	-	78.0

The summary of the calculated results of the percent conversion for the different loadings of HPW using 532nm and 355nm laser irradiation are displayed in **Figure 28** and **Table 5**.

Equation 3 was used for the calculation of the percent conversion to octyl acetate for the catalysts and **Equation 4** for percent selectivity. The lowest loading for 532 nm laser irradiation, which is 10 wt% HPW having conversion of 45.8% which is lower than 355 nm laser irradiation at 56.9 wt%. Both types of catalysts have a gradual increase as the loading increases except for the highest loading, 60wt% where 532 nm has 88.9% conversion while 355 nm has 85.4% conversion. This might be due to the dispersion of HPW on the support. These results present a small variance both catalysts. The following acid catalyzed reaction presents only 532 nm loadings. The selectivity for all the loadings is 100% since no other products are observed in GC-MS. When comparing these results we lower selectivity and lower conversion is obtained for the bulk HPW. The result shows about 79.5 % conversion and 78.0 % selectivity. The HPW-GO catalyst shows a greater conversion at 60 wt% compared to the bulk HPW. This suggests that the partially reduced GO helps increase the conversion and selectivity while using a smaller amount of HPW in the reaction.

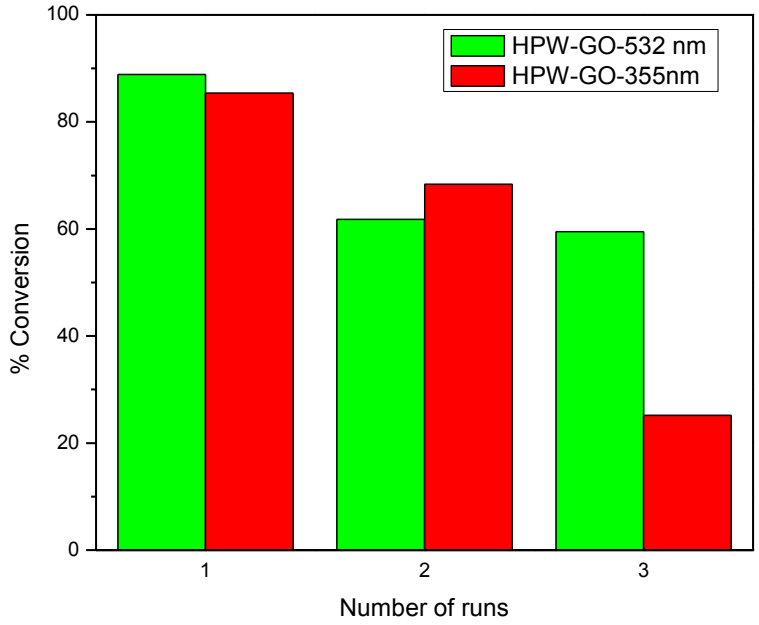

Figure 29. Esterification Recyclability for 60 wt% HPW-GO catalyst prepared by laser irradiation.

Table 6. Esterification Recyclability for 60 wt% HPW-GO catalyst prepared by laser irradiation

Number of Runs	% Conversion to Octyl-acetate 532nm	% Conversion to Octyl-acetate 355nm
1	88.9	85.4
2	61.2	68.4
3	59.5	25.2

One of the key features of a heterogeneous catalyst is its recyclability. The same 60 wt% HPW-GO was used to determine the catalysts response to each reaction. **Figure 29** and **Table 6** show how that the catalyst can be recycled twice. There is some loss of activity from the first run to the next two runs for the HPW-GO 532 nm. However, HPW-GO-355 nm shows a

significant loss of activity from the second run to the third run. This can be due to the leeching of the HPW from the surface of the partially reduced GO on each of the runs.

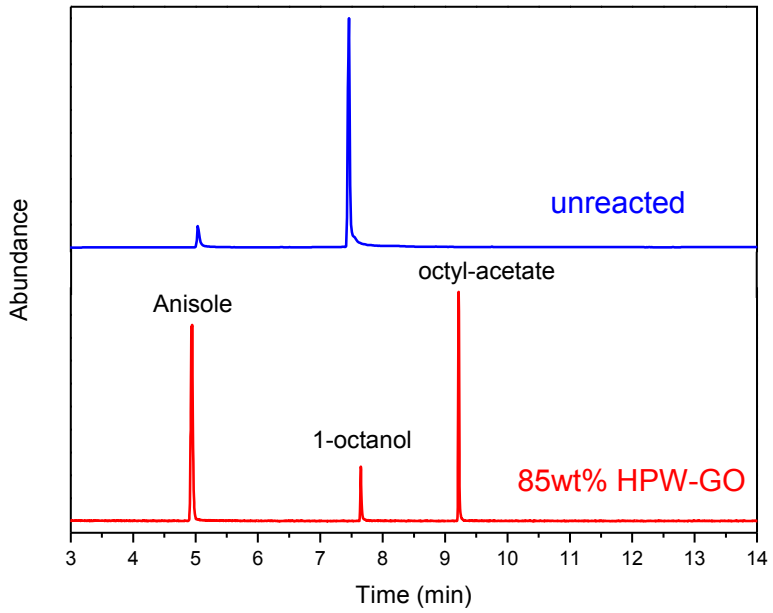

Figure 30. GC of Esterification Reaction for 85 wt% HPW-GO prepared by microwave irradiation as compared to the unreacted material.

Figure 30 shows the gas chromatograph (GC) of the esterification reaction for the microwave irradiation method. The esterification reaction uses acetic acid and 1-octanol as reactants and yields octyl-acetate as the major product. The anisole peak is shown because it is used as an internal standard. The internal standard is added after the reaction for GC analysis. The acetic acid is the limiting reagent in the reaction; therefore, it is completely consumed. The esterification reaction terminates once the acetic acid is consumed. The amount of 1-octanol in excess is utilized for the calculation of the percent conversion. The GC for other loadings of HPW is similar to this result with varying intensity and peak area.

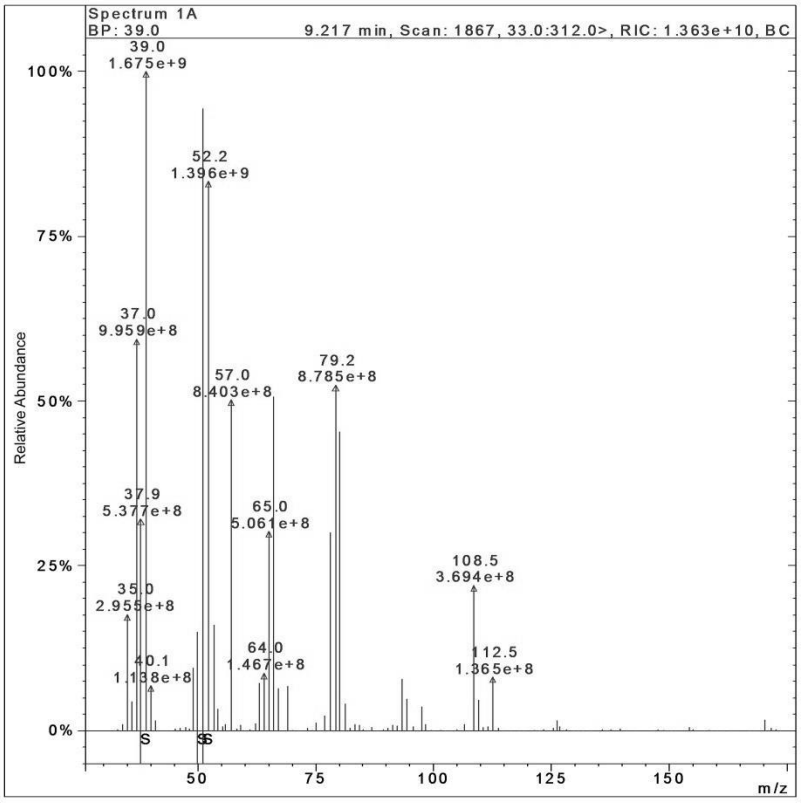

Figure 31. Mass Spectrum of Octyl-Acetate 85 wt% HPW-GO prepared by microwave irradation.

The gas chromatography (GC) is coupled with mass spectroscopy (MS) to help identify the molecules in a given sample. The GC separates the different components of a mixture and the MS identifies each compound. The MS occurs when the sample is bombarded with electrons and it generates molecular fragments. The detector measures the mass-to-charge ratio of each fragment. **Figure 31** displays the mass spectra of octyl-acetate that occurs around nine minutes in the GC. This is the product that is expected for the esterification reaction. The mass spectra in **Figure 31** corresponds to the standard mass spectrum of octyl acetate in the National Institute of Standards of Technology (NIST) database [147]. The results for the other loadings of HPW are

similar to the mass spectrum in **Figure 31**, which proves that the octyl acetate is the major product for catalyst that was prepared.

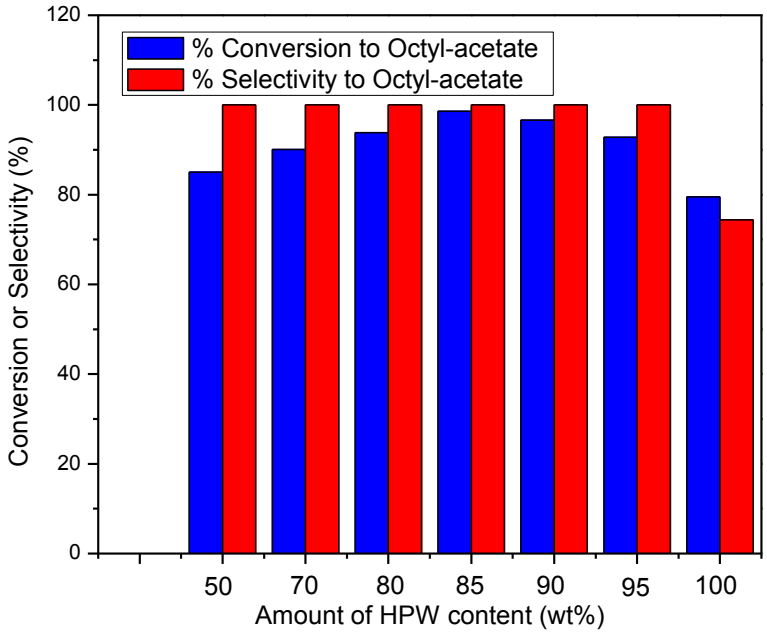

Figure 32. Percent Conversion and selectivity to octyl acetate of HPW-GO catalysts prepared by microwave irradiation.

Table 7. Percent Conversion and selectivity to octyl acetate of HPW-GO catalysts prepared by microwave irradiation.

Catalyst	% Conversion to Octyl-acetate	% Selectivity to Octyl-acetate
50 wt% HPW-GO	85.0	100.0
70 wt% HPW-GO	90.1	100.0
80 wt% HPW-GO	96.0	100.0
85 wt% HPW-GO	98.6	100.0
90 wt% HPW-GO	96.6	100.0
95 wt% HPW-GO	92.8	100.0
HPW	79.5	78.0

The percent conversion and percent selectivity for the different loadings of HPW supported are displayed in **Figure 32** and **Table 7**. Similar to the laser method, **Equation 4** was used for the calculation of the percent conversion to octyl acetate for the catalysts and **Equation 5** for percent selectivity. The lowest loading at 50wt% HPW shows 85.0% conversion. The 85wt% HPW has highest conversion with 98.6%. This is due to the dispersion of HPW on the support, which makes the acidic sites very reactive. However, the gradual decrease of the conversion occurs after loadings of 85wt% HPW. This might be from the agglomeration of the HPW on the surface of GO. Furthermore, the selectivity for all the loadings is 100% since no other products are observed in GC-MS. When comparing these results, lower selectivity and lower conversion for the bulk HPW is obtained. The result shows about 79.5 % conversion and 78.0 % selectivity. The HPW-GO catalyst show a greater conversion starting from 50 wt% compared to the bulk HPW. This suggests that the GO microwave helps increase the conversion and selectivity while using a smaller amount of HPW in the reaction.

The effect of calcination temperature was studied for the Esterification reaction using 80, 250, 350, 450ºC. **Figure 33** and **Table 8** show the effect of calcination temperature on the % yield of octyl-acetate and acid strength. It shows that the increase of calcination temperature increases the acid strength. The maximum acid strength is observed at 350ºC. Furthermore, the increase in acid strength results in the increase of % yield of octyl-acetate.

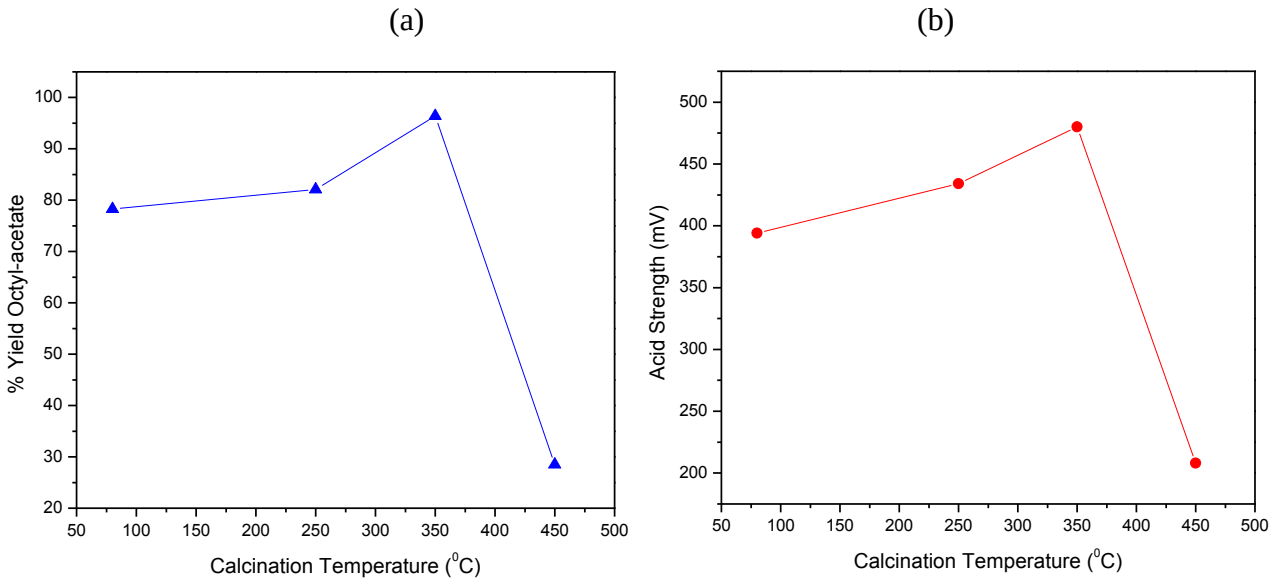

Figure 33. Effect of Calcination Temperature compared to (a) Percent Yield of octyl-acetate (b) acid strength prepared by microwave irradation.

Table 8. Effect of Calcination Temperature compared to Percent Yield of octyl-acetate and acid strength prepared by microwave irradiation.

Calcination Temperature	% Yield of octyl-acetate	Acid Strength (mV)
80ºC	78.3	394.0
250ºC	82.1	434.0
350ºC	96.4	480.0
450ºC	28.5	208.0

5.2 Friedel-Crafts Acylation

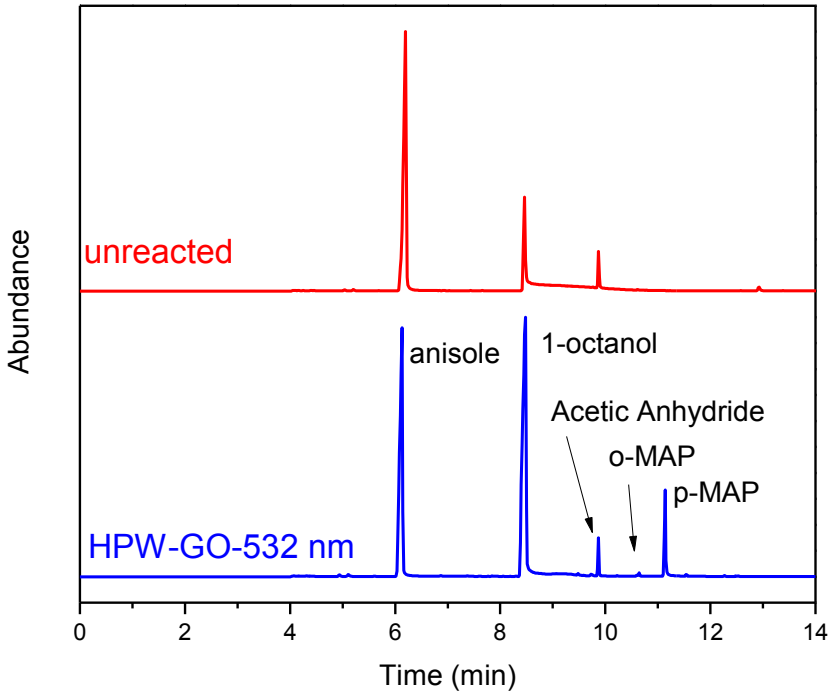

Figure 34. GC-MS of Friedel-Crafts Acylation of HPW-GO 60wt% prepared by laser irradiation at 532nm compared to the unreacted.

The Friedel Crafts Acylation involves the reaction of acetic anhydride (AA) and anisole to yield o-MAP and p-MAP. **Figure 34** shows the GC-MS of the reaction for 60wt% HPW-GO compared to the unreacted material. The 1-octanol was used as an internal standard for the reaction. Here it shows two product peaks when compared to the unreacted material by GC-MS. It is also significant that the selectivity of the para product is greater than towards the ortho product. **Equation 5** was used for calculating the % conversion while **Equation 6** was used for calculating the percent selectivity toward ortho or para products.

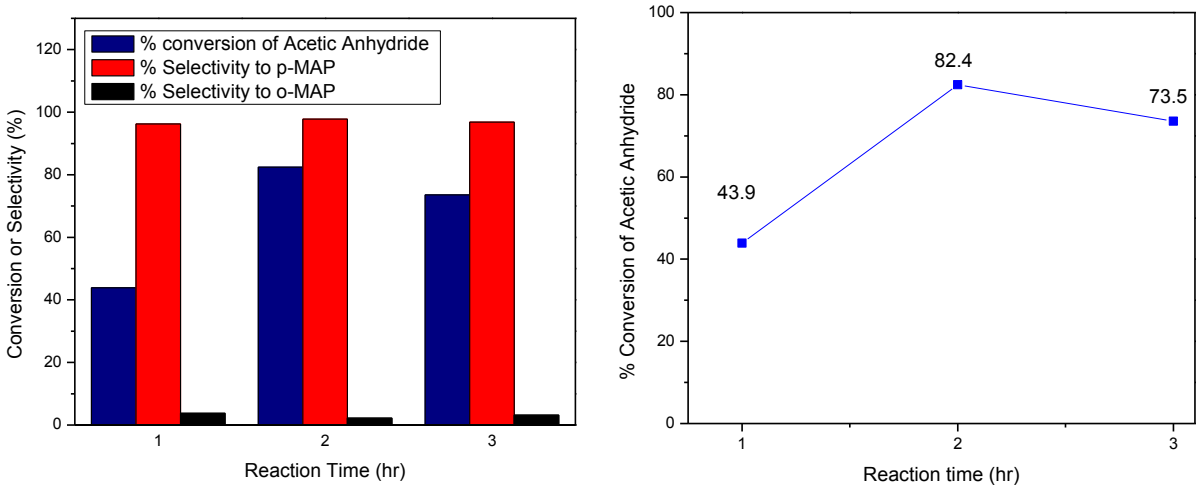

Figure 35. Percent Conversion of Acetic Anhydride at 1, 2, and 3 hours using 60 wt% HPW-GO prepared by laser Irradiation.

The Friedel-Crafts acylation reaction was subjected to different reaction times as shown in **Figure 35** in order to optimize the product yield. It shows that the optimum condition is with a reaction time of 2 hours. The conversion for 2 hours is 82.4% while 3 hours is 73.5%. The selectivity of p-MAP at 2 hours is also slightly higher than 3 hours. Therefore, this time was chosen for this reaction.

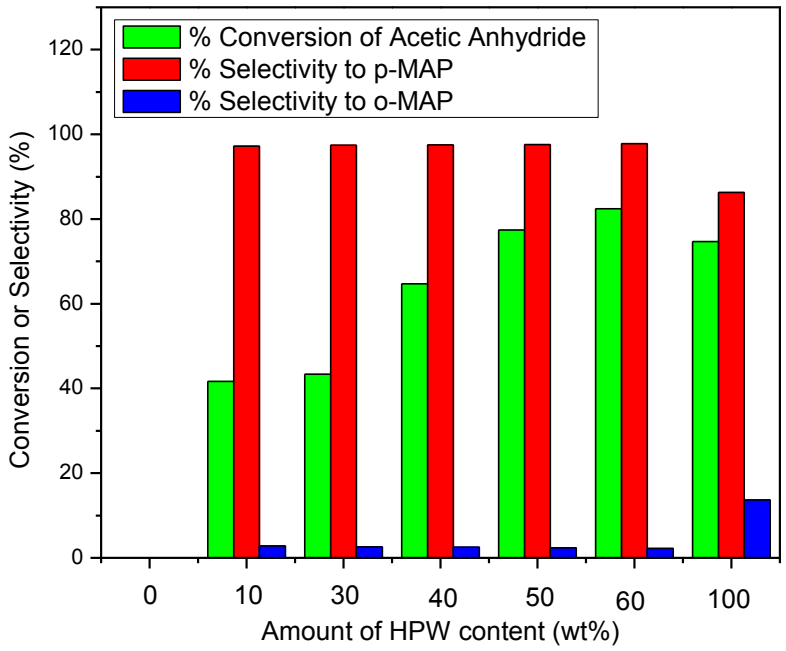

Figure 36. Percent Conversion and Selectivity to Acetic Anhydride of HPW-GO 532 nm to p-MAP and o-MAP products

Table 9. Percent Conversion and Selectivity to Acetic Anhydride of HPW-GO 532 nm to p-MAP and o-MAP products

Catalyst	% Conversion to Acetic Anhydride	% Selectivity to p-MAP	% Selectivity to o-MAP
10 wt% HPW-GO	41.7	97.2	2.8
30 wt% HPW-GO	43.3	97.4	2.6
40 wt% HPW-GO	64.7	97.5	2.5
50 wt% HPW-GO	77.4	97.6	2.4
60 wt% HPW-GO	82.4	97.8	2.2
HPW	74.7	86.3	13.7

The percent conversion and selectivity of the different loadings of HPW on partially reduced GO are shown on **Figure 36** and **Table 9**. The best conversion we obtained from 60 wt% HPW-GO is 82.4% with selectivity of 97.8% towards p-MAP and about 2.2% towards o-MAP. The selectivity is approximately the same for different loadings of HPW. This may suggest that selectivity is independent of the acid strength. Furthermore, the % conversion of bulk HPW is about 74.7%. At lower loadings of HPW at 50 wt%, the conversion is higher than the bulk. It should be noted that lower HPW loadings that exceed the conversion of the bulk HPW is desirable. These results suggest that HPW-GO is a good candidate for a heterogeneous catalyst.

The reusability of HPW-GO towards Friedel-Crafts acylation is only once. After the second reaction the percent conversion significantly decreases. This suggests that there is a great leeching of the HPW on the surface of the partially reduced GO.

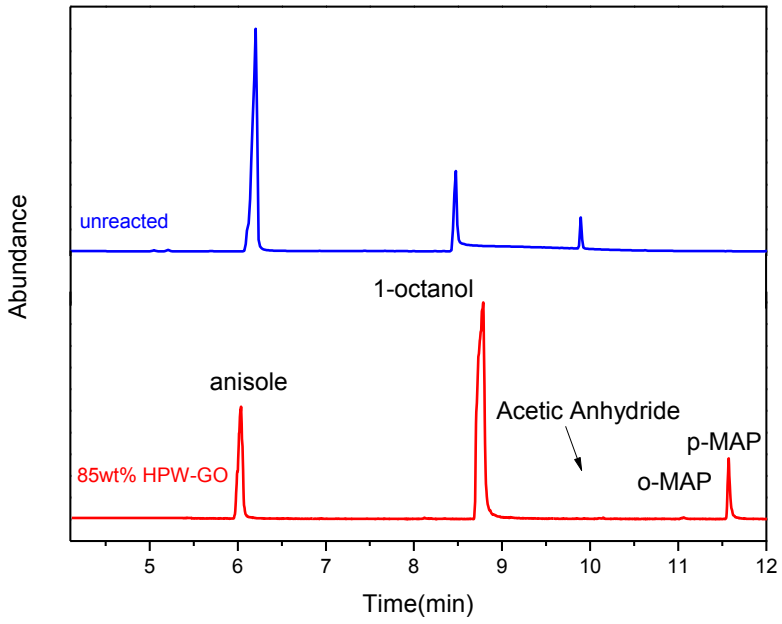

Figure 37. GC of 85wt% HPW-GO prepared by microwave irradiation compared to unreacted material.

Figure 37 shows the GC-MS of the reaction for 85wt% HPW-GO compared to the unreacted material. 1-octanol was used as an internal standard for the reaction. Here it shows two product peaks when compared to the unreacted GC-MS. It is also significant that the selectivity toward the para product is greater than for the ortho product for most of the loadings of HPW.

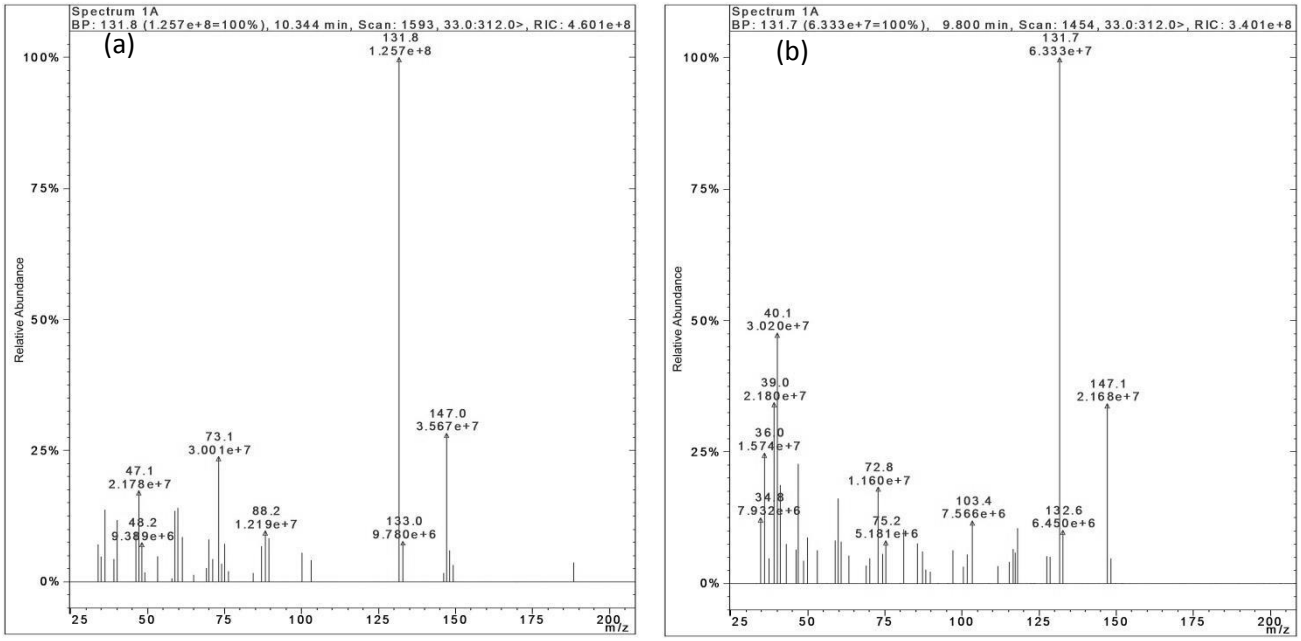

Figure 38. Mass Spectrum of (a) p-MAP (b) o-MAP prepared by microwave irradiation.

The mass spectrum shown in **Figure 38** corresponds to the two products (a) p-MAP and (b) p-MAP. The National Institute of Standards of Technology (NIST) database confirms these two products. Moreover, the molecular fragments of both spectra are very similar since the only difference between these two compounds is the position of the $-OCH_3$ group in either the meta or

para position. As a result, a similar MS is expected and is sufficient to show that the major product is the para position.

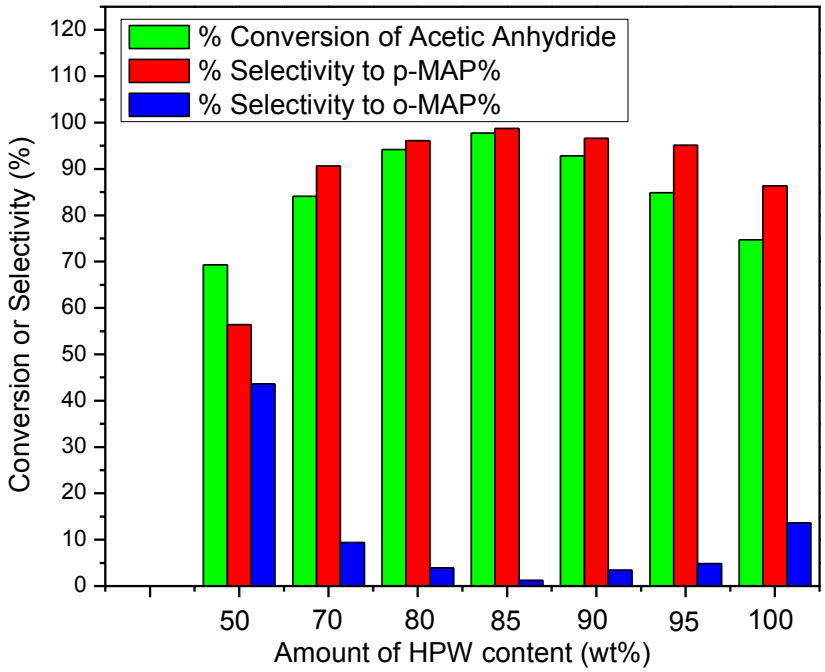

Figure 39. Percent Conversion and Selectivity of Acetic Anhydride to p-MAP and o-MAP products prepared by microwave irradiation.

Table 10. Percent Conversion and Selectivity of Acetic Anhydride to p-MAP and o-MAP products prepared by microwave irradiation.

Catalyst	% Conversion to Acetic Anhydride	% Selectivity to p-MAP	% Selectivity to o-MAP
50 wt% HPW-GO-MW	69.3	56.4	43.6
70 wt% HPW-GO-MW	84.1	95.2	9.4
80 wt% HPW-GO-MW	94.2	96.6	3.9
85 wt% HPW-GO-MW	97.7	98.8	1.2
90 wt% HPW-GO-MW	92.8	96.6	3.4
95 wt% HPW-GO-MW	84.9	95.1	4.8
HPW	74.7	86.3	13.7

The percent conversion and selectivity of the different loadings of HPW on GO are shown on **Figure 39** and **Table 10**. The best conversion obtained from 85 wt% HPW-GO is about 97.7% with selectivity of 98.8% towards p-MAP and 1.2% towards o-MAP. The selectivity toward p-MAP increases as the amount of HPW is increased. This may suggest that increasing the amount of support enhances the selectivity toward p-MAP. Furthermore, the % conversion of bulk HPW is about 74.7%. At loadings of HPW starting from 70 wt%, the conversion is higher than in the bulk. It should be noted that lower HPW loadings that exceed the conversion of the bulk HPW is desirable. Moreover, the conversion after 85wt% decreases, which suggest that there is agglomeration of the HPW on the surface of GO. As a result the conversion declines to lower than the bulk HPW.

5.3 Pechmann Condensation

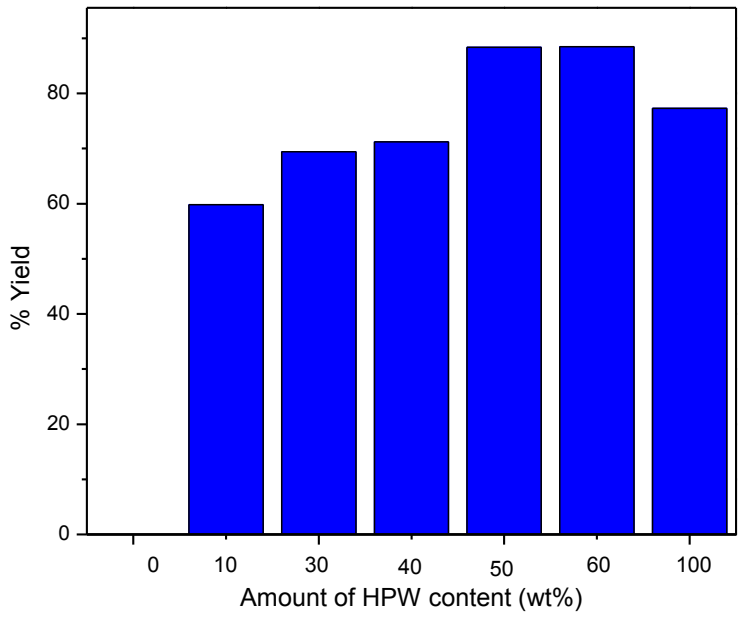

Figure 40. Percent Yield of 7-hydroxy-4-methyl coumarin for HPW-GO prepared by laser irradiation.

Table 11. Percent Yield of 7-hydroxy-4-methyl coumarin for HPW-GO prepared by laser irradiation.

Catalyst	% Yield
10 wt% HPW-GO	59.8
30 wt% HPW-GO	69.5
40 wt% HPW-GO	71.2
50 wt% HPW-GO	88.4
60 wt% HPW-GO	88.6
HPW	77.3

The results of the yield for the Pechmann condensation are shown in **Figure 40** and **Table 11**. The percent yield is calculated using **Equation 7**. The bulk HPW has a yield of 77.3% when comparing to the HPW-GO catalyst. The 50 wt% gives a yield of 88.4% which is a significant increase compared to the bulk. The best yield for the 60 wt% HPW-GO is about 88.6% which suggest that partially reduced GO is a plausible support for HPW in generating 7-hydroxy-4-methyl coumarin.

Table 12. Melting point of Pechmann reaction prepared by laser irradiation.

HPW-GO (wt%)	Melting point (^{0}C)
HPW bulk	177-189
10	178-188
30	179-188
40	183-188
50	179-189
60	178-189

The melting point of 7-hydroxy-4-methyl coumarin was measured to determine the purity of the product. The results are presented in **Table 12**. The melting point corresponds to what is reported in the literature which is 185-186ºC [148]. The wide range of the melting point suggests that an additional purification is needed to achieve its optimal purity.

The reusability for Pechmann condensation was tested using the HPW-GO 60 wt%. The reusability of the catalyst is twice. There is a minimal loss of yield as the catalyst is being recycled.

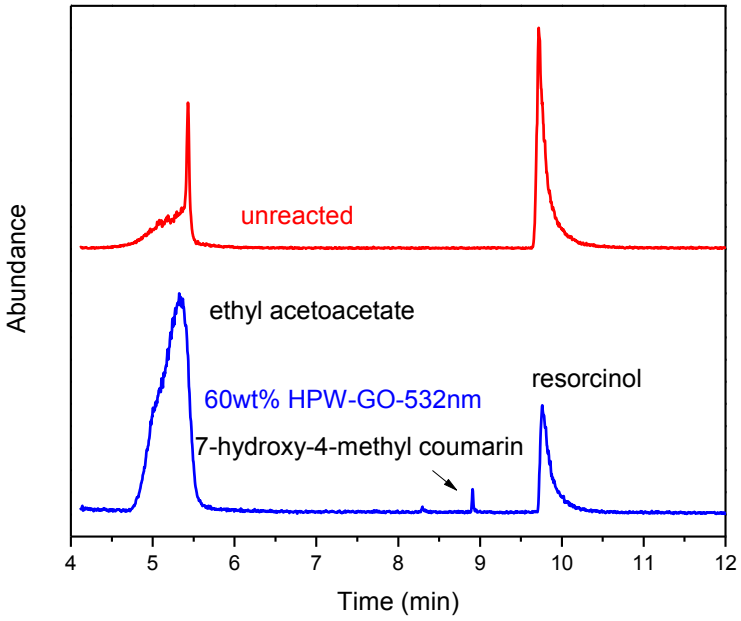

Figure 41. GC of 60wt% HPW prepared by laser irradiation at 532nm compared with the unreacted material.

Figure 41 shows the GC-MS of the reaction of ethyl acetoacetate with resorcinol which yields 7-hydroxy-4-methyl coumarin for 60wt% HPW-GO-532 nm compared to the unreacted material. The coumarin product peak is present as compared to the unreacted material. Furthermore, the mass spectrum shown in **Figure 41** corresponds to 7-hydroxy-4-methyl coumarin. The National Institute of Standards of Technology (NIST) database confirms this product.

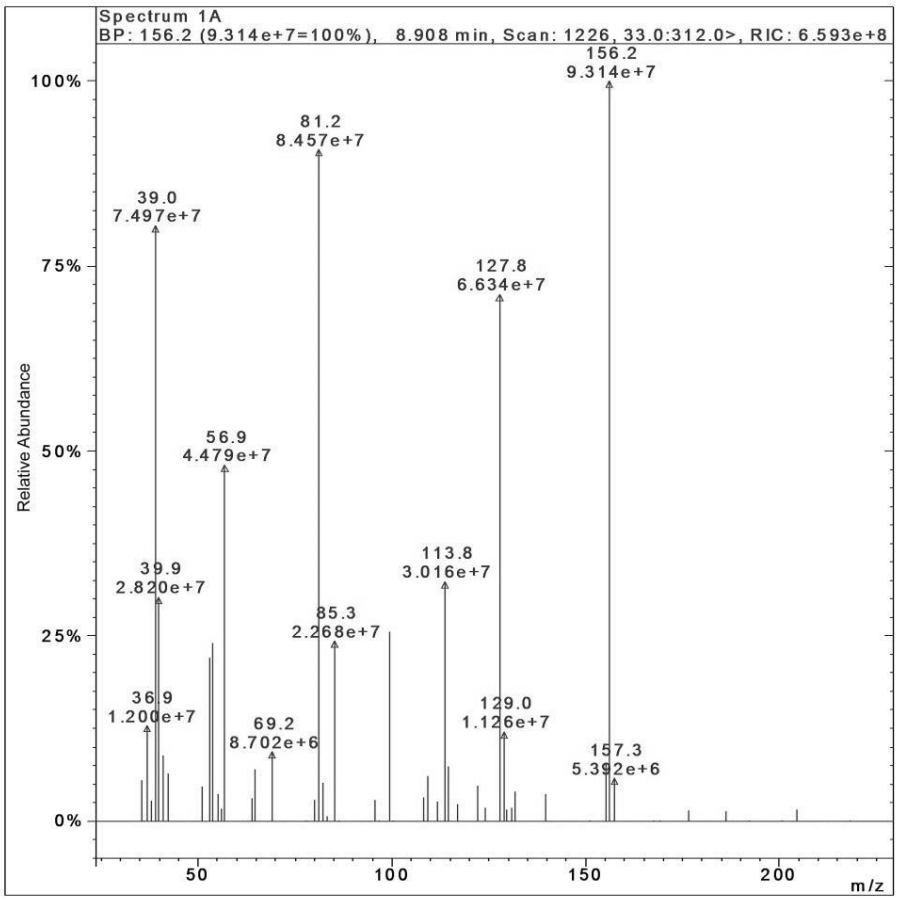

Figure 42. Mass Spectrum of 7-hydroxy-4-methyl coumarin prepared by microwave irradiation.

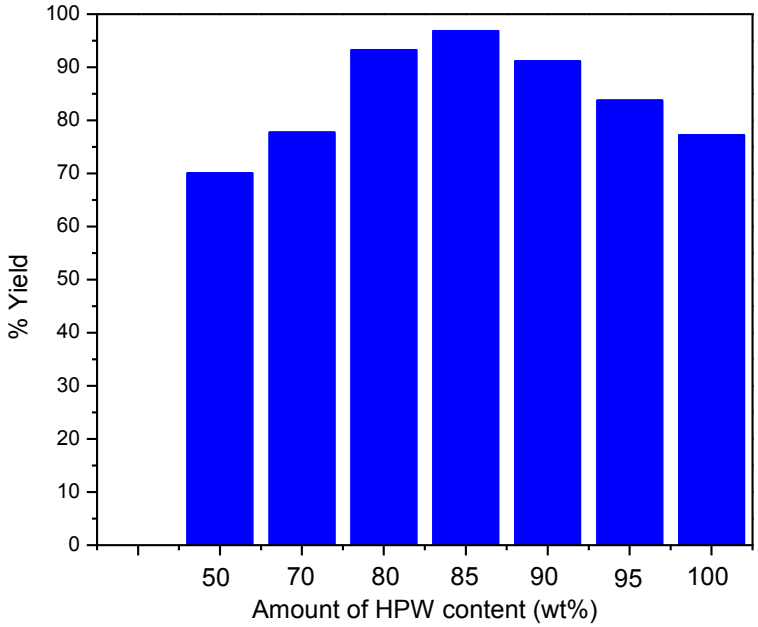

Figure 43. Percent Yield of 7-hydroxy-4-methyl coumarin synthesized from HPW-GO catalyst prepared by microwave irradiation.

Table 13. Percent Yield of 7-hydroxy-4-methyl coumarin synthesized from HPW-GO catalyst prepared by microwave irradiation.

Catalyst	% Yield
50 wt% HPW-GO	70.1
70 wt% HPW-GO	77.8
80 wt% HPW-GO	93.3
85 wt% HPW-GO	96.9
90 wt% HPW-GO	91.2
95 wt% HPW-GO	83.8
HPW	77.3

The results of the yield for the Pechmann condensation are shown in **Figure 43** and **Table 13**. The percent yield is calculated using equation 6. The bulk HPW has a yield about 77.3% when compared to the HPW-GO catalyst. The 80 wt% gives a yield of about 93.3% which is a great increase compared to the bulk. The other loadings provide an increasing yield

up to 85 wt% and declines thereafter. The best yield for the 85 wt% HPW-GO is about 96.9% which suggests that GO is a plausible support for HPW in generating 7-hydroxy-4-methyl coumarin.

One of the promising features of the Pechmann condensation is its recyclability. It was observed that its recyclability can be up to five times without significant loss of activity as show in **Figure 44**. After the fifth run, it was observed that there was a great loss of activity due to the leeching of the HPW catalyst to the surface of GO.

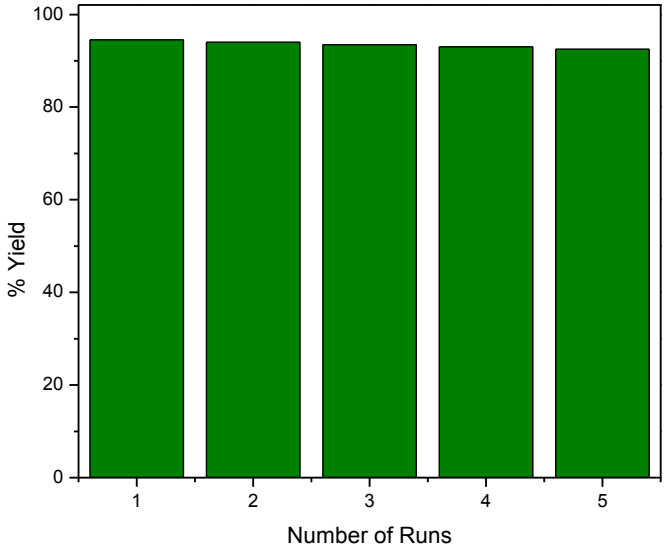

Figure 44. Recylability of Pechmann Condensation prepared by microwave irradiation.

5.4 Comparison of Results

The comparison of the results of HPW-GO with Esterification, Friedel Crafts Acylation, and Pechmann Condensation is shown in **Table 14**, **Table 15** and **Table 16.** The work presented by Khder and et.al shows a high conversion, selectivity yield, and conversion for the three acid-

catalyzed reaction [20]. However, the preparation for the MCM-41 support is extensive. Also, the amount of catalyst needed in some reactions is relatively higher. Bhorodwaj, and et. al presented work on using AT-Mont as a support for Esterification reaction[66]. However, the amount of catalyst is higher, the molar ratio required is more, and the reaction time is longer. Kozhevnikov and et. al presented the SiO_2 as a support and gives good selectivity [12]. Ghodke and et. al presented a ZrO_2 as a support for Pechmann condensation[80]. The reaction time is longer, and the % yield is lower. Therefore, a HPW-GO support is presented because of economic, lower amount of support, and reasonable conversion and yield.

Table 14. Esterification Reaction

References	**Catalyst**	**Reaction conditions(a)**	**Conversion (%)**	**Selectivity (%)**
[20]	MCM-41/HPW	0.05;1:1;80;1	99.0	100.0
[66]	HPW/AT-Mont	0.3;1:2;150;12	88.0	100.0
[22]	HPW/MIL-101	0.05;1:1;120;1	92.3	100.0
Present work	HPW-GO-532nm	0.04;1:1;80:1	89.0	100.0
	HPW-GO-MW	0.04;1:1;80:1	98.6	100.0

a. Reaction conditions: Mass of catalyst (g); molar ratio: n-octanol/acetic acid; reaction temperature °C; reaction time h.

Table 15. Friedel-Crafts Acylation

References	Catalyst	Reaction conditions(b)	Conversion (%)	Selectivity to p-MAP (%)	Selectivity to o-MAP (%)
[20]	MCM-41/HPW	0.1;4:1;120;1	99.2	98.1	1.9
[12]	PW/SiO_2	9.5;4:1;110;2	-	98.0	2.1
[22]	HPW/MIL-101	0.05;4:1;120;1	62.5	99.1	0.9
Present work	HPW-GO-532nm	0.02;4:1;120;2	82.0	98.0	2.0
	HPW-GO-MW	0.02;4:1;120;1	97.7	98.8	1.2

b. Reaction conditions: Mass of catalyst (g); molar ratio: anisole/acetic anhydride; reaction temperature °C; reaction time h.

Table 16. Pechmann Condensation

References	Catalyst	Reaction conditions(c)	% Yield
[20]	MCM-41/HPW	0.1;1:2;120;1	96.0
[80]	12-TPA/ZrO2	0.20;1:1.5;130;8	57.01
[22]	HPW/MIL-101	0.1;1:2;120,1	74.0
Present work	HPW-GO-532nm	0.04;1:2;120;1	88.0
	HPW-GO-MW	0.04;1:2;120;1	96.9

c. Reaction conditions: Mass of catalyst (g); molar ratio: resorcinol/ethyl acetoacetate; reaction temperature °C; reaction time h.

CHAPTER 6

6. Concluding Remarks

The HPW-GO catalysts have been prepared by the loading of the HPW into GO via the impregnation method. The solution was treated further for the reduction of GO using laser irradiation. The solution was subjected to microwave irradiation for the incorporation of GO onto GO. Different loadings of HPW were examined in these two methods to determine which loading will give the best result. The catalysts were characterized by different analytical techniques such as UV-Vis, FTIR, XRD, XPS, and potentiometric titration in order to demonstrate a successful catalyst.

The characterization techniques provided sufficient evidence for the successful loadings of HPW on the surface of GO and partially reduced GO. UV-Vis confirms that there is a shift in absorbance for the bulk HPW and GO when compared to the catalyst. The difference of the absorption of ultraviolet of visible radiation in the catalyst suggests the HPW integration on the surface of partially reduced GO. FTIR provides evidence of what is occurring with the functional groups of the catalyst. The reduction of GO implies the disappearance of the functional groups containing oxygen. In fact, the carbonyl groups intensity decreased while the carbon double bonds' intensity increased. Furthermore, the infrared characteristic peaks of HPW are present in the catalysts. XRD is useful for crystalline compounds and gives it phase information. The GO has a diffraction peak at $2\theta = 10.9^{o}$. However, the HPW-GO catalysts show the disappearance of

that diffraction peak. Also, the some of the HPW diffraction peaks are present in the catalyst. XPS provides the chemical information and elemental analysis on the surface of GO. The C1s profile shows the carbonyl peaks of GO decreased and the carbon-carbon bonds increased. Moreover, the HPW's tungsten and phosphorous information is observed. The elemental composition of P2p and W4f profile confirms HPW is present on the surface of partially reduced GO. Potentiometric titration gives the acidity information of the catalytic surface. The acidity is correlated to the number of acidic sites. Therefore, increasing the acidic sites enhances the acidity of the catalysts. The HPW-GO catalyst acidity increased because more acidic sites are available for the acid-catalyzed organic reactions.

The acid-catalyzed reactions used to test the catalytic activity of the catalysts are Esterification, Friedel-Crafts acylation, and Pechmann condensation. The optimum condition for each reaction was tested in order to obtain the maximum catalytic activity. The catalytic activity such as the conversion, selectivity and yield were calculated using the GC-MS peaks observed for the reactions. The best HPW-GO catalyst for the laser synthesis was the 60 wt% for both 532 nm and 355 nm. The conversion for octyl-acetate in the Esterification reaction was 88.9 % for 532 nm and 85.0 % with selectivity of 100% for both sources. The reusability for this reaction is twice. The conversion for acetic anhydride in the Friedel-Crafts acylation for HPW-GO 532nm was 82.4% with 97.8 % selectivity to p-MAP and 2.2% towards o-MAP. The reusability for this reaction is once. The yield for 7-hydroxy-4-methyl coumarin in the Pechmann condensation is 88.6% with a melting point of 178-189ºC.

The catalytic activity for the microwave synthesis obtained was similar to the laser synthesis. The best HPW-GO catalyst was the 85wt% in all the acid-catalyzed reactions. The conversion for the Esterification reaction was at 98.6% with 100% selectivity to the octyl ester

product. Moreover, the conversion for Friedel Crafts acylation was 97.7% with selectivity of 98.8% towards p-MAP and about 1.2% towards o-MAP. Then, the percent yield for the Pechmann condensation is 96.9%. The summary of results for both reactions is shown in **Table 17**.

The HPW-GO is a plausible candidate for the heterogeneous catalyst for acid-catalyzed reactions. Reducing the amount of HPW in each reaction is preferable as it is economical. The loading of 60 wt% HPW, the conversion and yield are its maximum compared to bulk HPW. Also, the selectivity toward the major products is advantageous as it provides a way for synthesis of the products desired. These products can be isolated for the desired applications. Furthermore, the time for the synthesis of the reaction is lower compared to the other catalysts. Also, the catalyst can be reused for different runs. Therefore, HPW-GO catalysts are cost-effective, reusable, and time-efficient.

Table 17. Summary of Results for Laser (60wt% HPW-GO 532nm) and Microwave Synthesis (85wt% HPW-GO)

	Esterification		**Friedel-Crafts Acylation**			**Pechmann Condensation**
	Conversion (%)	Selectivity (%)	Conversion (%)	Selectivity p-MAP (%)	Selectivity o-MAP(%)	Yield (%)
Laser	89.0% (532nm) 85.0% (355nm)	100.0	82.0	98.0	2.0	88.0
Microwave	98.6	100.0	97.7	98.8	1.2	96.9

LIST OF REFERENCES

LIST OF REFERENCES

1. Haber, J., et al., *Catalytic performance of the dodecatungstophosphoric acid on different supports.* Applied Catalysis A: General, 2003. **256**(1): p. 141-152.
2. Hill, C.L. and C.M. Prosser-McCartha, *Homogeneous catalysis by transition metal oxygen anion clusters.* Coordination Chemistry Reviews, 1995. **143**: p. 407-455.
3. Izumi, Y., K. Hisano, and T. Hida, *Acid catalysis of silica-included heteropolyacid in polar reaction media.* Applied Catalysis A: General, 1999. **181**(2): p. 277-282.
4. Khder, A.E.R.S., *Preparation, characterization and catalytic activity of tin oxide-supported 12-tungstophosphoric acid as a solid catalyst.* Applied Catalysis A: General, 2008. **343**(1): p. 109-116.
5. Kozhevnikov, I.V., *Catalysis by heteropoly acids and multicomponent polyoxometalates in liquid-phase reactions.* Chemical Reviews, 1998. **98**(1): p. 171-198.
6. Micek-Ilnicka, A., et al., *Carbon nanotubes, silica and titania supported heteropolyacid $H_3PW_{12}O_{40}$ as the catalyst for ethanol conversion.* Applied Catalysis A: General, 2012. **421**: p. 91-98.
7. Mizuno, N. and M. Misono, *Heterogeneous catalysis.* Chemical Reviews, 1998. **98**(1): p. 199-217.
8. Okumura, K., et al., *Enhancement of the Catalytic Activity of a Dawson-type Heteropoly Acid Induced by the Loading on a Silica Support.* Topics in Catalysis, 2009. **52**(6-7): p. 649-656.

9. Yang, X., et al., *Study of the Keggin structure and catalytic properties of Pt-promoted heteropoly compound/Al-MCM-41 hybrid catalysts.* Catalysis Today, 2009. **148**(1): p. 160-168.

10. Zhu, K., et al., *Characterization of Dispersed Heteropoly Acid on Mesoporous Zeolite Using Solid-State P-31 NMR Spin-Lattice Relaxation.* Journal of the American Chemical Society, 131 (28): 9715-9721, 2009. **131**(PNNL-SA-68413).

11. Zhu, Z. and W. Yang, *Preparation, Characterization and Shape-Selective Catalysis of Supported Heteropolyacid Salts K2. 5H0. 5PW12O40,(NH4) 2.5 H0. 5PW12O40, and Ce0. 83H0. 5PW12O40 on MCM-41 Mesoporous Silica.* The Journal of Physical Chemistry C, 2009. **113**(39): p. 17025-17031.

12. Kozhevnikov, I., *Friedel–Crafts acylation and related reactions catalysed by heteropoly acids.* Applied Catalysis A: General, 2003. **256**(1): p. 3-18.

13. Dupont, P. and F. Lefebvre, *Esterification of propanoic acid by butanol and 2-ethylhexanol catalyzed by heteropolyacids pure or supported on carbon.* Journal of Molecular Catalysis A: Chemical, 1996. **114**(1): p. 299-307.

14. Dias, J.A., et al., *Preparation and characterization of supported H3PW12O40 on silica gel: a potential catalyst for green chemistry processes.* Catalysis Today, 2003. **85**(1): p. 39-48.

15. Caliman, E., et al., *Solvent effect on the preparation of $H_3PW_{12}O_{40}$ supported on alumina.* Catalysis Today, 2005. **107**: p. 816-825.

16. Kumbar, S.M. and S. Halligudi, *Tungstophosphoric acid supported on titania: A solid acid catalyst in benzylation of phenol with benzylalcohol.* Catalysis Communications, 2007. **8**(5): p. 800-806.

17. Llanos, A., et al., *Synthesis and characterization of HPW/MCM-41 (Si) and HPW/MCM-41 (Si/Al) catalysts: Activity for toluene alkylation with 1-dodecene.* Catalysis Today, 2008. **133**: p. 20-27.

18. Caliman, E., et al., *Preparation and characterization of H_3 $PW_{12}O_{40}$ supported on niobia.* Microporous and Mesoporous Materials, 2010. **132**(1): p. 103-111.

19. Oliveira, C.F., et al., *Esterification of oleic acid with ethanol by 12-tungstophosphoric acid supported on zirconia.* Applied Catalysis A: General, 2010. **372**(2): p. 153-161.

20. Khder, A.E.R.S., H. Hassan, and M.S. El-Shall, *Acid catalyzed organic transformations by heteropoly tungstophosphoric acid supported on MCM-41.* Applied Catalysis A: General, 2012. **411**: p. 77-86.

21. Chen, Y., et al., *Facile synthesis and characterization of 12-tungstophosphoric acid anchoring MCM-41 mesoporous materials.* Materials Letters, 2014. **114**: p. 72-75.

22. Abd El Rahman, S.K., H.M. Hassan, and M.S. El-Shall, *Metal-organic frameworks with high tungstophosphoric acid loading as heterogeneous acid catalysts.* Applied Catalysis A: General, 2014. **487**: p. 110-118.

23. Baroi, C. and A.K. Dalai, *Esterification of free fatty acids (FFA) of Green Seed Canola (GSC) oil using HY zeolite supported 12-Tungstophosphoric acid (TPA).* Applied Catalysis A: General, 2014. **485**: p. 99-107.

24. Tessonnier, J.-P., et al., *Structure, Stability, and Electronic Interactions of Polyoxometalates on Functionalized Graphene Sheets.* Langmuir, 2012. **29**(1): p. 393-402.

25. Kim, Y. and S. Shanmugam, *Polyoxometalate–Reduced Graphene Oxide Hybrid Catalyst: Synthesis, Structure, and Electrochemical Properties.* ACS applied materials & interfaces, 2013. **5**(22): p. 12197-12204.

26. Jiang, M., et al., *Electrocatalytic Hydrogen Evolution and Oxygen Reduction on Polyoxotungstates/Graphene Nanocomposite Multilayers.* The Journal of Physical Chemistry C, 2014. **118**(26): p. 14371-14378.

27. Nipane, S.V., M.G. Mali, and G.S. Gokavi, *Reduced graphene oxide supported silicotungstic acid for efficient conversion of thiols to disulfides by hydrogen peroxide.* Industrial & Engineering Chemistry Research, 2014. **53**(10): p. 3924-3930.

28. Liu, R., et al., *Polyoxometalate-Mediated Green Synthesis of Graphene and Metal Nanohybrids: High-Performance Electrocatalysts.* Journal of Cluster Science, 2014. **25**(3): p. 711-740.

29. Bolotin, K.I., et al., *Ultrahigh electron mobility in suspended graphene.* Solid State Communications, 2008. **146**(9): p. 351-355.

30. Balandin, A.A., et al., *Superior thermal conductivity of single-layer graphene.* Nano letters, 2008. **8**(3): p. 902-907.

31. Lee, C., et al., *Measurement of the elastic properties and intrinsic strength of monolayer graphene.* science, 2008. **321**(5887): p. 385-388.

32. Morozov, S., et al., *Giant intrinsic carrier mobilities in graphene and its bilayer.* Physical Review Letters, 2008. **100**(1): p. 016602.

33. Cai, W., et al., *Large area few-layer graphene/graphite films as transparent thin conducting electrodes.* Applied Physics Letters, 2009. **95**(12): p. 123115.

34. Li, X., et al., *Transfer of large-area graphene films for high-performance transparent conductive electrodes.* Nano letters, 2009. **9**(12): p. 4359-4363.

35. Geim, A.K., *Graphene: status and prospects.* Science, 2009. **324**(5934): p. 1530-1534.

36. Geim, A.K. and K.S. Novoselov, *The rise of graphene.* Nature materials, 2007. **6**(3): p. 183-191.

37. Herring, N.P., et al., *Enhanced photocatalytic activity of ZnO–graphene nanocomposites prepared by microwave synthesis.* Journal of Nanoparticle Research, 2012. **14**(12): p. 1-13.

38. Kamat, P.V., *Graphene-based nanoarchitectures. Anchoring semiconductor and metal nanoparticles on a two-dimensional carbon support.* The Journal of Physical Chemistry Letters, 2009. **1**(2): p. 520-527.

39. Moussa, S., V. Abdelsayed, and M. Samy El-Shall, *Laser synthesis of Pt, Pd, CoO and Pd–CoO nanoparticle catalysts supported on graphene.* Chemical Physics Letters, 2011. **510**(4): p. 179-184.

40. Singh, R.N. and C.S. Sharma, *Preparation of Bimetallic Pd-Co Nanoparticles on Graphene Support for Use as Methanol Tolerant Oxygen Reduction Electrocatalysts.* Engineering, Technology & Applied Science Research, 2012. **2**(6): p. pp. 295-301.

41. Moussa, S., et al., *Graphene Supported Iron-based Nanoparticles for Catalytic Production of Liquid Hydrocarbons from Synthesis Gas. The Role of the Graphene Support in Comparison to Carbon Nanotubes.* ACS Catalysis, 2013.

42. He, H. and C. Gao, *Graphene nanosheets decorated with Pd, Pt, Au, and Ag nanoparticles: Synthesis, characterization, and catalysis applications.* Science China Chemistry, 2011. **54**(2): p. 397-404.

43. Machado, B.F. and P. Serp, *Graphene-based materials for catalysis.* Catalysis Science & Technology, 2012. **2**(1): p. 54-75.

44. Mwakikunga, B.W. and K.T. Hillie, *Graphene synthesis, catalysis with transition metals and their interactions by laser photolysis.* 2011.

45. Haag, D. and H.H. Kung, *Metal Free Graphene Based Catalysts: A Review.* Topics in Catalysis: p. 1-12.

46. Zhang, C., et al., *Synthesis of amino-functionalized graphene as metal-free catalyst and exploration of the roles of various nitrogen states in oxygen reduction reaction.* Nano Energy, 2013. **2**(1): p. 88-97.

47. Ji, J., et al., *Sulfonated graphene as water-tolerant solid acid catalyst.* Chemical Science, 2011. **2**(3): p. 484-487.

48. A. D. McNaught, A.W., *IUPAC. Compendium of Chemical Terminology, 2nd ed. (the "Gold Book").* 1997, Blackwell Scientific Publications: Oxford.

49. Farnetti, E., R. Di Monte, and J. Kašpar, *HOMOGENEOUS AND HETEROGENEOUS CATALYSIS.*

50. Lower, S., *Catalyst reduce activation energy*. 2013, University of California Davis.

51. Cole-Hamilton, D.J., *Homogeneous catalysis--new approaches to catalyst separation, recovery, and recycling.* Science, 2003. **299**(5613): p. 1702-1706.

52. Sawant, D.P., et al., *Catalytic performances of silicotungstic acid/zirconia supported SBA-15 in an esterification of benzyl alcohol with acetic acid.* Journal of Molecular Catalysis A: Chemical, 2007. **276**(1): p. 150-157.

53. Timofeeva, M., et al., *Esterification of n-butanol with acetic acid in the presence of heteropoly acids with different structures and compositions.* Kinetics and catalysis, 2001. **42**(6): p. 791-795.

54. Clark, J.H., D.J. Macquarrie, and K. Wilson, *Functionalised mesoporous materials for green chemistry.* Studies in Surface Science and Catalysis, 2000. **129**: p. 251-264.

55. Keggin, J., *The structure and formula of 12-phosphotungstic acid.* Proceedings of the Royal Society of London. Series A, 1934. **144**(851): p. 75-100.

56. Kozhevnikov, I.V., *Heteropoly acids and related compounds as catalysts for fine chemical synthesis.* Catalysis Reviews, 1995. **37**(2): p. 311-352.

57. Pope, M.T., *Heteropoly and Isopoly Oxometalates*. Springer. 1983, Berlin.

58. Himmel, D., et al., *A unified pH scale for all phases.* Angewandte Chemie International Edition, 2010. **49**(38): p. 6885-6888.

59. Kozhevnikov, I., *Advances in catalysis by heteropolyacids.* Russian Chemical Reviews, 1987. **56**(9): p. 811.

60. Chuvaev, V., K. Popov, and V. Spitsyn. *High temperature hydrogen ion self-diffusion in solid heteropoly acids*. in *Dokl. Akad. Nauk. SSSR*. 1980.

61. Furuta, M., et al., *Structure and acidity of 12-molybdophosphoric acid and its salts in solid state as characterized by infrared spectroscopy.* Chemistry Letters, 1979(1): p. 31-34.

62. Guisnet, M. and P. Magnoux, *Organic chemistry of coke formation.* Applied Catalysis A: General, 2001. **212**(1–2): p. 83-96.

63. Izumi, Y., K. Urabe, and M. Onaka, *Zeolite, clay, and heteropoly acid in organic reactions*. Vol. 99. 1992: Kodansha Tokyo.

64. Singh, S. and A. Patel, *12-Tungstophosphoric acid supported on mesoporous molecular material: Synthesis, Characterization and Performance in biodiesel production.* Journal of Cleaner Production, 2014.

65. Srilatha, K., et al., *Efficient Esterification and Transesterification of Used Cooking Oil Using 12-Tungstophosphoric Acid (TPA)/Nb2O5 Catalyst†.* Energy & Fuels, 2010. **24**(9): p. 4748-4755.

66. Bhorodwaj, S.K., M.G. Pathak, and D.K. Dutta, *Esterification of acetic acid with n-butanol using heteropoly acid supported modified clay catalyst.* Catalysis letters, 2009. **133**(1-2): p. 185-191.

67. Chu, W., et al., *Immobilization of the heteropoly acid (HPA) H4SiW12O40 (SiW12) on mesoporous molecular sieves (HMS and MCM-41) and their catalytic behavior.* Catalysis letters, 1996. **42**(3-4): p. 201-208.

68. Jermy, B.R. and A. Pandurangan, *A highly efficient catalyst for the esterification of acetic acid using n-butyl alcohol.* Journal of Molecular Catalysis A: Chemical, 2005. **237**(1): p. 146-154.

69. Bardock, G.A., *Fenaroli's Handbook of Flavor Ingredients*. 3 ed. Vol. 11. 1994: CRC Press.

70. Kirumakki, S.R., N. Nagaraju, and K.V. Chary, *Esterification of alcohols with acetic acid over zeolites Hβ, HY and HZSM5.* Applied Catalysis A: General, 2006. **299**: p. 185-192.

71. Wang, M., et al., *Synthesis and characterization of transition metal methanesulfonates and their catalytic behavior in Biginelli reactions.* Transition metal chemistry, 2005. **30**(7): p. 792-796.

72. Barbosa, S.L., et al., *Solvent free esterification reactions using Lewis acids in solid phase catalysis.* Applied Catalysis A: General, 2006. **313**(2): p. 146-150.

73. Chu, W., et al., *Vapor phase esterification catalyzed by immobilized dodecatungstosilicic acid (SiW< sub> 12</sub>) on activated carbon.* Applied Catalysis A: General, 1996. **145**(1): p. 125-140.

74. Olah, G.A., *Friedel-crafts chemistry*. 1973: Wiley New York.

75. Olah, G.A., *Friedel-Crafts and related reactions*. 1965: Interscience Publishers.

76. Ma, Y., et al., *Friedalr̂Crafts acylation of anisole over zeolite catalysts.* Applied Catalysis A: General, 1997. **165**(1): p. 199-206.

77. Freese, U., F. Heinrich, and F. Roessner, *Acylation of aromatic compounds on H-Beta zeolites.* Catalysis today, 1999. **49**(1): p. 237-244.

78. Bogdał, D., *Coumarins: fast synthesis by Knoevenagel condensation under microwave irradiation.* J. Chem. Res.(s), 1998(8): p. 468-469.

79. Reddy, B.M., M.K. Patil, and P. Lakshmanan, *Sulfated Ce< sub> x</sub> Zr< sub> 1− x</sub> O< sub> 2</sub> solid acid catalyst for solvent free synthesis of coumarins.* Journal of Molecular Catalysis A: Chemical, 2006. **256**(1): p. 290-294.

80. Ghodke, S. and U. Chudasama, *Solvent Free Synthesis of Coumarins Using Environment Friendly Solid Acid Catalysts.* Applied Catalysis A: General, 2013.

81. Sudha, S., et al., *Single step synthesis of coumarin derivatives over Al-MCM-41 and its supported catalysts under solvent-free condition.* Journal of Molecular Catalysis A: Chemical, 2008. **291**(1): p. 22-29.

82. Novoselov, K., et al., *Electric field effect in atomically thin carbon films.* Science, 2004. **306**(5696): p. 666-669.

83. *The Nobel Prize in Physics 2010*. 2010 [cited 2013 June 14]; Available from: http://nobelprize.org/nobel_prizes/physics/laureates/2010/press.html.

84. Tasis, D., et al., *Chemistry of carbon nanotubes.* Chemical reviews, 2006. **106**(3): p. 1105-1136.

85. Zhu, Y., et al., *Graphene and graphene oxide: synthesis, properties, and applications.* Advanced materials, 2010. **22**(35): p. 3906-3924.

86. Tour, J.M., *Top-Down versus Bottom-Up Fabrication of Graphene-Based Electronics.* Chemistry of Materials, 2013.

87. Lotya, M., et al., *Liquid phase production of graphene by exfoliation of graphite in surfactant/water solutions.* Journal of the American Chemical Society, 2009. **131**(10): p. 3611-3620.

88. Hummers, W.S. and R.E. Offeman, *Preparation of Graphitic Oxide.* Journal of the American Chemical Society, 1958. **80**(6): p. 1339-1339.

89. Staudenmaier, L., *Verfahren zur darstellung der graphitsäure.* Berichte der deutschen chemischen Gesellschaft, 1898. **31**(2): p. 1481-1487.

90. Brodie, B.C., *On the atomic weight of graphite.* Philosophical Transactions of the Royal Society of London, 1859: p. 249-259.

91. Pei, S. and H.-M. Cheng, *The reduction of graphene oxide.* Carbon, 2012. **50**(9): p. 3210-3228.

92. Chua, C.K. and M. Pumera, *Chemical reduction of graphene oxide: a synthetic chemistry viewpoint.* Chemical Society Reviews, 2014. **43**(1): p. 291-312.

93. Hassan, H.M., et al., *Microwave synthesis of graphene sheets supporting metal nanocrystals in aqueous and organic media.* Journal of Materials Chemistry, 2009. **19**(23): p. 3832-3837.

94. Moussa, S., et al., *Laser assisted photocatalytic reduction of metal ions by graphene oxide.* Journal of Materials Chemistry, 2011. **21**(26): p. 9608-9619.

95. El-Shall, M.S., *Heterogeneous Catalysis by Metal Nanoparticles Supported on Graphene.* Graphene: Synthesis, Properties, and Phenomena, 2013: p. 303-338.

96. Zhu, Y., et al., *Exfoliation of graphite oxide in propylene carbonate and thermal reduction of the resulting graphene oxide platelets.* ACS nano, 2010. **4**(2): p. 1227-1233.

97. Zedan, A.F., et al., *Ligand-controlled microwave synthesis of cubic and hexagonal CdSe nanocrystals supported on graphene. Photoluminescence quenching by graphene.* The Journal of Physical Chemistry C, 2010. **114**(47): p. 19920-19927.

98. Abdelsayed, V., et al., *Photothermal deoxygenation of graphite oxide with laser excitation in solution and graphene-aided increase in water temperature.* The Journal of Physical Chemistry Letters, 2010. **1**(19): p. 2804-2809.

99. Acik, M., et al., *The role of oxygen during thermal reduction of graphene oxide studied by infrared absorption spectroscopy.* The Journal of Physical Chemistry C, 2011. **115**(40): p. 19761-19781.

100. Huh, S.H., *Thermal reduction of graphene oxide.* Physics and Applications of Graphene-Experiments, Nanotechnology and Nanomaterials, 2011.

101. Boehm, H., et al., *Dünnste kohlenstoff-folien.* Z. Naturforschg, 1962. **17**: p. 150-157.

102. Kudin, K.N., et al., *Raman spectra of graphite oxide and functionalized graphene sheets.* Nano letters, 2008. **8**(1): p. 36-41.

103. Schniepp, H.C., et al., *Functionalized single graphene sheets derived from splitting graphite oxide.* The Journal of Physical Chemistry B, 2006. **110**(17): p. 8535-8539.

104. Seger, B. and P.V. Kamat, *Electrocatalytically active graphene-platinum nanocomposites. Role of 2-D carbon support in PEM fuel cells.* The Journal of Physical Chemistry C, 2009. **113**(19): p. 7990-7995.

105. Xu, T., et al., *Significantly enhanced photocatalytic performance of ZnO via graphene hybridization and the mechanism study.* Applied Catalysis B: Environmental, 2011. **101**(3): p. 382-387.

106. Chang, H., et al., *Graphene fluorescence resonance energy transfer aptasensor for the thrombin detection.* Analytical Chemistry, 2010. **82**(6): p. 2341-2346.

107. Lu, C.H., et al., *A graphene platform for sensing biomolecules.* Angewandte Chemie, 2009. **121**(26): p. 4879-4881.

108. Wang, Y., et al., *Aptamer/graphene oxide nanocomplex for in situ molecular probing in living cells.* Journal of the American Chemical Society, 2010. **132**(27): p. 9274-9276.

109. Wang, S., et al., *Graphene as Atomic Template and Structural Scaffold in the Synthesis of Graphene− Organic Hybrid Wire with Photovoltaic Properties.* Acs Nano, 2010. **4**(10): p. 6180-6186.

110. Han, T.H., et al., *Peptide/graphene hybrid assembly into core/shell nanowires.* Advanced materials, 2010. **22**(18): p. 2060-2064.

111. Alsharaeh, E.H. and A.A. Othman, *Microwave irradiation synthesis and characterization of RGO-AgNPs/polystyrene nanocomposites.* Polymer Composites, 2014.

112. Kim, H., A.A. Abdala, and C.W. Macosko, *Graphene/polymer nanocomposites.* Macromolecules, 2010. **43**(16): p. 6515-6530.

113. Jahan, M., et al., *Structure-directing role of graphene in the synthesis of metal− organic framework nanowire.* Journal of the American Chemical Society, 2010. **132**(41): p. 14487-14495.

114. Petit, C. and T.J. Bandosz, *MOF–graphite oxide composites: combining the uniqueness of graphene layers and metal–organic frameworks.* Advanced Materials, 2009. **21**(46): p. 4753-4757.

115. Tung, V.C., et al., *Low-temperature solution processing of graphene− carbon nanotube hybrid materials for high-performance transparent conductors.* Nano Letters, 2009. **9**(5): p. 1949-1955.

116. Jiao, L., et al., *Narrow graphene nanoribbons from carbon nanotubes.* Nature, 2009. **458**(7240): p. 877-880.

117. Liu, Z.-B., et al., *Porphyrin and fullerene covalently functionalized graphene hybrid materials with large nonlinear optical properties.* The Journal of Physical Chemistry B, 2009. **113**(29): p. 9681-9686.

118. Yu, D., et al., *Fullerene-grafted graphene for efficient bulk heterojunction polymer photovoltaic devices.* The Journal of Physical Chemistry Letters, 2011. **2**(10): p. 1113-1118.

119. Hoffmann, M.R., et al., *Environmental applications of semiconductor photocatalysis.* Chemical Reviews, 1995. **95**(1): p. 69-96.

120. Li, Y., et al., *Gold nanoparticles–graphene hybrids as active catalysts for Suzuki reaction.* Materials Research Bulletin, 2010. **45**(10): p. 1413-1418.

121. Shao, Y., et al., *Nitrogen-doped graphene and its electrochemical applications.* Journal of Materials Chemistry, 2010. **20**(35): p. 7491-7496.

122. Rao, K.N., et al., *Structure and reactivity of zirconium oxide-supported ammonium salt of 12-molybdophosphoric acid catalysts.* Applied Catalysis A: General, 2006. **300**(2): p. 139-146.

123. Khder, A. and A. Ahmed, *Selective nitration of phenol over nanosized tungsten oxide supported on sulfated SnO_2 as a solid acid catalyst.* Applied Catalysis A: General, 2009. **354**(1): p. 153-160.

124. Clark, B.L.D.a.C.M. *X-ray Powder Diffraction (XRD).* 2013 [cited 2014 February 7]; Available from: http://serc.carleton.edu/research_education/geochemsheets/techniques/XRD.html.

125. Soled, S., et al., *Preparation of bulk and supported heteropolyacid salts.* Catalysis today, 1997. **36**(4): p. 441-450.

126. Watts, J.F. and J. Wolstenholme, *An introduction to surface analysis by XPS and AES.* An Introduction to Surface Analysis by XPS and AES, by John F. Watts, John Wolstenholme, pp. 224. ISBN 0-470-84713-1. Wiley-VCH, May 2003., 2003. **1**.

127. Fan, X., et al., *Deoxygenation of exfoliated graphite oxide under alkaline conditions: a green route to graphene preparation.* Advanced Materials, 2008. **20**(23): p. 4490-4493.

128. Jalil, P.A., et al., *Surface investigation on thermal stability of tungstophosphoric acid supported on MCM-41 using synchrotron radiation.* Applied Catalysis A: General, 2004. **257**(1): p. 1-6.

129. Damyanova, S. and J. Fierro, *Surface properties of titania-supported 12-molybdophosphoric acid hydrodesulphurization catalysts.* Applied Catalysis A: General, 1996. **144**(1): p. 59-77.

130. Paredes, J., et al., *Graphene oxide dispersions in organic solvents.* Langmuir, 2008. **24**(19): p. 10560-10564.

131. Nomiya, K., et al., *Charge-transfer absorption spectra of some tungsten (VI) and molybdenum (VI) polyoxoanions.* Polyhedron, 1987. **6**(3): p. 519-524.

132. Siesler, H.W., et al., *Near-infrared spectroscopy: principles, instruments, applications*. 2008: Wiley. com.

133. Brown, G., et al., *Dodecatungstophosphoric acid hexahydrate,(H5O2+) 3 (PW12O403-). The true structure of Keggin'spentahydrate'from single-crystal X-ray and neutron diffraction data.* Acta Crystallographica Section B: Structural Crystallography and Crystal Chemistry, 1977. **33**(4): p. 1038-1046.

134. Hashimoto, M., G. Koyano, and N. Mizuno, *In Situ IR Spectrum of 12-Tungstophosphoric Acid Hexahydrate with Planar H5O2+*. The Journal of Physical Chemistry B, 2004. **108**(33): p. 12368-12374.

135. Park, S., et al., *Colloidal suspensions of highly reduced graphene oxide in a wide variety of organic solvents.* Nano letters, 2009. **9**(4): p. 1593-1597.

136. Bourlinos, A.B., et al., *Graphite oxide: chemical reduction to graphite and surface modification with primary aliphatic amines and amino acids.* Langmuir, 2003. **19**(15): p. 6050-6055.

137. Hernandez, Y., et al., *High-yield production of graphene by liquid-phase exfoliation of graphite.* Nature Nanotechnology, 2008. **3**(9): p. 563-568.

138. Berciaud, S., et al., *Probing the intrinsic properties of exfoliated graphene: Raman spectroscopy of free-standing monolayers.* Nano letters, 2008. **9**(1): p. 346-352.

139. Dresselhaus, M., A. Jorio, and R. Saito, *Characterizing graphene, graphite, and carbon nanotubes by Raman spectroscopy.* Annu. Rev. Condens. Matter Phys., 2010. **1**(1): p. 89-108.

140. Tuinstra, F. and J. Koenig, *Characterization of graphite fiber surfaces with Raman spectroscopy.* Journal of Composite Materials, 1970. **4**(4): p. 492-499.

141. Dimitrijevic, R., *Davidovie, M.; Nedic, ZP; Mitrovic, MM; Colomban, Ph.* J. Mater. Sci, 1994. **29**: p. 3705.

142. Hernandez-Cortez, J., et al., *Thermally induced phase transformation on 12-tungstophosphoric acid/ZrO2 sol-gel.* Journal of sol-gel science and technology, 2003. **26**(1-3): p. 213-216.

143. Rocchiccioli-Deltcheff, C., et al., *Vibrational investigations of polyoxometalates. 2. Evidence for anion-anion interactions in molybdenum (VI) and tungsten (VI) compounds related to the Keggin structure.* Inorganic Chemistry, 1983. **22**(2): p. 207-216.

144. Graf, D., et al., *Spatially resolved Raman spectroscopy of single-and few-layer graphene.* Nano letters, 2007. **7**(2): p. 238-242.

145. Bennardi, D., et al., *Supported trifluoromethanesulfonic acid as catalyst in the synthesis of flavone and chromone derivatives.* Applied Catalysis A: General, 2007. **324**: p. 62-68.

146. Szabó, T., et al., *Enhanced acidity and pH-dependent surface charge characterization of successively oxidized graphite oxides.* Carbon, 2006. **44**(3): p. 537-545.

147. NIST. *Standard Reference Database 69: NIST Chemistry WebBook*. 2014 [cited 2014 March 12]; Available from: http://webbook.nist.gov/cgi/inchi/InChI%3D1S/C10H20O2/c1-3-4-5-6-7-8-9-12-10(2)11/h3-9H2%2C1-2H3.

148. Valizadeh, H. and A. Shockravi, *An efficient procedure for the synthesis of coumarin derivatives using TiCl< sub> 4</sub> as catalyst under solvent-free conditions.* Tetrahedron letters, 2005. **46**(20): p. 3501-3503.

VITA

Mark Paul Jimena Dailo was born on May 21, 1985, in Quezon City, Philippines. He migrated to the United States in June 2000, and became a citizen of the United States. He graduated from Richard Gahr High School, Cerritos, California in 2003. He received his Bachelor of Science in Chemistry with a minor in Mathematics from University of California Irvine, Irvine, California in 2007. Since 2011, he is pursuing Master's degree in Chemistry at Virginia Commonwealth University.